無給電素子及びブリッジ素子を用いた多素子の平板逆Fアンテナのデカップリング手法に関する研究

(DECOUPLING METHOD FOR MULTIPLE PLANAR INVERTED-F ANTENNAS USING PARASITIC ELEMENTS AND BRIDGE LINES)

防衛大学校理工学研究科後期課程

電子情報工学系専攻 エレクトロニクス工学教育研究分野

フン　クァン　クァン

PHUNG QUANG QUAN

令和 4 年 12 月

Contents

Chapter 1 Introduction 1

1.1 Background 1

1.1.1 Advancement of IoT Devices 1

1.1.2 Multiple Input Multiple Output Technique 1

1.1.3 Conventional Decoupling Methods 3

1.1.4 Mobile Terminal Antennas 5

1.2 Objective of This Dissertation 7

1.3 Configuration of This Dissertation 8

Chapter 2 Decoupling Method for Two PIFAs 10

2.1 Introduction 10

2.2 Structure and Characteristic of Two PIFAs 10

2.2.1 Structure of PIFA Element and Ground Plane 10

2.2.2 Structure and Characteristic of Two PIFAs 11

2.3 Effect of BL Connected Directly to Two PIFAs 16

2.4 Proposed Decoupling Method for Two PIFAs 19

2.4.1 Structure and Effects of PEs and BL 19

2.4.2 Space-saving of PEs 22

2.4.3 Comparison of Characteristics 24

2.5 Discussion on Decoupling Principle using Characteristic Mode Analysis 29

2.5.1 Overview of Characteristic Mode Analysis 29

2.5.2 Discussion on Decoupling Principle 30

2.6 Fabrication and Measurement 36

2.7 Comparison with Other Previous Studies 39

2.8 Summary 40

Chapter 3 Dual-band Design and Decoupling Method for Two PIFAs 41

3.1 Introduction 41

3.2 Dual-band Design for 1-element PIFA....43
3.2.1 Antenna Structure and Characteristics....43
3.2.2 Dual-band Design....45
3.3 Decoupling for Two PIFAs in Dual Band....51
3.3.1 Proposed Decoupling Method....51
3.3.2 Comparison of Characteristics....55
3.3.3 Discussion on Decoupling Principle....57
3.4 Fabrication and Measurement....60
3.5 Versatility of Proposed Decoupling Method....63
3.6 Comparison with Other Previous Studies....66
3.7 Summary....67

Chapter 4 Decoupling Method for Four PIFAs....68
4.1 Introduction....68
4.2 Effects of Previously Proposed PEs and BLs on Four PIFAs....70
4.2.1 Structure and Characteristic of Four PIFAs....70
4.2.2 Effects of Previously Proposed PEs and BLs....71
4.3 Proposed Decoupling Method Using PEs and BLs for Four PIFAs ...74
4.3.1 Structure and Effects of PEs and BLs....74
4.3.2 Space-saving of BLs....78
4.4 Comparison of Characteristics and Discussion on Decoupling Principle 79
4.4.1 Comparison of Characteristics....79
4.4.2 Discussion on Decoupling Principle....85
4.5 Fabrication and Measurement....88
4.6 Comparison with Other Previous Studies....90
4.7 Summary....91

Chapter 5 Conclusion....92

Appendices....94
A Decoupling Method for Two PIFAs Using CMA....94
A.1 Ground Plane Current Modes and Proposed Decoupling

Method 94
A.2 Comparison of Characteristics 97
A.3 Fabrication and Measurement 101
B Antenna Design for WiMAX Using CMA.....103
B.1 Antenna structure and CMA result.....103
B.2 Antenna Design 107
B.3 Fabrication and Measurement 109

Acknowledgements.....111

References 112

Research Achievements..... 120
Journal Papers.....120
International Conferences.....121
Technical Reports and Domestic Conferences 122
Other Research Activities 124

Chapter 1
Introduction

1.1 Background

1.1.1 Advancement of IoT Devices

Recently, the Internet of things (IoT) has become prevalent with applications in countless areas such as medical, consumer, industrial, etc., and maybe even automobile and aerospace in the future [1]. It can be said that the Internet has become an indispensable part, contributing to improving people's quality of life. In addition to common devices such as computers and smartphones, everything from communication devices, home appliances, cars to buildings and factories, etc., is and will be connected to the Internet. Along with the significant annual increase in the number of IoT devices, data traffic will increase, especially mobile data traffic. In Japan, mobile data traffic in December 2021 averaged 5,258.8 Gbps, up approximately 1.2 times from last year [2]. Therefore, large channel capacity and high-speed communication is required to satisfy the needs of all users of these devices.

In order to meet these requirements, increasing the number of base stations is one of the solutions, but the location of the base stations and the power consumption of each base station are problems that are not easy to solve. Therefore, there is a need for technology that enables large channel capacity and high-speed communication without increasing the number of base stations.

1.1.2 Multiple Input Multiple Output Technique

To enhance the transmission system performances with large channel capacity and high-speed communication without increasing the number of base stations, multiple-input multiple-output (MIMO) technique has been invented and continuously developed in recent years. It is considered as a potential technique and plays a major role in developing the next generation communication [3]. Figure 1.1 shows an illustrative example of the MIMO technique. An important feature of this technique is that multiple antenna elements are installed in the same system, including not only base station but also terminal devices.

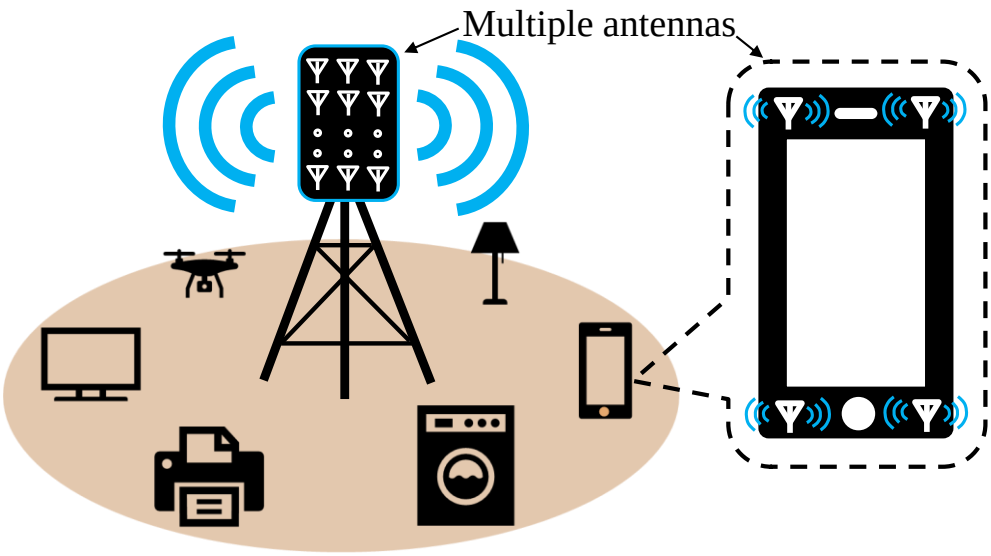

Figure 1.1: Illustrative example of the MIMO technique

Figure 1.2 shows a comparison of signal path between Single Input Single Output (SISO) and 2×2 MIMO technique. In a SISO system, a single antenna is used for both transmitting and receiving functions; therefore, the signal path between the base station and the terminal device is limited to one. In the other hand, by increasing the number of antenna elements as in 2×2 MIMO, which has two antenna elements on both the base station and terminal device, four signal paths can be simultaneously achieved. Therefore, the 2×2 MIMO can obtain two times more communication capacity than the SISO. Furthermore, the communication capacity can increase even more if a large number of antenna elements are used as in Massive MIMO technique. Massive MIMO is a further development of MIMO technique, and it is considered as an elemental technology for next generation communications. The number of antennas used by the base station in a Massive MIMO system is estimated to be dozens or even 100 or more antennas.

As mentioned above, MIMO is an effective technique in improving transmission performance by using multiple antennas in the same system. However, this technique also has a major problem that needs to be solved. Since the space for antennas installation is limited in small terminal devices, it is necessary to place each antenna element close to each other. However, when the antennas are closely spaced, the strong mutual coupling occurs between them and adversely affects the antenna efficiency. Therefore, in order to

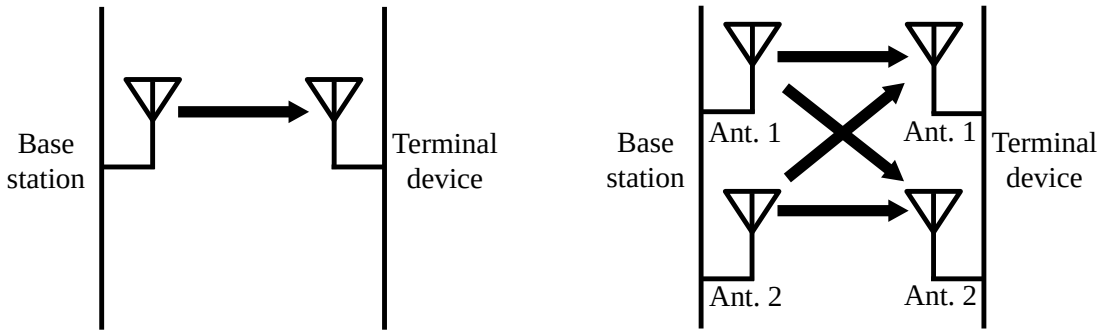

(a) SISO (b) 2×2 MIMO

Figure 1.2: Comparison of signal path between SISO and 2×2 MIMO

improve the efficiency of the antenna, it is necessary to reduce the mutual coupling (hereafter referred to as decoupling) between them.

1.1.3 Conventional Decoupling Methods

To date, many decoupling solutions using various arrays of conventional antenna elements have been proposed. Figure 1.3 shows several typical decoupling methods. The method using slot on the ground plane is regarded as a simple method because it does not increase the volume of the original antenna [4-6]. By creating one or several slots, the current path on the ground plane is physically eliminated. Therefore, coupling current cannot directly flow from radiating antenna to non-radiating antenna through the ground plane, resulting in a reduction in mutual coupling. However, since slots are usually created on the ground plane where the antennas are located, the space for mounting electronic components in this area is reduced. In addition, placing electromagnetic band gap (EBG) structures on the ground plane is also considered as an effective method [7-8]. An outstanding characteristic of the EBG structures is that they can create a stopband to suppress electromagnetic waves of certain frequency bands. Therefore, placing the EBG structures between antenna elements can reduce the mutual coupling. However, the EBG structure requires considerable space, rendering it difficult to use it in array antennas, which are spaced closely. Other methods using decoupling circuit have been proposed in [9-11]. These circuits can cancel the mutual coupling that occurred between the adjacent

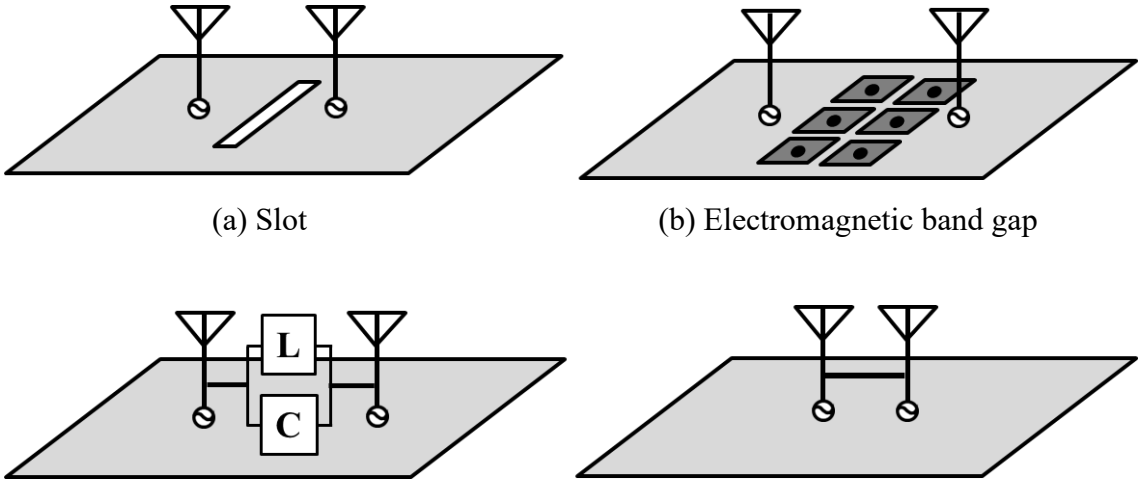

(a) Slot (b) Electromagnetic band gap

(c) Decoupling circuit (d) Bridge line

Figure 1.3: Several typical decoupling methods

antenna elements by providing a negative coupling. However, this method requires the use electronic components to form the decoupling circuit. A disadvantage of the decoupling circuits is that their structure is complex, and the operating bandwidth is reduced significantly. The method using a thin metal line to directly connect antenna elements is a well-known and effective method and is known by various names, such as suspended lines, neutralization lines, or bridge lines [12-16]. Among the four typical decoupling methods presented in Fig. 1.3, this method is considered to be the simplest and most effective, and therefore this dissertation will focus mainly on it. For convenience, the method will be referred to as a bridge line (BL) hereinafter. Thus far, the BL has only been studied for decoupling two antenna elements. Moreover, the resonant frequency shifts to a different frequency when the antenna elements are connected directly by a BL, particularly in the case where the antennas operate in a narrow band. Hence, to shift the resonant frequency toward the desired frequency, the original size of the antenna elements must be adjusted individually. This is considered to be disadvantageous if the methods are applied under design conditions that hinder the implementation, for example, for small wireless modules with antenna.

In fact, there are many cases when small wireless modules are implemented in mobile terminal devices. Figure 1.4 illustrates an example of MIMO system consisting

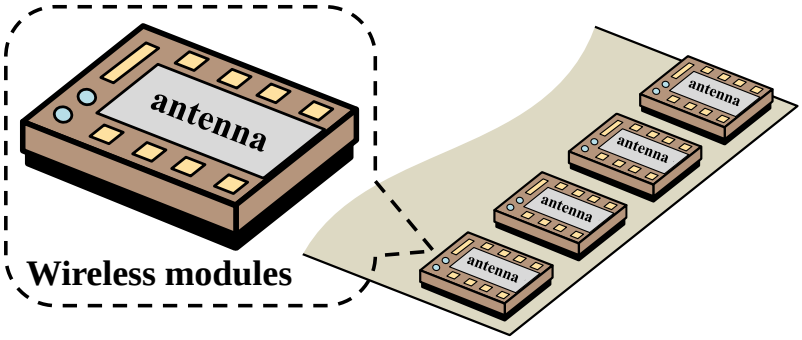

Figure 1.4: Example of MIMO system composed of multiple wireless modules

of multiple wireless modules. When the individual modular antennas are placed close together inside a small device, mutual coupling occurs. So that, they must be decoupled, and redesign of modular antennas is required to achieve this. However, there are many electronic components around the antenna and the initial size of the antenna is also fixed, so the redesign of modular antennas or direct connection with additional elements is difficult. Moreover, fifth-generation technology standard 5G has become popular in recent years, and it is still in the development process to be widely available. Compared to the fourth generation 4G which uses the frequency bands below 3.6 GHz, 5G requires the higher frequency bands of 3.7 GHz, 4.5 GHz (Sub6) and 28 GHz (millimeter wave). To operate in these high frequency bands, the antennas need to be smaller in size. Thus, it becomes even more difficult to redesign the original antenna.

For these reasons, to easily decouple the antennas in such cases, an approach that does not require the adjustment of the original antenna sizes or structure is required.

1.1.4 Mobile Terminal Antennas

In the past, terminal devices such as mobile phones were usually large in size and the antennas were placed on the outside of the device. This type of antenna design affects the aesthetics of the devices as well as makes their total size larger. In addition, placing the antennas outside the device also adversely affects the performance of the antenna because most of the radiated signal is reflected and absorbed by the user's head.

Nowadays, in order to meet the aesthetic requirements as well as the convenience for users, the size and weight of these devices have been greatly reduced. Furthermore, to reduce their total size, the antennas have been placed inside instead of outside the devices. However, placing antennas inside a compact device is also an issue because the space

available for the antenna is limited by a large number of other electronic components. Therefore, antenna miniaturization has been an interesting topic for a long time, and so far, various antenna miniaturization methods have been proposed by many researchers and antenna designers. For example, several typical techniques of miniaturization for monopole antenna can be mentioned such as folding the top of the antenna into a meander or inverted-L shape; or changing the structure to an inverted-F shape. In practical design of mobile device antenna, the inverted-F is considered as one of the most effective structures because of its low profile, and especially it does not require any external components such as matching circuit. Therefore, inverted-F antenna is widely used in compact mobile terminal devices, including mobile phones and tablet computers. However, one drawback of this antenna is that its bandwidth is extremely narrow. Therefore, in order to widen the bandwidth, the wire radiator element of inverted-F antennas is replaced by a plate. Since then, the inverted-F antenna with the plate element is known as the planar inverted-F antenna (PIFA).

Figure 1.5 shows a basic layout of PIFA. As shown, the PIFA usually composes of a rectangular plate (PIFA patch), a feeding strip and a shorting strip. In addition, the bandwidth and gain can be further improved by placing the PIFA on a ground plane. This is because when the PIFA is excited, the current flowing on the ground plane makes the effective size of the PIFA larger. Another feature of the PIFA can be mentioned is that the impedance matching can be easily adjusted by changing the distance between the feeding strip and the shorting strip. Furthermore, the resonant frequency depends on the peripheral length of the PIFA patch and the width of shorting strip, as following equation (1.1) [17]:

$$f = \frac{\mathrm{c}}{4\times(l_{\mathrm{f}} + w_{\mathrm{f}} - w_{\mathrm{s}})} \tag{1.1}$$

where c is the speed of electromagnetic waves in vacuum; l_{f} and w_{f} are the length and the width of the PIFA patch, respectively; w_{s} is the width of the shorting strip.

In addition, PIFA has other advantages such as omnidirectional radiation pattern and less hazardous effects on the human brain. Because of these advantages, it is commonly used for built-in antennas in many devices such as mobile phones [18-23]. Moreover, a decoupling method using a bridge line has already been studied for two-

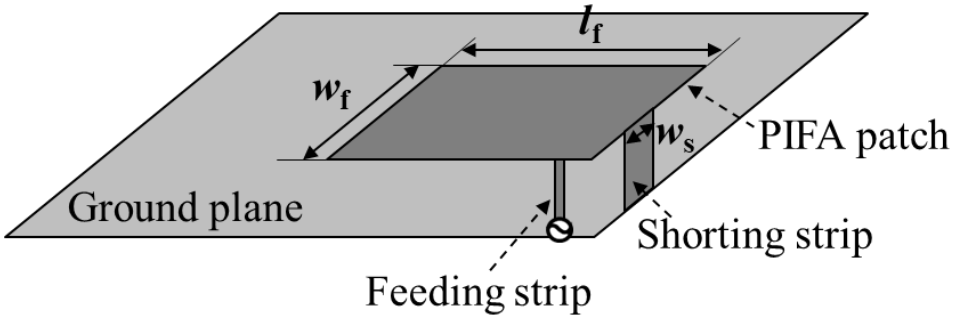

Figure 1.5: Basic layout of PIFA

element PIFAs [12]. However, the two-element PIFA used in [12] is not a MIMO antenna, because they operate at different frequency.

In this dissertation, the multiple PIFA elements that operate at the same frequency as a MIMO antenna for mobile terminals are selected as the research target to investigate the decoupling method that can reduce the mutual coupling between them.

1.2 Objective of This Dissertation

As mentioned in 1.1.3, to easily decouple the antennas in cases where the design conditions render it difficult to redesign the original antenna sizes or structure, an approach that does not require the redesign of the original antenna sizes or structure is required. A simple idea to implement a decoupling method that meets these requirements is to use parasitic elements (PEs), since PEs will electromagnetically couple to the antenna if they are placed in suitable locations. And thus, the antenna characteristics can be adjusted using PEs instead of directly redesigning the original antenna. So that, there is no need to redesign the original antenna. Previously, PEs are generally utilized to adjust either the directivity of the antenna to the desired direction or to enhance the bandwidth, as discussed in [24-26]. However, utilizing PEs to reduce the mutual coupling of MIMO antennas are few.

Based on this idea, this dissertation will utilize the combination of PEs and BLs to reduce the mutual coupling between multiple PIFAs, without having to redesign the original antenna sizes or structure. Moreover, the design target of this dissertation is to reduce and maintain all the return loss and mutual coupling for less than −10 dB, which

are acceptable levels for MIMO antennas. Besides, in this dissertation, the desired frequency is set at 2.0 GHz because this frequency still supports a lot of mobile devices today, and the size of PIFA operating at 2.0 GHz is suitable to perform the fabrication and measurement processes easier.

1.3 Configuration of This Dissertation

The results obtained in this study have been summarized in this dissertation, which consists of five chapters as shown in Fig. 1.6. In Chapter 1, background, motivation, and objective of this dissertation were presented.

Chapter 2 investigates a decoupling method using PEs and BL for two PIFAs as a primary study to confirm the possibility of the proposed method. The decoupling principle of the proposed method is discussed in more detail using Characteristic Mode Analysis (CMA), which is a useful analysis method for antenna design and for clarifying the operating principle of antennas.

Chapter 3 presents a dual-band design and decoupling method for the two PIFAs. In this chapter, the proposed method using PEs and BLs in Chapter 2 will be developed to increase the operating frequency band and decouple the two PIFAs at these frequency bands. First, a dual-band design for 1-element PIFA using PE is performed. The PEs are then connected by a BL to decouple the two PIFAs in dual-band.

In Chapter 4, a decoupling method for four PIFAs is investigated. In this chapter, the proposed method using PEs and BLs in Chapter 2 will be developed to reduce the mutual coupling between four PIFAs, which are closely spaced in a horizontal row on a ground plane.

Chapter 5 summarizes the overall conclusions of this dissertation.

The simulations in this study are performed using the simulator CST Studio Suite, and the validity of simulation results will be confirmed by the comparison with the measurement results of several fabricated antenna prototypes.

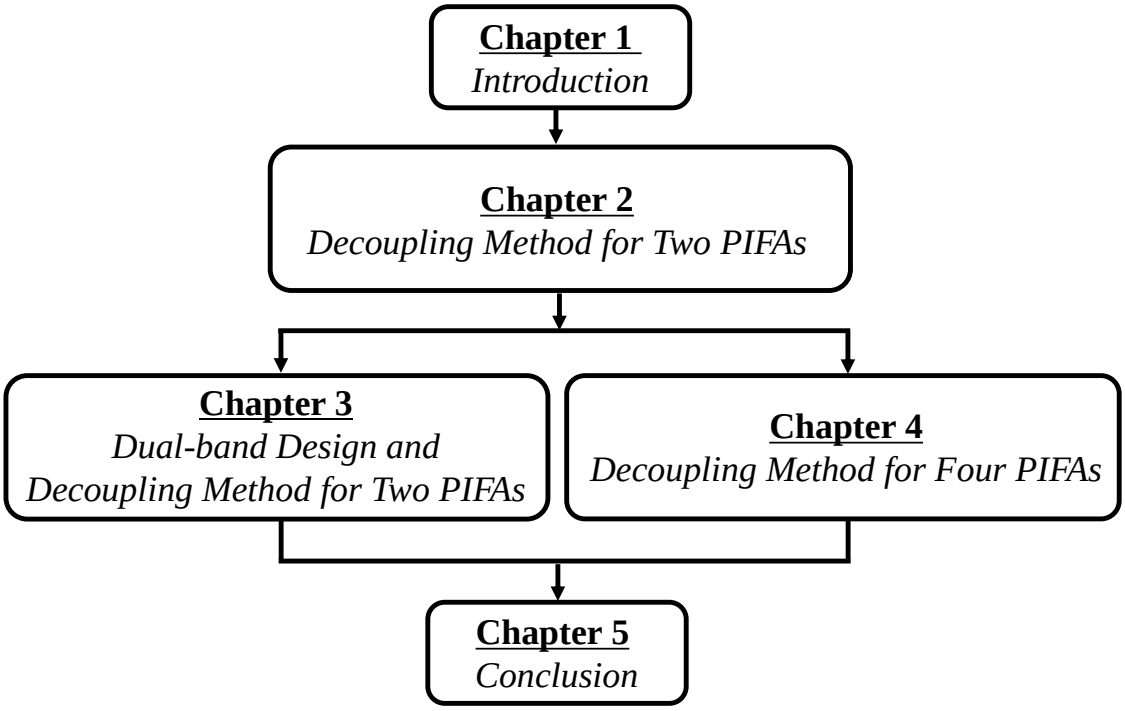

Figure 1.6: Configuration of this dissertation

Chapter 2
Decoupling Method for Two PIFAs

2.1 Introduction

In this chapter, a decoupling method using PEs and BL is proposed without having to redesign the original sizes of the two PIFAs. Section 2.2 first describes the structure of a PIFA element and ground plane, then investigates the characteristics of two PIFA elements when they are mounted on the ground plane with different arrangement and different positions of feeding pin. In Section 2.3, the two PIFAs with close feeding pins are directly connected by a BL to investigate the effect of BL to the resonant frequency of the two PIFAs. Section 2.4 describes the design progress of proposed decoupling method, which uses the combination of PEs and BL. The operating principle of the proposed decoupling method is discussed in more detail using Characteristic Mode Analysis (CMA) in Section 2.5. Section 2.6 shows the fabrication prototypes and examines the agreement between simulation and measurement results to confirm the validity of the proposed decoupling method. Section 2.7 compares the proposed method in this chapter with some other previous studies. Finally, Section 2.8 gives a summary of this chapter.

2.2 Structure and Characteristic of Two PIFAs

2.2.1 Structure of PIFA Element and Ground Plane

Figure 2.1 shows the structure of the PIFA element and ground plane, which are used to construct the MIMO antenna in this dissertation. The ground plane is represented as a shielding plate in a mobile handset terminal measuring 120 mm × 45 mm. The PIFA element consists of a PIFA patch and two pins, of which one is for feeding and the other is for shorting. As explained in Chapter 1, the resonant frequency of the PIFA depends on the peripheral length of the PIFA patch and the width of shorting pin. Therefore, the PIFA patch is optimized to a size of 20 mm × 19 mm, and the width of shorting pin is set to 1 mm, such that the PIFA can resonate at a frequency of approximately 2.0 GHz. The height of the PIFA patch is 7 mm. An advantage of the PIFA is that its impedance matching

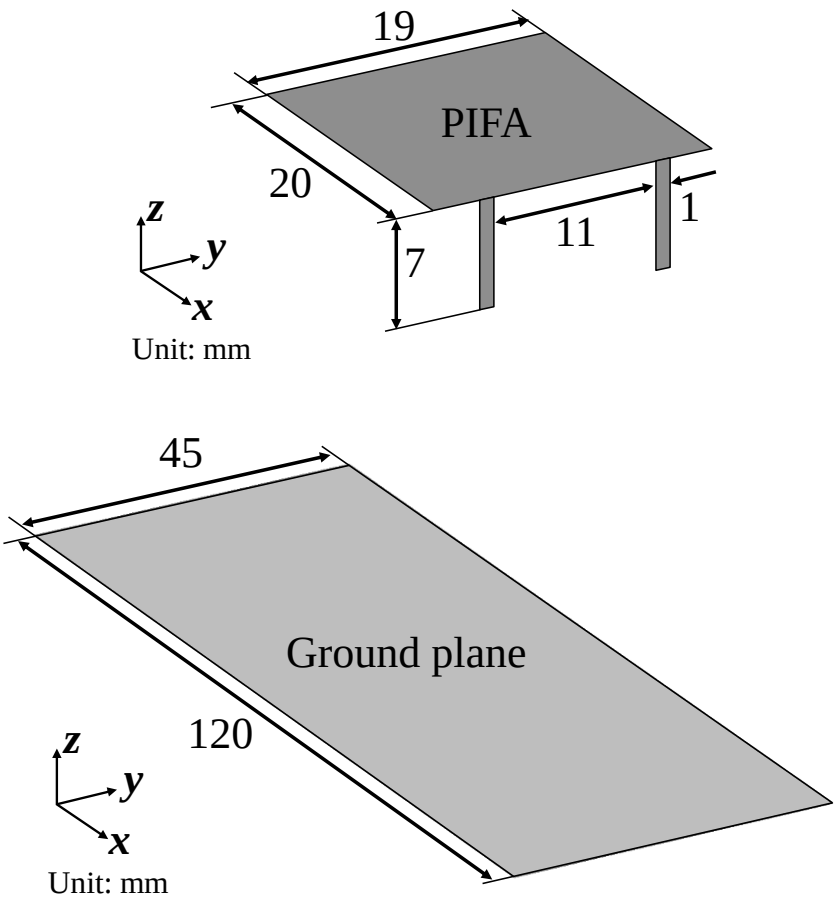

Figure 2.1: Structure and size of PIFA element and ground plane

can be easily accomplished by adjusting the positions of the feeding and shorting pin. Therefore, the distance between the feeding and shorting pin is set to 11 mm after performing a parametric study. The PIFA element and ground plane are made of copper and measured 0.3 and 0.5 mm thick, respectively.

2.2.2 Structure and Characteristic of Two PIFAs

Figure 2.2 shows four models A, B, C, and D with different arrangements of two PIFAs. In each model, the two PIFA elements are symmetrically mounted at the edge of the ground plane and fed by 50-Ω sources. Figure 2.3 shows S-parameters (return loss S_{11} and mutual coupling S_{21}) of these four models. As shown in Fig. 2.3(a), although the PIFA elements in the four model are designed to be able to resonate at the desired frequency of approximately 2.0 GHz as mentioned above, their resonant frequency and input impedance vary greatly depending on the arrangement method. Specifically, the resonant

frequency of Model A is 2.0 GHz, which is the desired frequency of this study, and the S_{11} is less than −10 dB. Meanwhile, the S_{11} in Models B and D is less than −10 dB, but the resonance appears at 2.4 GHz. In addition, the S_{11} in Model C deteriorates for beyond −10 dB and no resonance appeared at 2.0 GHz. From these results, Model A is considered to be the most suitable for the objective of this study as it provides a good impedance matching at the desired frequency. However, as shown in Fig. 2.3(b), since the mutual coupling in Model A at 2.0 GHz is strong (S_{21} = −6.6 dB), it is necessary to reduce the mutual coupling between the two PIFAs to improve its performance at the desired frequency.

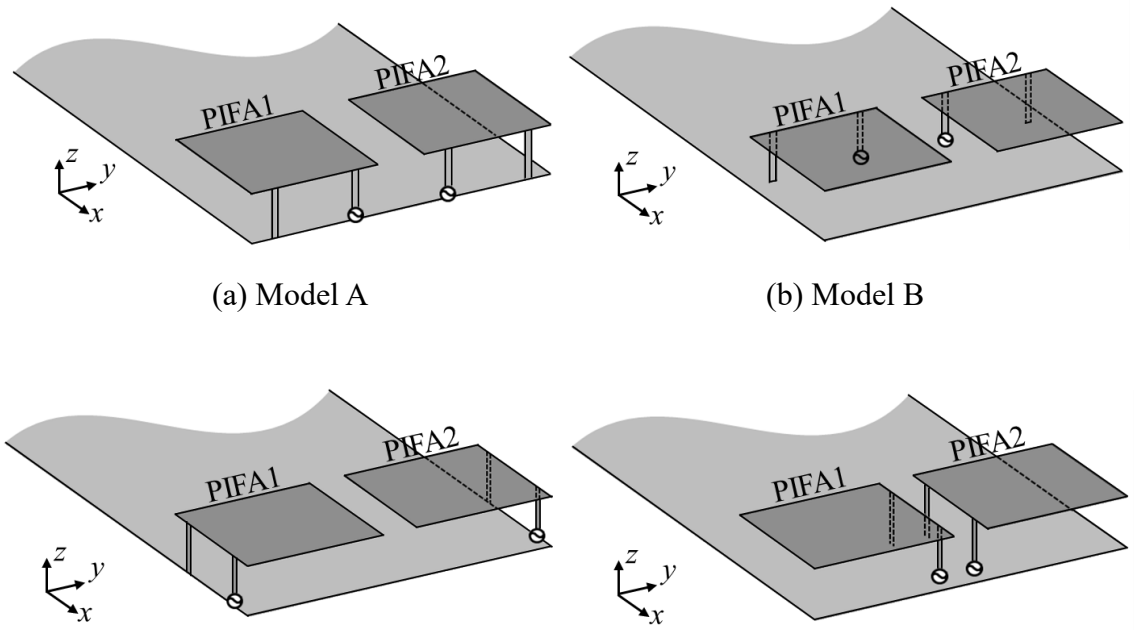

(a) Model A (b) Model B

(c) Model C (d) Model D

Figure 2.2: Structure of two PIFAs mounted on ground plane with different arrangements

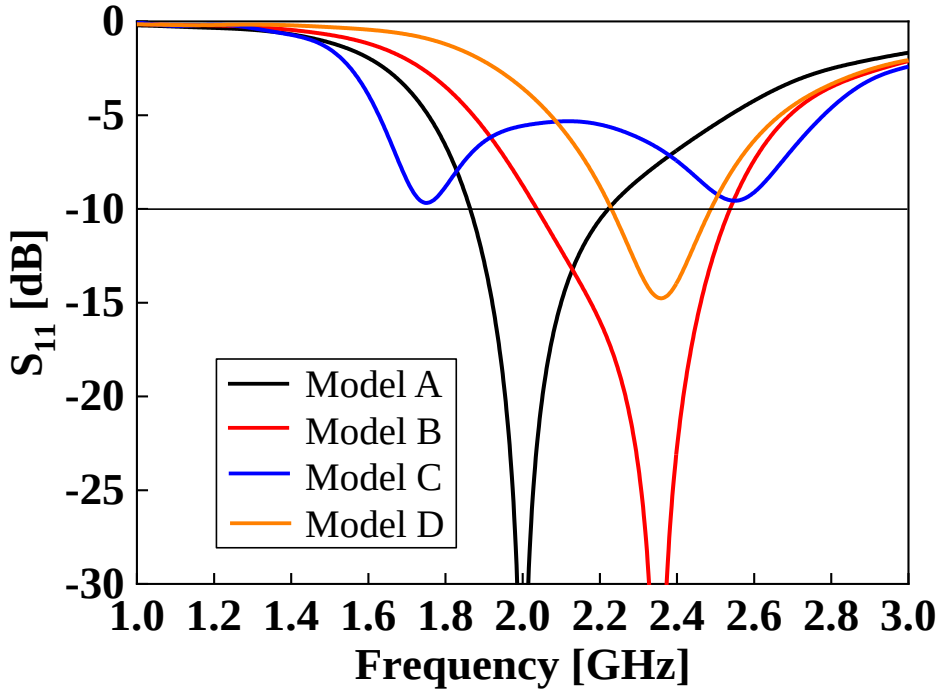

(a) S_{11}

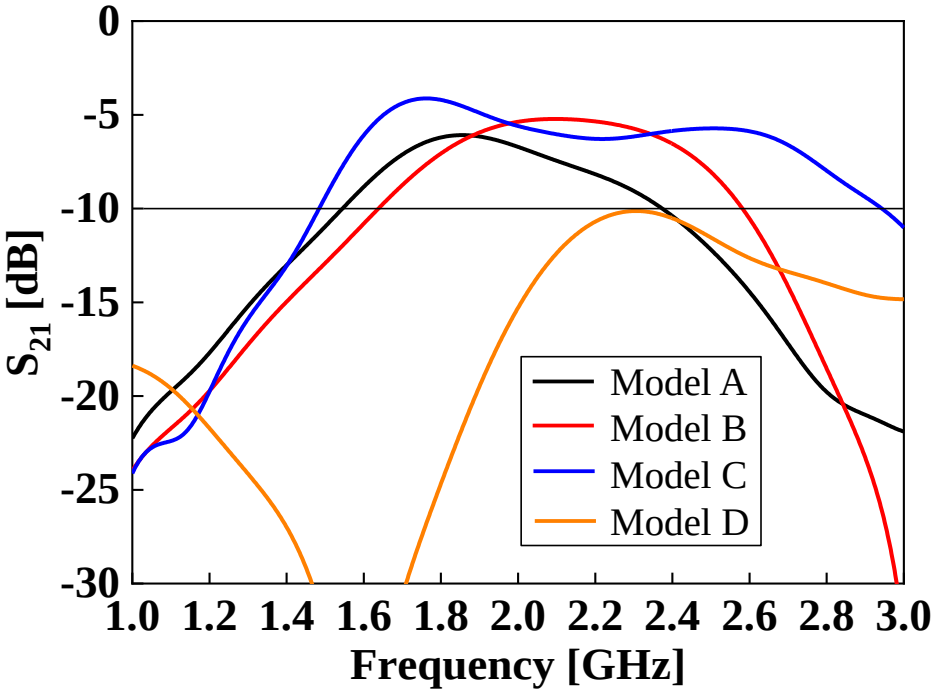

(b) S_{21}

Figure 2.3: S-parameters of four models

Next, the effect of feeding position on the characteristics of the two PIFAs will be investigated. Figure 2.4 shows two models of two PIFAs, called Model A and Model A', with different positions of feeding pin and shorting pin. As shown in Fig. 2.4(a), the feeding pin of the two PIFAs in Model A is arranged close to each other on the inside, and the shorting pin is arranged on the outside. On the other hand, as shown in Fig. 2.4(b), the shorting pin of PIFAs in Model A' is arranged close to each other on the inside and the feeding pin is arranged on the outside. Each PIFA element of Models A and A' is fed by a 50-Ω source.

Figure 2.5 shows the simulation result of S-parameters of Model A and Model A'. The result shows that the resonant frequency of both models is 2.0 GHz. However, in the case of Model A, a strong mutual coupling (S_{21} = −6.6 dB) occurs between two PIFAs at their resonant frequency. Meanwhile, the mutual coupling between the two PIFAs in Model A' is only −10.0 dB, which is an acceptable level for MIMO antennas. From these results, it is clear that the positions of the feeding pins and the shorting pins slightly effect on the resonant frequency, but strongly effect on the mutual coupling between the two PIFAs.

Figure 2.6 shows the simulation result of total antenna efficiency of Model A and Model A'. The total antenna efficiency (η_{total}) is presented in Eq. (2.1) as follows [27]:

$$\eta_{total} = \eta_{rad}\,(1 - |S_{11}|^2 - |S_{21}|^2) \tag{2.1}$$

where η_{rad} represents the radiation efficiency, which is the ratio of the radiated power to

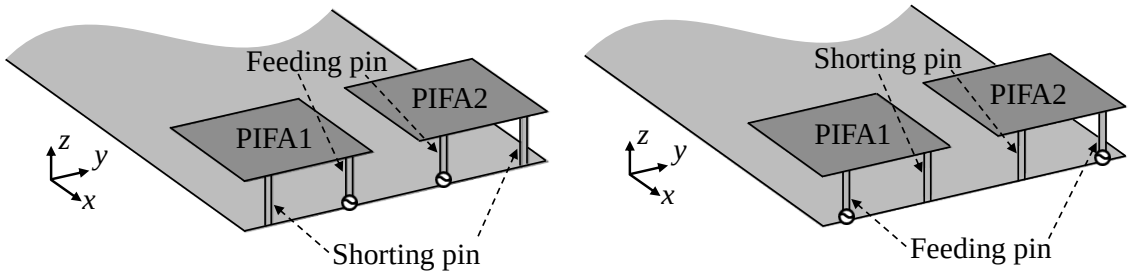

(a) Model A (b) Model A'

Figure 2.4: Structure of two PIFAs with different positions of feeding pin and shorting pin

the accepted power. From Eq. (2.1), it can be known that if the radiation efficiency of a single PIFA element is maintained with a good impedance matching, the total antenna efficiency mainly depends on the magnitude of the mutual coupling between the two PIFAs. As shown in Fig. 2.6, the total antenna efficiency at 2.0 GHz of Model A is 77.6%, meanwhile that of Model A' is 89.3%.

From these results, it can be concluded that by selecting suitable position of feeding and shorting pins such as Model A', mutual coupling can be reduced significantly, and a high total antenna efficiency can be achieved at the desired frequency without any additional decoupling methods. However, in the case of a MIMO system consisting of a larger number of PIFA elements than two, it is unavoidable to arrange the feeding pins close to each other as show in Model A. Therefore, a decoupling method to reduce the mutual coupling between the two PIFAs in case their feeding pins are close to each other is also required. For this reason, in the following studies, the structure of Model A will be considered as the original model of two PIFAs, and decoupling methods to reduce mutual coupling between them will be investigated.

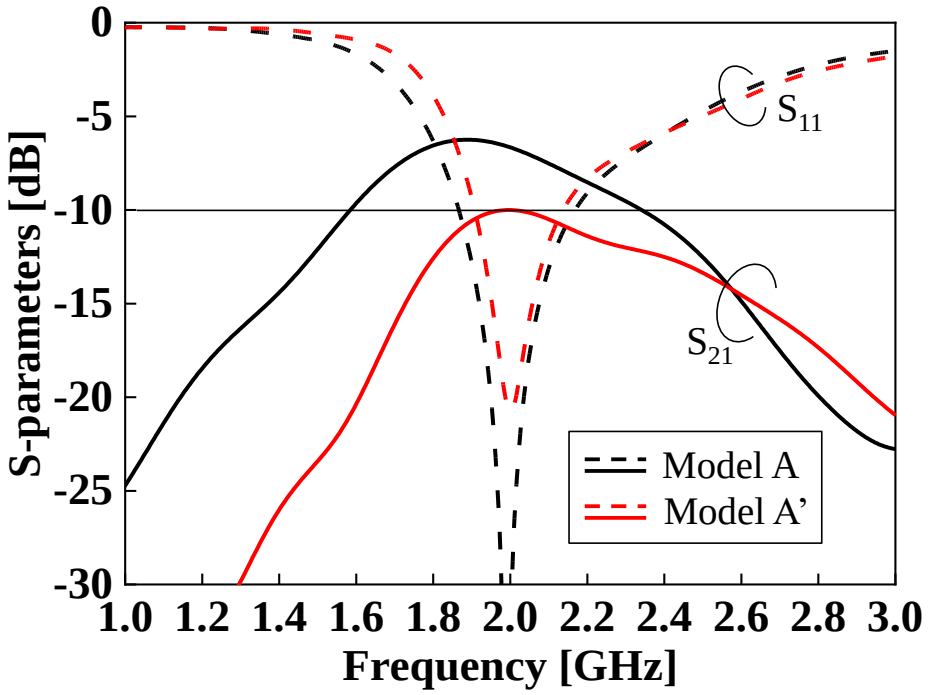

Figure 2.5: S-parameters of Model A and Model A'

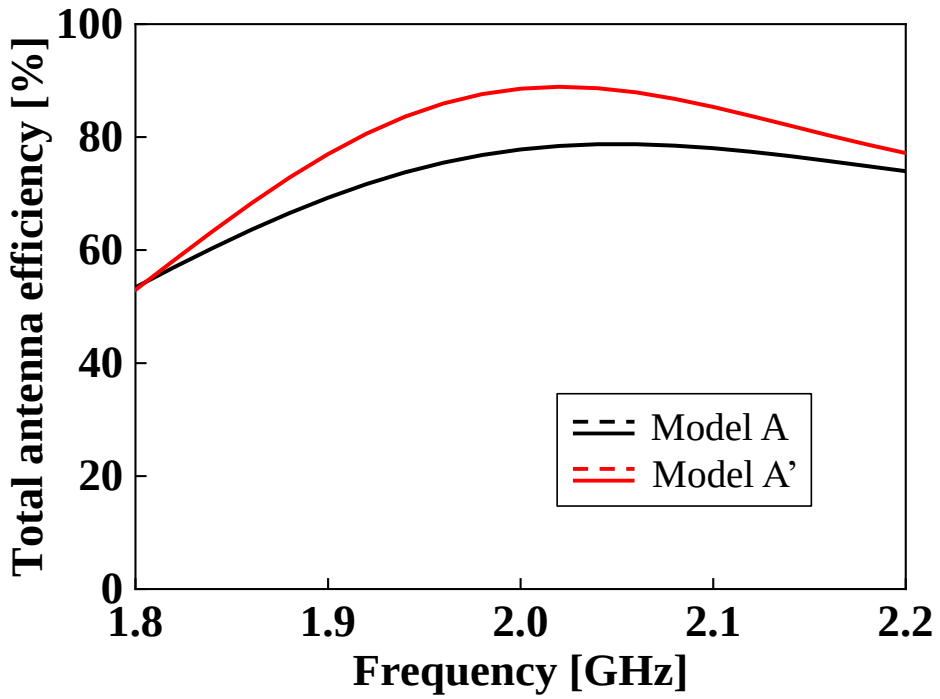

Figure 2.6: Total antenna efficiency of Model A and Model A'

2.3 Effect of BL Connected Directly to Two PIFAs

In a previous study pertaining to two L-shaped folded monopole antennas (LFMAs), as shown in [15], it was observed that the mutual coupling reduced when the two LFMAs were connected directly by a BL, but the resonant frequency shifted to a higher frequency. However, the LFMA exhibited a certain structure that might have caused a change in the resonant frequency. In this section, a BL is applied to two PIFAs to evaluate the effect of the BL on the resonant frequency more effectively. First, the BL should be connected at the feeding pin of the antennas, where the currents have the highest intensity [12]. Figure 2.7 shows the structure of two PIFAs connected directly to their feeding pins by the BL. The BL is positioned at the same height as the PIFAs.

Figure 2.8 shows the S-parameters of PIFAs with and without a BL. As shown, when the PIFAs are connected by a BL, S_{21} reduces significantly at approximately 2.3 GHz. However, the resonant frequency shifts from 2.0 to 2.3 GHz, and the impedance matching deteriorates compared with the case of PIFAs without a BL. The reason contributing to the shift in the resonant frequency to a different frequency at a higher band after directly connecting the PIFAs will be explained by comparing the current

distribution in Section 2.4.

The antenna size can be increased to shift the resonance to a lower frequency. However, this may not be appropriate from the viewpoint of miniaturization but acceptable in cases where the design conditions facilitate the technique. Figure 2.9 shows the S-parameters when the PIFA patch length l_f is varied. As shown, the resonant frequency is 2.0 GHz when l_f = 24 mm. Furthermore, the lowest S_{21} increases when l_f increases, but it is still less than −18 dB at 2.0 GHz.

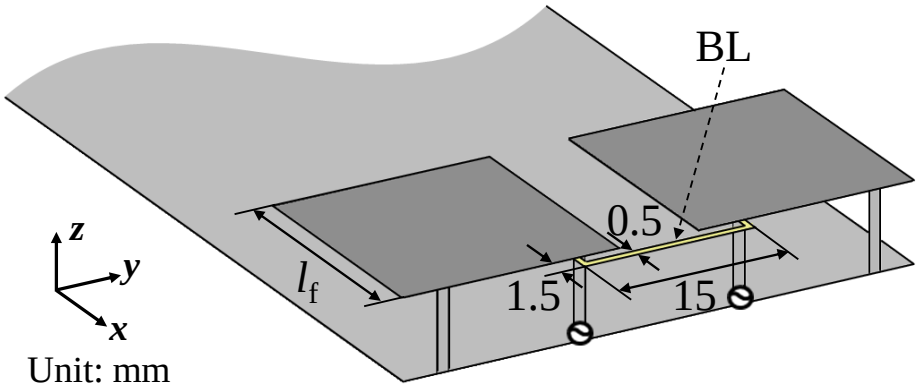

Figure 2.7: Structure of PIFAs connected directly by a BL (l_f = 20 mm)

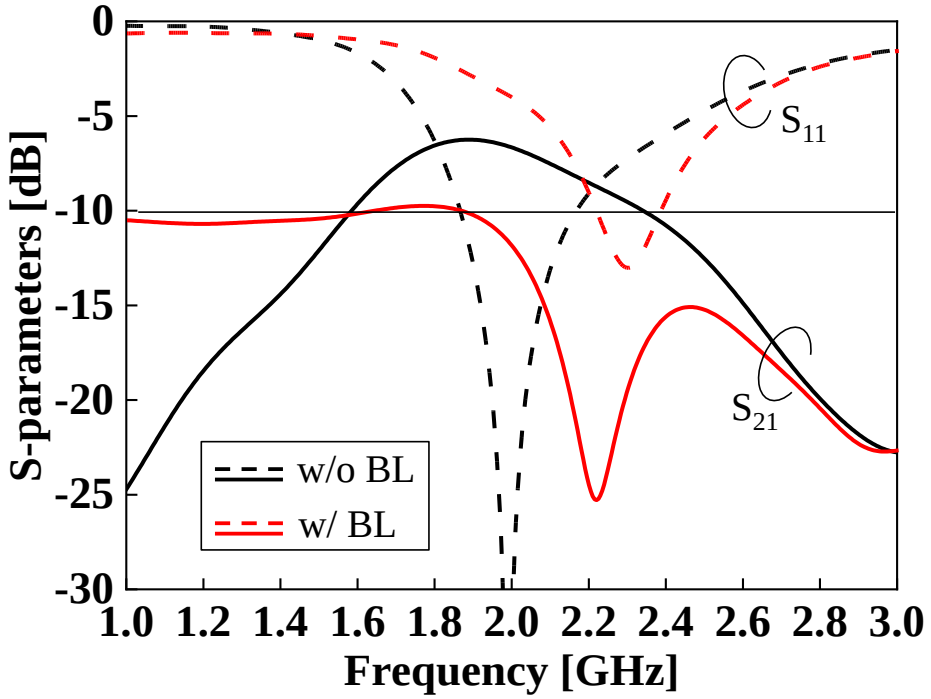

Figure 2.8: S-parameters of PIFAs with and without BL (l_f = 20 mm)

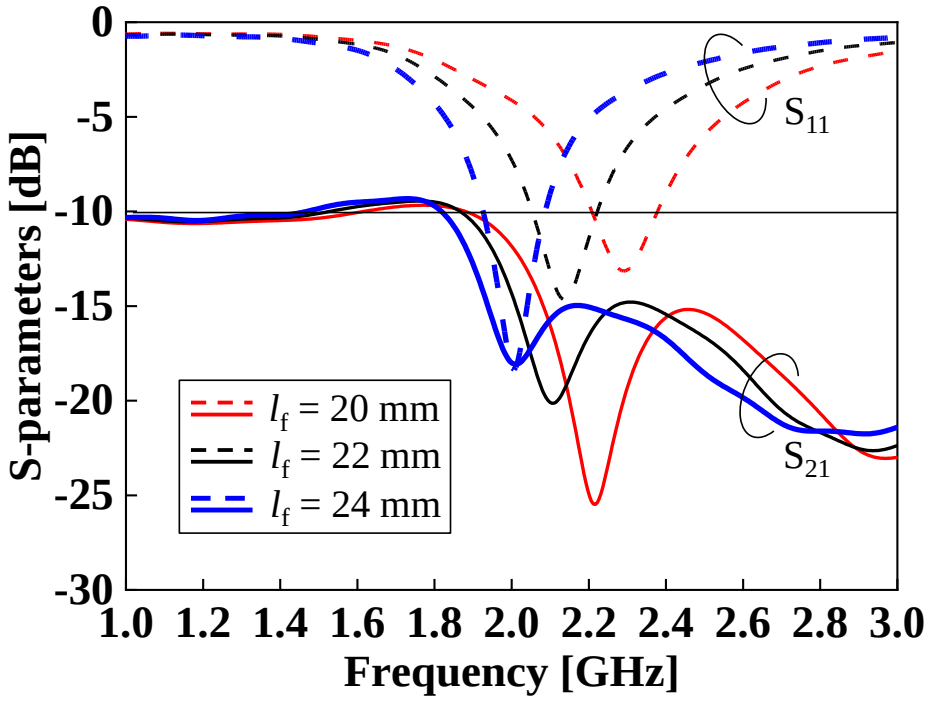

Figure 2.9: S-parameters of varying PIFA patch length l_f (with a BL)

It is noteworthy that the objective of this investigation is not to determine the amount of mutual coupling that can be reduced when the PIFAs are directly connected by the BL. However, based on the results, the following salient points should be emphasized: 1) Although the LFMAs and PIFAs have different structures, the resonant frequencies remain similar when the abovementioned antennas are connected directly by the BL. In other words, the BL significantly affects the resonant frequency regardless of the antenna structure; 2) when the BL is used to directly connect the antennas, the antenna size must be adjusted to shift the resonant frequency toward the desired frequency or improve the impedance matching.

As mentioned above, when the design condition enables the antennas to be directly connected by the BL and the size of the original antennas to be adjusted, then it is easy and effective to decouple the antennas using this method. However, for decoupling the antennas when the design condition is difficult to achieve, another decoupling method known as parasitic elements (PEs) connected by a BL will be proposed and discussed in the next section.

2.4 Proposed Decoupling Method for Two PIFAs

In this section, the decoupling method using PEs that are connected by a BL and loaded onto the two PIFAs will be presented. Previously, PEs are generally utilized to adjust either the directivity of the antenna to the desired direction or to enhance the operating bandwidth, as discussed in [24-26]. Studies utilizing PEs to reduce the mutual coupling of MIMO antennas are few. Moreover, the novelty of the proposed method is that the advantages of the PEs and BL are utilized to reduce the mutual coupling as well as to maintain the impedance matching at the desired frequency without having to redesign the original size and structure of the two PIFAs.

2.4.1 Structure and Effects of PEs and BL

Figure 2.10 shows the structure of two PEs connected by a BL and then loaded onto the two PIFAs. In order for electromagnetic coupling of the PEs and the two PIFAs to be effective, the PEs should be loaded in parallel onto PIFA patches near the feeding pins, where a strong current is flowing. Therefore, in the first step of the design process, two PEs made of rectangular copper plates will be used. The size of each PE is $l_p \times w_p$, and the air gap between PEs and PIFAs is h_p. The spacing between the two PEs is the same as that of the two PIFAs (7 mm). The BL is used to connect them at points closest to the feeding pin of the PIFAs. To determine the optimal position and size of the PEs, several parameters individually are varied while the other parameters are fixed.

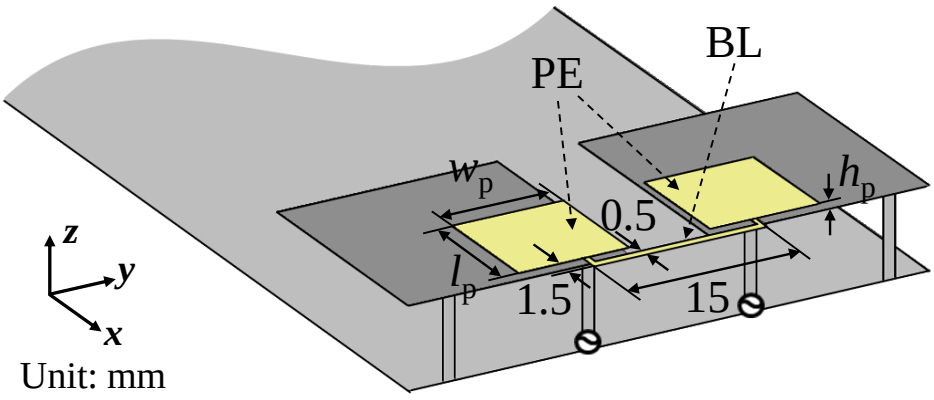

Figure 2.10: Structure of two PIFAs with PEs and BL

First, h_p is varied to investigate the effects of the PEs on the PIFAs when the space between them is small. The reason for loading PEs onto PIFAs by a small air gap is that it does not significantly increase the volume of PIFAs with PEs. In this investigation, the dimensions of the PEs are fixed to l_p = 10 mm and w_p = 9.5 mm. As shown from the results in Fig. 2.11, when h_p = 1.5 mm, two resonances are observed; one appears at a lower frequency, whereas the other at a higher frequency of 2.0 GHz. For convenience, the resonances appearing at the lower and higher frequencies are referred as the first and the second resonances, respectively. The mutual coupling at the first resonant frequency is extremely strong. Meanwhile, the mutual coupling at the second resonant frequency is considerably reduced. Hence, the second resonance should be focused for the next investigation. Moreover, the second resonance shifts to a lower frequency when h_p decreases. In particular, when h_p is 0.5 mm, a resonance with S_{11} < −10 dB is observed at 2.35 GHz. This resonance will shift to a frequency lower than 2.35 GHz if h_p is decreased to less than 0.5 mm; however, the shift is not significant. Therefore, h_p is fixed to 0.5 mm, and the other parameters of the PEs must be investigated to shift the resonance from 2.35 to 2.0 GHz.

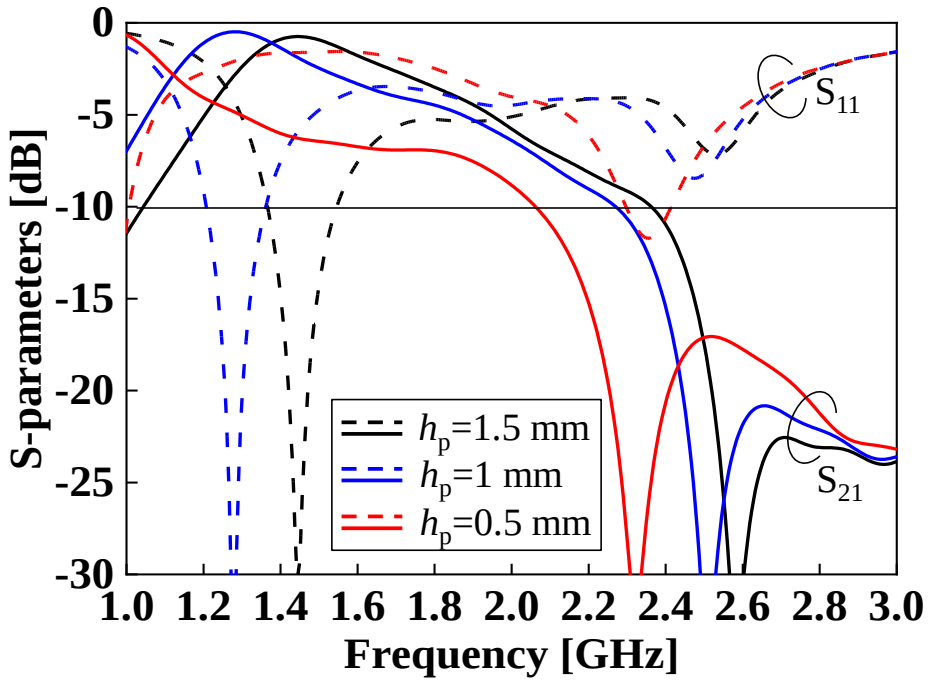

Figure 2.11: Effects of varying h_p (l_p = 10 mm and w_p = 9.5 mm)

In the next step, the size of the PEs is investigated by varying w_p and l_p. The objective of this investigation is to determine the size of PEs that enables the following two targets to be achieved simultaneously: 1) shifting the resonance from 2.35 to 2.0 GHz and improving or at least maintaining S_{11} for less than −10 dB; and 2) maintaining S_{21} at less than −10 dB at 2.0 GHz.

Figure 2.12 shows the S-parameters of the PIFAs when w_p is varied from 9.5 to 25.5 mm, while l_p is fixed at 10 mm. It is obvious that, even though w_p increases considerably, the resonance only shifts slightly from 2.35 GHz to a lower frequency. Moreover, when w_p = 25.5 mm, S_{11} deteriorates for beyond −10 dB. Hence, it is evident that the first target of this investigation cannot be achieved by varying w_p. Therefore, w_p is fixed at 9.5 mm. Meanwhile, as shown in Fig. 2.13, when l_p increased from 10 to 26 mm, the resonance shifts from 2.35 GHz to a lower frequency. In particular, when l_p = 26 mm, the resonance appears at 2.0 GHz, and S_{11} improves significantly for less than −30 dB. Additionally, S_{21} is maintained at less than −16.7 dB at 2.0 GHz. Hence, the two targets of this investigation are achieved.

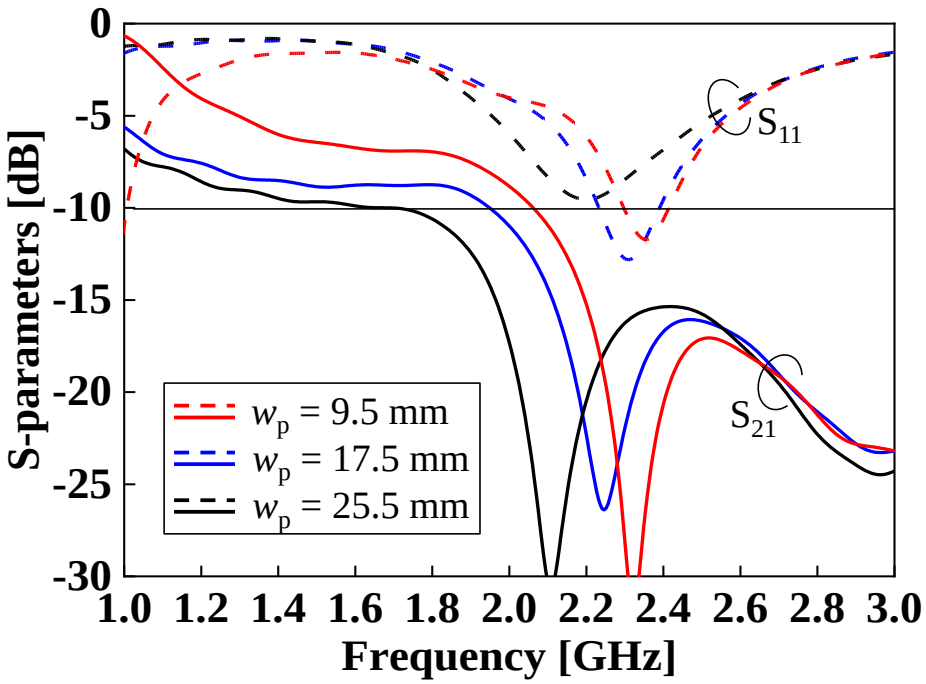

Figure 2.12: Effects of varying w_p (h_p = 0.5 mm and l_p = 10 mm)

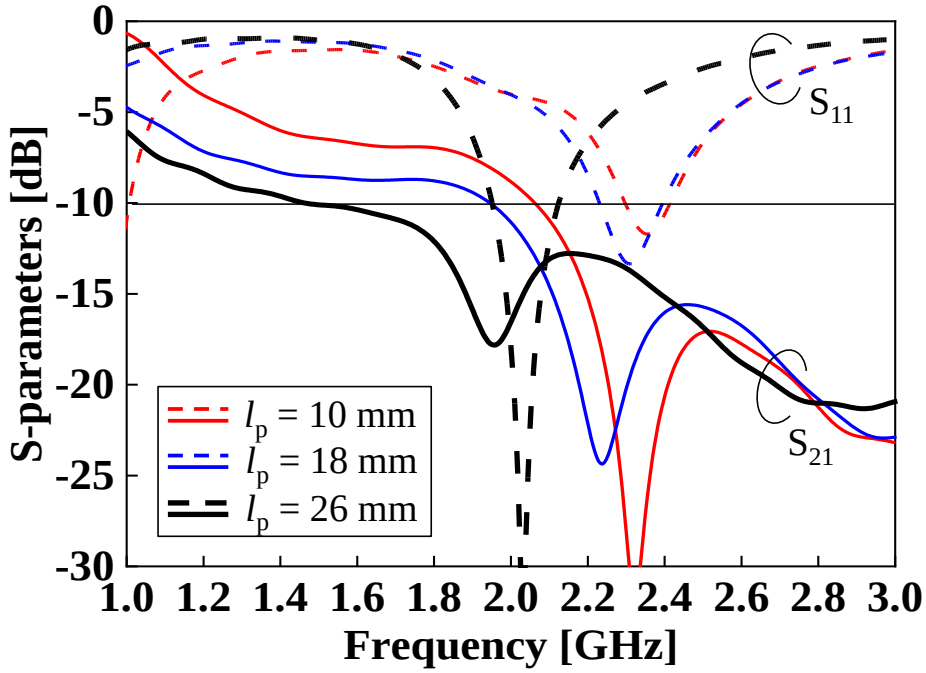

Figure 2.13: Effects of varying l_p (h_p = 0.5 mm and w_p = 9.5 mm)

By varying the parameters, the optimal position and size of the PEs can be determined, where h_p = 0.5 mm, l_p = 26 mm, and w_p = 9.5 mm. The other parameters of the PEs may also affect the performances of the PIFAs, although insignificantly.

2.4.2 Space-saving of PEs

By loading the PEs with the parameters determined above, a low level of mutual coupling and impedance matching is obtained at 2.0 GHz without having to redesign the original size and structure of two PIFAs. However, the volume of the PIFAs including PEs and the BL increases. Therefore, the space-saving of PEs needs to be considered. To achieve this, the PEs are bent at a certain position, as shown in Fig. 2.14(a), and the results are shown in Fig. 2.14(b). The total length l_p of the PEs is maintained at 26 mm in this investigation. The results demonstrate that when the PEs are bent, the resonant frequency remains unchanged. In addition, the mutual coupling level remains at 2.0 GHz for less than −10 dB. Therefore, the two targets mentioned in this section are still achieved.

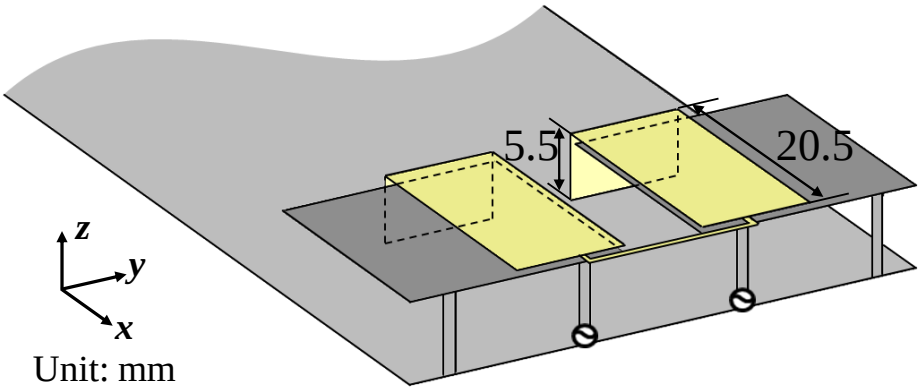

(a) Structure of two PIFAs with bent PEs

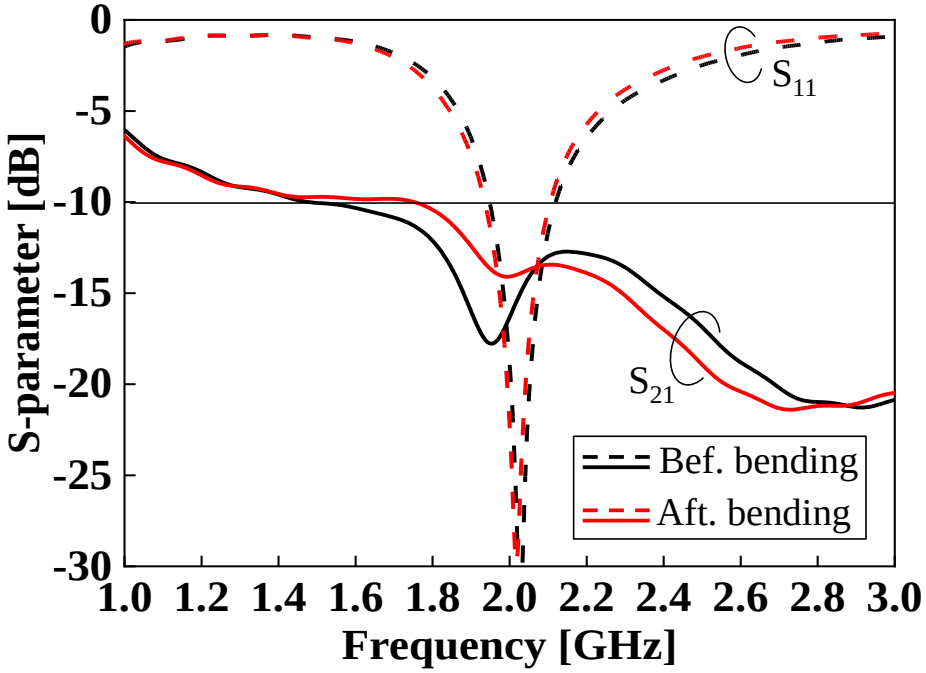

(b) S-parameters of two PIFAs before and after bending PEs

Figure 2.14: Space-saving of PEs

2.4.3 Comparison of Characteristics

The effectiveness of the proposed decoupling method is studied by comparing several important characteristics such as the S-parameters, total antenna efficiency and envelope correlation coefficient (ECC) between the two PIFAs with and without PEs and BL. Subsequently, the decoupling principle of the proposed decoupling method will be discussed by comparing the current distributions.

Figure 2.15 shows the S-parameters of the PIFAs with and without PEs and BL. As shown, by loading the PEs and BL onto the PIFAs, the mutual coupling reduces appreciably from –6.6 to –14.1 dB at 2.0 GHz. Furthermore, although the bandwidth is slightly narrower, the resonant frequency at 2.0 GHz with good impedance matching is maintained. Figure 2.16 shows the total antenna efficiency of the PIFAs with and without PEs and BL. As shown, the use of PEs and BL can significantly improve the total antenna efficiency from 77.4% to 94.6% at the desired frequency of 2.0 GHz. The ECC of the PIFAs with and without PEs and BL is shown in Fig. 2.17. In the case of PIFAs without PEs and BL, the ECC is initially low at 2.0 GHz. Meanwhile, using the PEs and BL increases the ECC in the low-frequency band, but a low ECC is still maintained at the desired frequency.

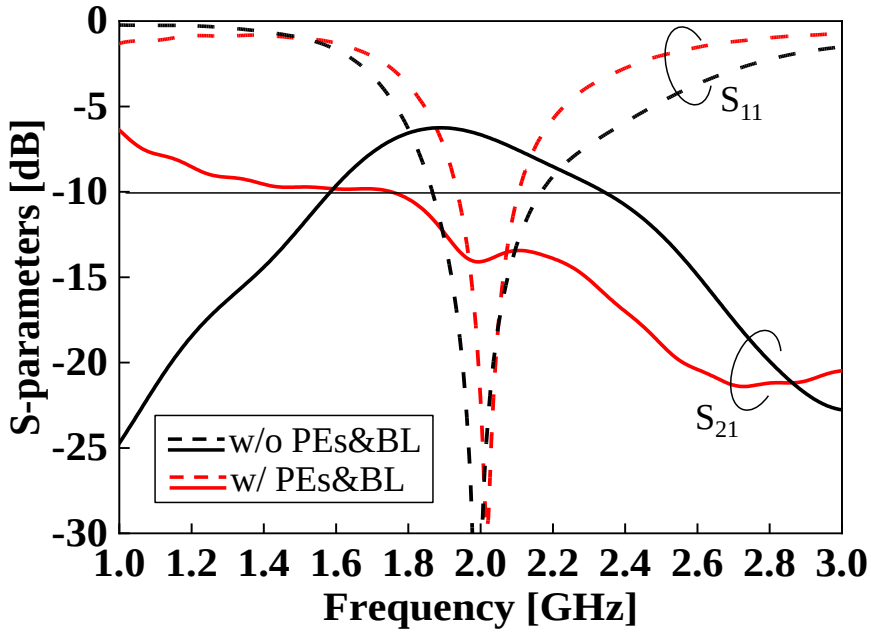

Figure 2.15: S-parameters of two PIFAs with and without PEs and BL

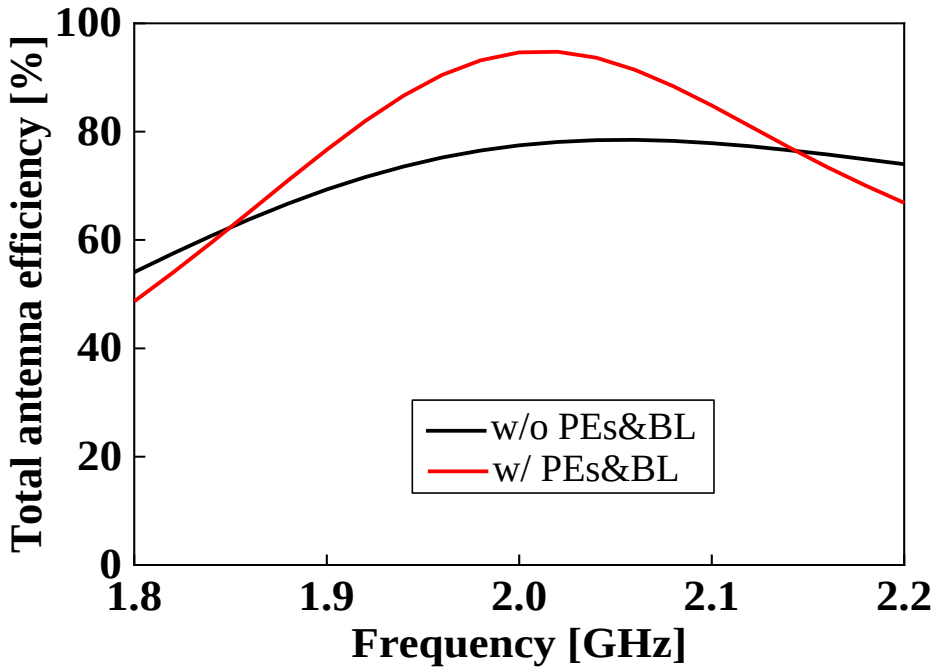

Figure 2.16: Total antenna efficiency of two PIFAs with and without PEs and BL

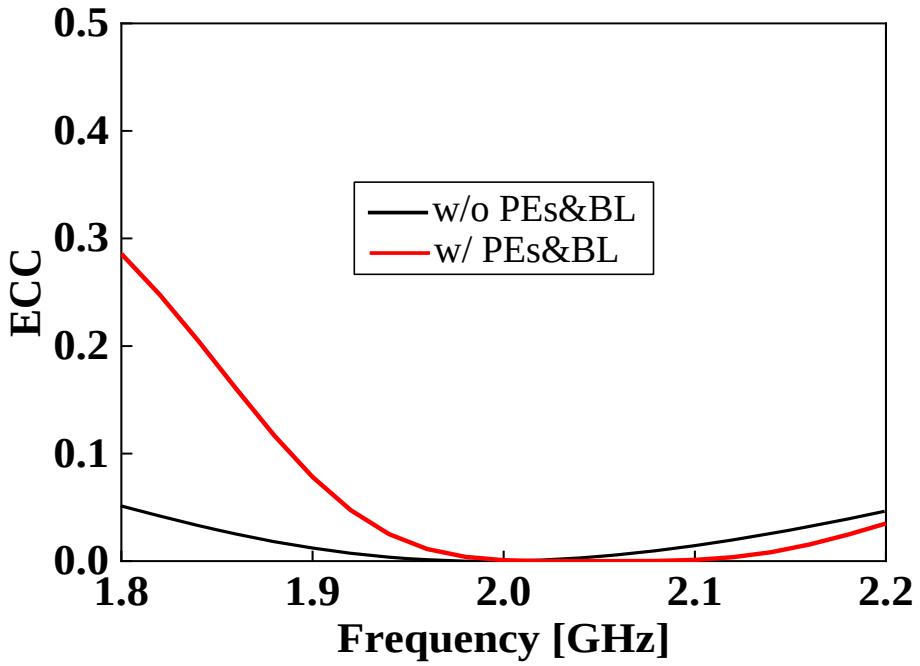

Figure 2.17: ECC of two PIFAs with and without PEs and BL

To understand why the resonant frequency shifts to a different frequency of higher band when the antennas are directly connected by the BL (see Fig. 2.8) and why using PEs connected by the BL can reduce the mutual coupling, the current distributions at the corresponding resonant frequency of each model are compared. Figures 2.18(a) and (b) show the current distributions of the original two PIFAs (2.0 GHz), and original two PIFAs connected directly by the BL (2.3 GHz), respectively. The current distribution of two PIFAs connected directly by the BL with patch lengths l_f = 24 mm (2.0 GHz), and original two PIFAs with PEs and BL (2.0 GHz) are shown in Figs. 2.19(a) and (b), respectively. In all cases, Port1 is excited and Port2 is terminated by a 50-Ω load.

First, in the original two PIFAs, when PIFA1 is excited, strong currents flow primarily on the side where PIFA1 is located; however, a portion of those currents flows through the ground plane and then flows strongly into PIFA2 as shown in Fig. 2.18 (a). This current is considered to be the main contributor to the strong mutual coupling and referred to as the coupling current. The coupling current adversely affects the antenna efficiency; however, it made part of PIFA2 served as an additional radiating element when PIFA1 is excited. In other words, when one PIFA element is excited, the currents on the ground plane and both PIFA elements enable an operation at a resonant frequency of 2.0 GHz. However, the coupling current is canceled when the two PIFAs are connected directly by the BL, as shown in Fig. 2.18 (b). Therefore, when PIFA1 is excited, the current flowing on PIFA2 and the ground plane weakened, causing the overall operating current to be reduced compared with the original two PIFAs. This is considered to be the main contributor to the increase in the resonant frequency from 2.0 to 2.3 GHz.

To determine how the coupling current might be canceled, the flow direction of the currents between Port1 and Port2 as shown in Fig. 2.18 (b) should be focused. It is clear that when the BL is used to directly connect the PIFAs, in addition to the current through the ground plane, other current newly appears on the BL. The two currents cancel each other at the feeding pin of PIFA2 because of the opposite phase. Hence, the mutual coupling between the two PIFAs reduces significantly. Furthermore, the canceled current is compensated for when the PIFA patch length l_f is increased to 24 mm, as shown in Fig. 2.19 (a). Consequently, the resonant frequency shifts back from 2.3 to 2.0 GHz.

In the case of the original two PIFAs with PEs and BL, as shown in Fig. 2.19 (b), a similar current distribution as that shown in Fig. 2.19 (a) is observed. It can be assumed

that owing to the proximity between the PEs and PIFAs, the PEs electromagnetically couple to the PIFAs and hence behaved like radiating elements. Therefore, the role of the PEs is similar to that of the PIFAs patches. This implies that even if the PEs are connected by a BL, mutual coupling between elements can be reduced based on the principle shown in Fig. 2.19 (a).

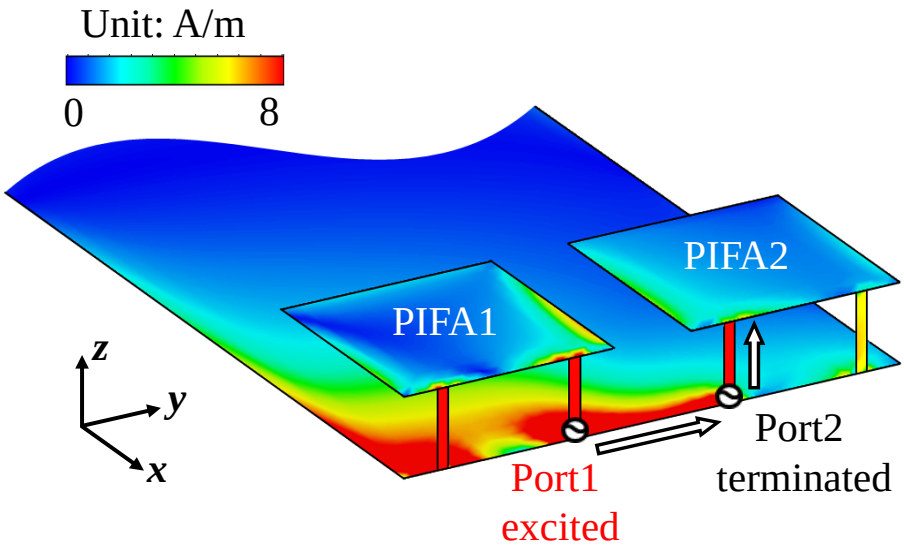

(a) Original two PIFAs (2.0 GHz)

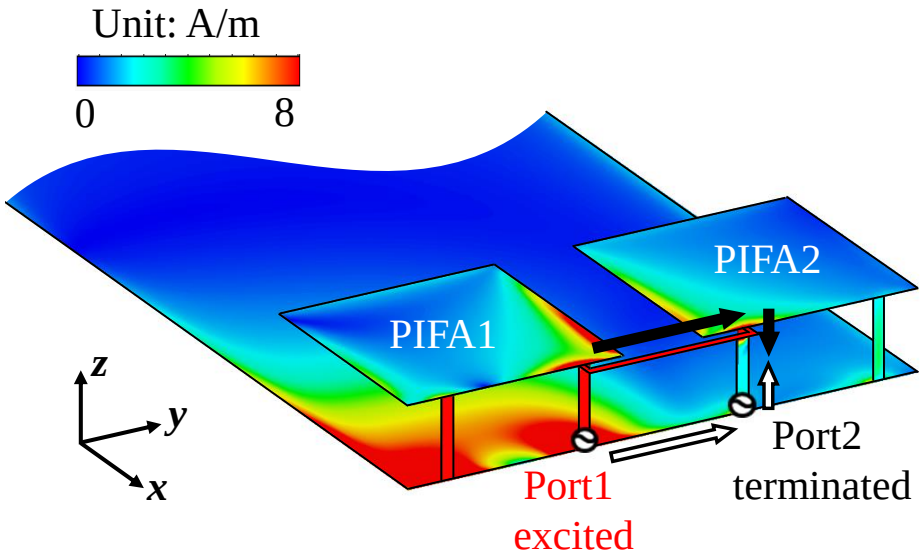

(b) Original two PIFAs directly connected by BL (2.3 GHz)

Figure 2.18: Current distribution of original two PIFAs and original two PIFAs directly connected by BL

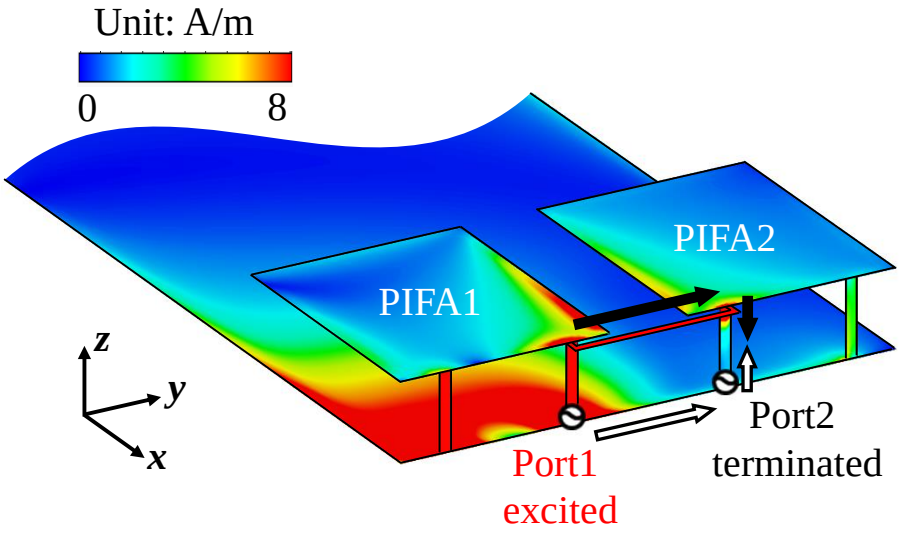

(a) Two PIFAs directly connected by BL with patches length l_f = 24 mm (2.0 GHz)

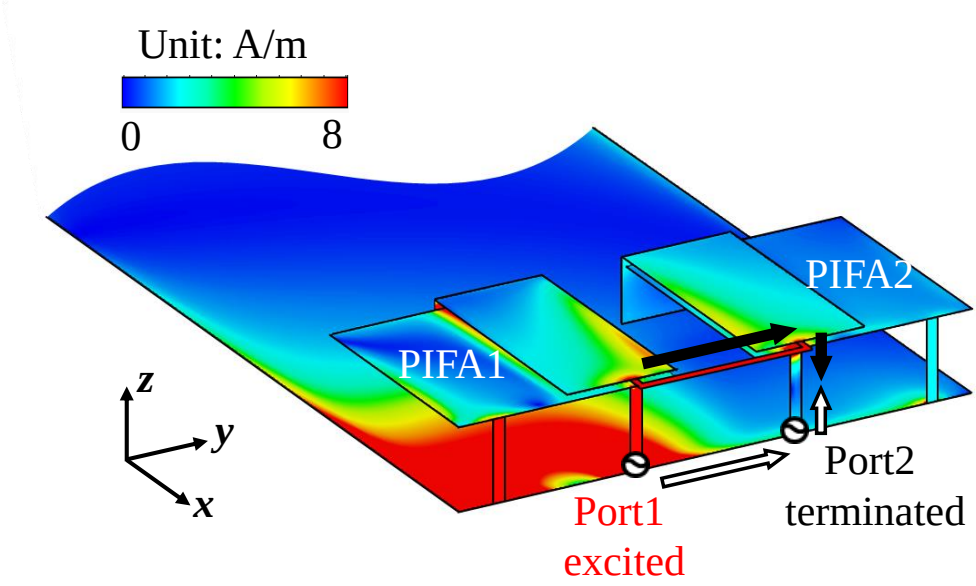

(b) Original two PIFAs with PEs and BL (2.0 GHz)

Figure 2.19: Current distribution of two PIFAs directly connected by BL with patches length l_f = 24 mm, and original two PIFAs with PEs and BL

2.5 Discussion on Decoupling Principle using Characteristic Mode Analysis

In previous section, a decoupling method using PEs and BL was proposed without having to redesign the original sizes and structure of the two PIFAs. The decoupling principle of the proposed method was discussed by comparing the changes in the current distribution of PIFAs with and without PEs and BL; but this was not quantitatively discussed. In [28], decoupling principle was quantitatively discussed by considering the current path length between the two ports through the BL, and the arguments in [28] can also be applied to explain the decoupling principle of the proposed decoupling method. However, in this study, another method called characteristic mode analysis (CMA) is used to do that because it is considered an extremely effective method and has received a lot of attention in recent years.

2.5.1 Overview of Characteristic Mode Analysis

The theory of characteristic modes was first introduced by Garbacz and Turpin in 1968 and then refined by Harrington and Mautz in 1971 [29,30]. The theory is effective for characterizing an arbitrarily shaped perfectly conducting body by providing a set of characteristic current modes that can be obtained from the following weighted eigenvalue equation:

$$\mathrm{X}(J_n) = \lambda_n \mathrm{R}(J_n) \tag{2.2}$$

where X and R are the imaginary and real parts of the impedance operator Z = R + *j*X, and J_n and λ_n denote the eigencurrents and eigenvalues of the n^{th} mode on the surface of the structure, respectively. The magnitude of the eigenvalue λ_n provides information on the property of the mode, and a mode can be considered as a resonance if its eigenvalue λ_n equals zero. In practice, however, another representation of the eigenvalues, called modal significance (MS), is preferred in the examination of the properties of modes, and it is given by the equation below:

$$\mathrm{MS}_n = \frac{1}{1 + j\lambda_n} \tag{2.3}$$

The MS represents the normalized amplitude of the current mode and depends on the magnitude of the eigenvalue λ_n. Therefore, when the eigenvalue λ_n is zero, MS_n reaches a maximum value of 1. A mode with MS = 1 at the resonant frequency can be considered as the dominant mode.

Unlike other methods for electromagnetic field analysis, by using CMA, a designer can express the unknown total current on the surface of the structure as a weighted sum of the characteristic current mode. The total current was obtained using the following equation:

$$J = \sum_{n=1}^{N} \alpha_n J_n \tag{2.4}$$

Where α_n is the modal weighting coefficient (MWC) of the n^{th} mode and becomes an important parameter, as it represents the contribution of each corresponding mode to the total current. Because of this advantage, CMA is a useful method for antenna design and for clarifying the operating principle of antennas.

2.5.2 Discussion on Decoupling Principle

In 2.4.3, the results showed that mutual coupling (S_{21}) decreased from −6.6 to −14.1 dB, and a good impedance matching was maintained simultaneously at the desired resonant frequency of 2.0 GHz after loading PEs and the BL onto PIFAs. In the following, the decoupling principle is discussed in detail by comparing several parameters obtained from the CMA between the two PIFAs with and without PEs and BL. The structure and size of two PIFAs with and without PEs and BL is the same as shown in the previous section. In the simulation performed with CMA, the materials of all structures are assumed to be perfect electric conductors (PECs).

Figures 2.20(a) and (b) show the MS characterisitc of the two PIFAs with and without PEs and BL, respectively. In the case of two PIFAs without PEs and BL, the first six modes with MS = 1 can be observed within the frequency range. The MS of Modes 1 and 2 are approximately equal to 1 at the resonant frequency of 2.0 GHz. Therefore, the two modes are considered the dominant modes of the two PIFAs. In other words, the characteristics of the two PIFAs mainly depends on these two modes. In the case of two PIFAs with PEs and BL, MS characteristic do not change significantly compared to the

case without PEs and BL, and the dominant modes in this case are still Modes 1 and 2. Therefore, it is clear that PEs and BL have almost no effect on the MS characteristic of the two PIFAs.

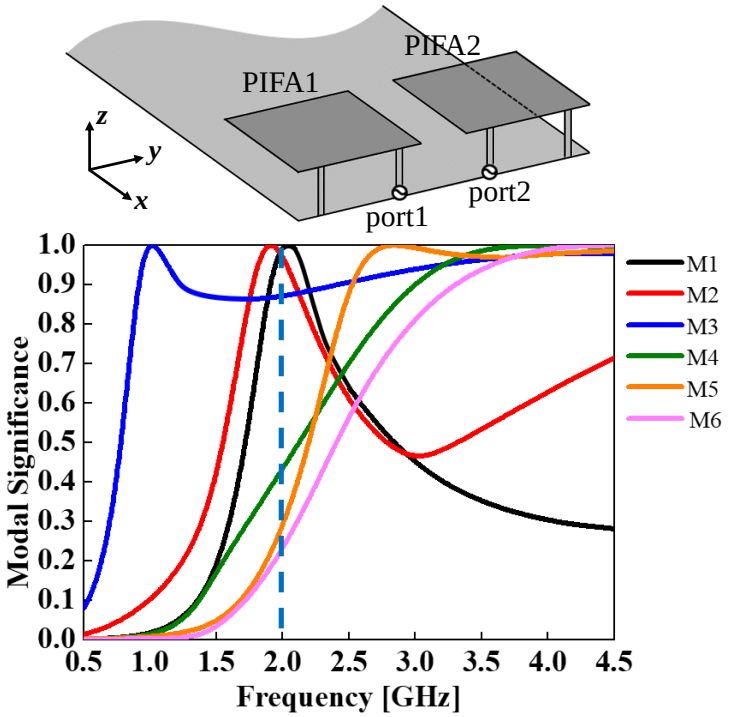

(a) without PEs and BL

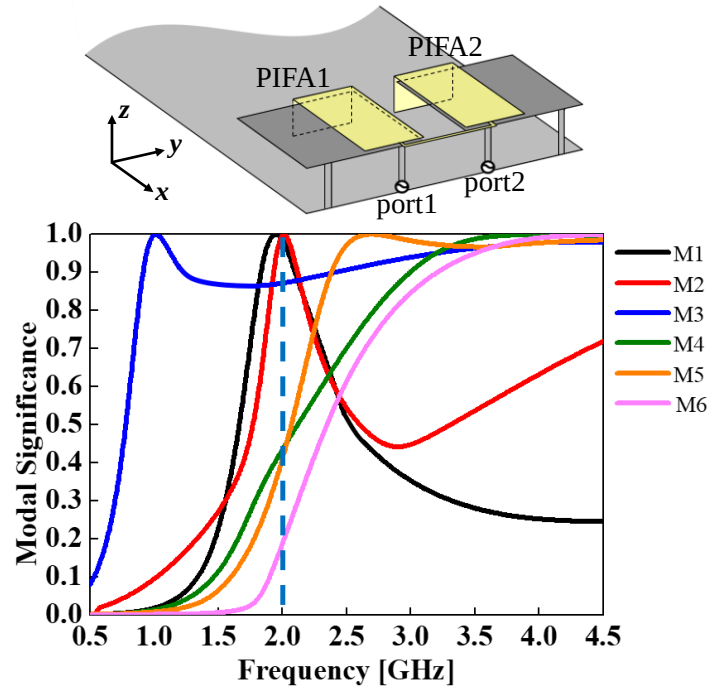

(b) with PEs and BL

Figure 2.20: Modal Significance of two PIFAs

The characteristic of two PIFAs with and without PEs and BL is discussed in more detail by comparing the current distributions in Modes 1 and 2, which are the dominant modes of the two PIFAs.

Figure 2.21 shows the changes of current distribution in Mode 1 (2.0 GHz). By observing the current distribution on the ground plane in the case without PEs and BL, it can be seen that no current flows through the ground plane between the two feeding ports. Therefore, it is obvious that in Mode 1, the two PIFA elements operate independently of each other. In addition, in the case with PEs and BL, the current flowing on the PIFA elements and ground plane is almost the same compared to the case without PEs and BL. This is because in Mode 1, the current flowing through the PEs and BL is extremely weak, so their effect on the two PIFAs is small.

Figure 2.22 shows the changes of current distribution in Mode 2 (2.0 GHz). Unlike the case of Mode 1 without PEs and BL, in the case of Mode 2 without PEs and BL, a strong current can be observed on the ground plane between two feeding ports. For this reason, Mode 2 is considered to be the mode that contributes to mutual coupling between the two PIFAs. On the other hand, in the case with PEs and BL, a decrease in current between the two feeding ports is observed compared to the case without PEs and BL. This is similar to the current distribution comparison results mentioned in the previous section; therefore, the validity of these results can be confirmed. Furthermore, the current flowing through PEs and BL in Mode 2 is extremely strong. This indicates that PEs and BL are effective in reducing the coupling current. However, this is only a qualitative discussion, so a quantitative discussion on decoupling principle is also required.

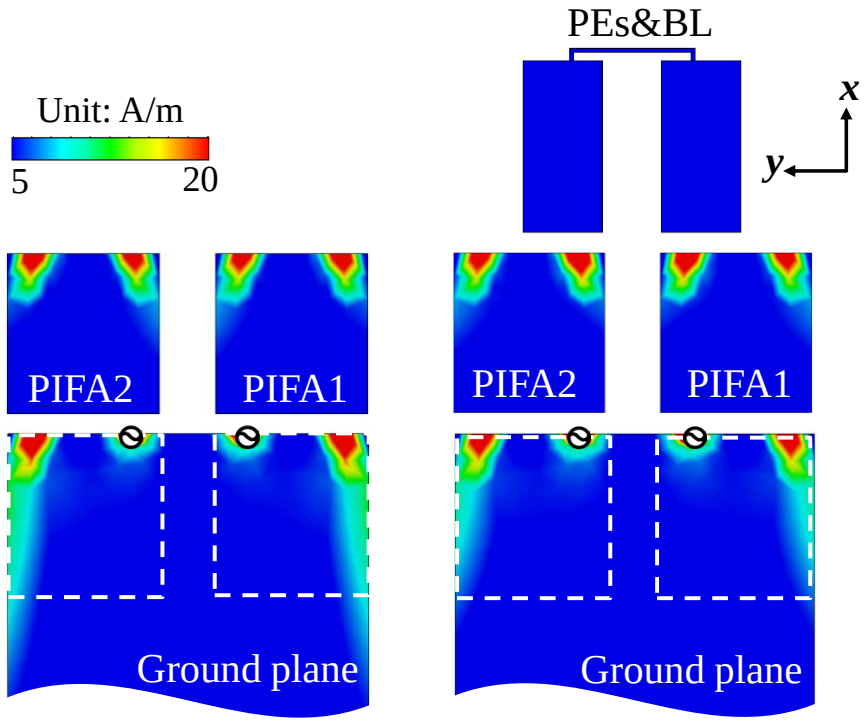

(a) without PEs and BL (b) with PEs and BL

Figure 2.21: Current distribution in Mode 1 (2.0 GHz)

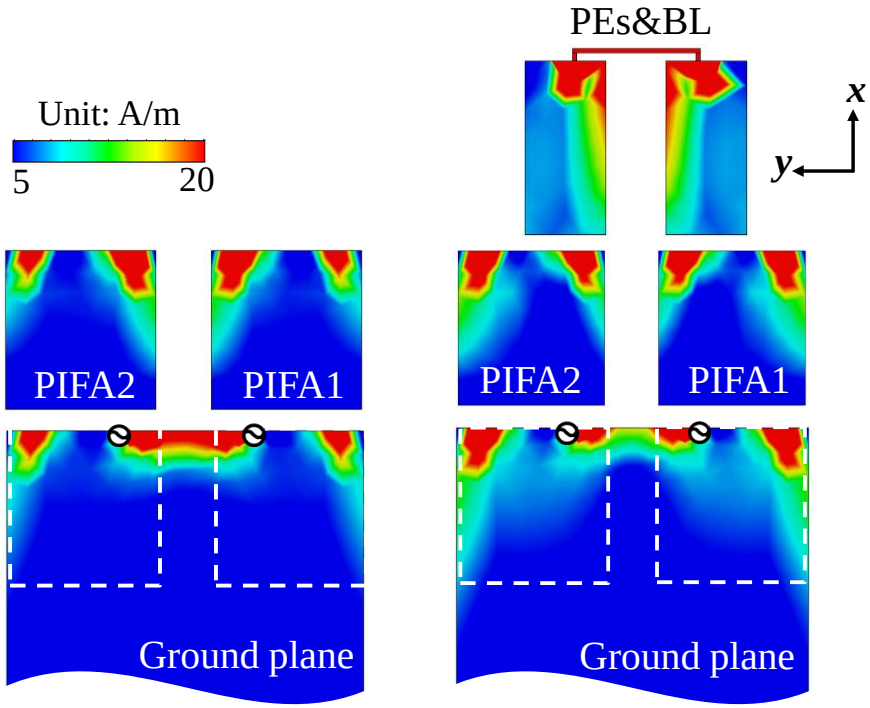

(a) without PEs and BL (b) with PEs and BL

Figure 2.22: Current distribution in Mode 2 (2.0 GHz)

The decoupling principle of the proposed method is quantitatively discussed by considering the MWC of each mode in cases with and without PEs and BL. For a two-element antenna, if the total currents excited from feeding Ports1 and 2 are J_{p1} and J_{p2}, they can be expressed by the following equations (2.5) and (2.6) as follows [31]:

$$J_{\mathrm{p1}} = \sum_{n=1}^{N} \alpha_{n\_\mathrm{p1}} J_n = \alpha_{1\_\mathrm{p1}} J_1 + \alpha_{2\_\mathrm{p1}} J_2 + \alpha_{3\_\mathrm{p1}} J_3 + \ldots + \alpha_{N\_\mathrm{p1}} J_N \tag{2.5}$$

$$J_{\mathrm{p2}} = \sum_{n=1}^{N} \alpha_{n\_\mathrm{p2}} J_n = \alpha_{1\_\mathrm{p2}} J_1 + \alpha_{2\_\mathrm{p2}} J_2 + \alpha_{3\_\mathrm{p2}} J_3 + \ldots + \alpha_{N\_\mathrm{p2}} J_N \tag{2.6}$$

The orthogonality of J_{p1} and J_{p2} can be determined using the total inner product value. The total inner product of these can be calculated from the MWC in each mode as follows:

$$J_{\mathrm{p1}}(J_{\mathrm{p2}})^* = \alpha_{1\_\mathrm{p1}}(\alpha_{1\_\mathrm{p2}})^* + \alpha_{2\_\mathrm{p1}}(\alpha_{2\_\mathrm{p2}})^* + \alpha_{3\_\mathrm{p1}}(\alpha_{3\_\mathrm{p2}})^* + \ldots + \alpha_{N\_\mathrm{p1}}(\alpha_{N\_\mathrm{p2}})^* \tag{2.7}$$

Tables 2.1 and 2.2 show the MWC of each mode current excited from feeding Port1 and Port2 in the case of the two PIFAs with and without PEs and BL, respectively. As shown, due to the symmetric structure of PIFA1 and PIFA2, the amplitude of MWC in the same mode excited by Port1 and Port2 has the same value. However, the phase difference of the MWC in the same mode is 0° (Modes 1, 3, 5) and 180° (Modes 2, 4, 6). A mode with a phase difference of 0° is called an in-phase mode, and a mode with a phase difference of 180° is called an anti-phase mode. As can be seen, the inner product of the in-phase mode has a positive value, while that of the anti-phase mode has a negative value. The total inner product value is the sum of the inner products corresponding to each mode. In case of PIFAs without PEs and BL, the total inner product value is −0.43, while it is −0.11 in case of PIFAs with PEs and BL. The correlation coefficient of the currents excited from feeding Port1 and Port2 can be calculated by dividing the total inner product value by the absolute value of all modes. As the result, the correlation coefficient is −0.41

in case of two PIFAs without PEs and BL, while it is −0.1 in case of two PIFAs with PEs and BL. This shows that the total inner product value and the correlation coefficient value change close to zero after loading PEs and BL onto the two PIFAs, indicating that J_{p1} and J_{p2} are orthogonal to each other. For this reason, the interplay between them becomes weaker, and thus, mutual coupling is reduced.

Table 2.1: MWC in each mode and total inner product value (without PEs and BL)

Mode	MWC (port1)		MWC (port2)		Phase difference (deg.)	Inner product of each mode	Total inner product
	Amplitude	Phase (deg.)	Amplitude	Phase (deg.)			
1	0.47	9.2	0.47	9.2	0	0.22	**-0.43**
2	0.85	-11.1	0.85	168.9	180	-0.72	
3	0.25	-35.2	0.25	-35.2	0	0.06	
4	0.05	64.2	0.05	-115.8	180	0	
5	0.16	73.9	0.16	73.9	0	0.03	
6	0.1	-103.2	0.1	76.8	180	-0.01	

Table 2.2: MWC in each mode and total inner product value (with PEs and BL)

Mode	MWC (port1)		MWC (port2)		Phase difference (deg.)	Inner product of each mode	Total inner product
	Amplitude	Phase (deg.)	Amplitude	Phase (deg.)			
1	0.54	173	0.54	173	0	0.29	**-0.11**
2	0.76	6.9	0.76	-173.1	180	-0.58	
3	0.38	141.2	0.38	141.2	0	0.14	
4	0.05	64.1	0.05	-115.9	180	0	
5	0.2	66.3	0.2	66.3	0	0.04	
6	0.06	103.4	0.06	-76.6	180	0	

2.6 Fabrication and Measurement

In order to validate the simulation results, the two PIFAs with and without PEs and BL are fabricated and measured. Figure 2.23(a) and (b) show photograph of the fabricated two PIFAs without and with PEs and BL, respectively. In the prototype of the two PIFAs with PEs and BL, two pieces of Styrofoam with a thickness of 0.5 mm are inserted between the PIFAs and PEs to maintain an air gap between them.

Figure 2.24 shows the simulation and measurement S-parameters results of the PIFAs with and without PEs and BL. A good agreement is observed between the simulation and measurement results; hence, the proposed decoupling method is validated.

The simulation and measurement radiation patterns at 2.0 GHz of the PIFAs without and with PEs are shown in Figs. 2.25(a) and (b), respectively. Owing to the symmetrical structure of the PIFAs, only the radiation patterns of PIFA1 are shown. By comparing the simulation results shown in Figs. 2.25(a) and (b), it is clear that the radiation pattern changes at some positions, although insignificantly. In addition, the gains are still maintained in all planes when the PEs and BL are loaded onto the two PIFAs. Therefore, it can be concluded that the PEs and BL do not significantly affect the radiation pattern of the two PIFAs. Moreover, the simulation results are validated by their consistency with the measurement results.

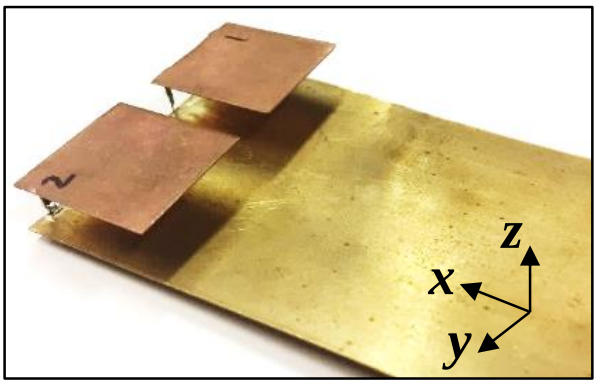

(a) without PEs and BL

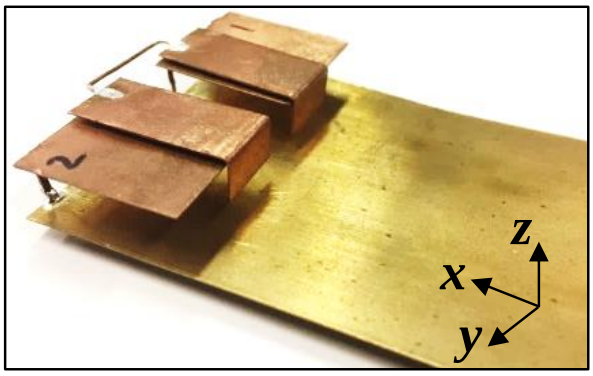

(b) with PEs and BL

Figure 2.23: Fabricated prototype of two PIFAs

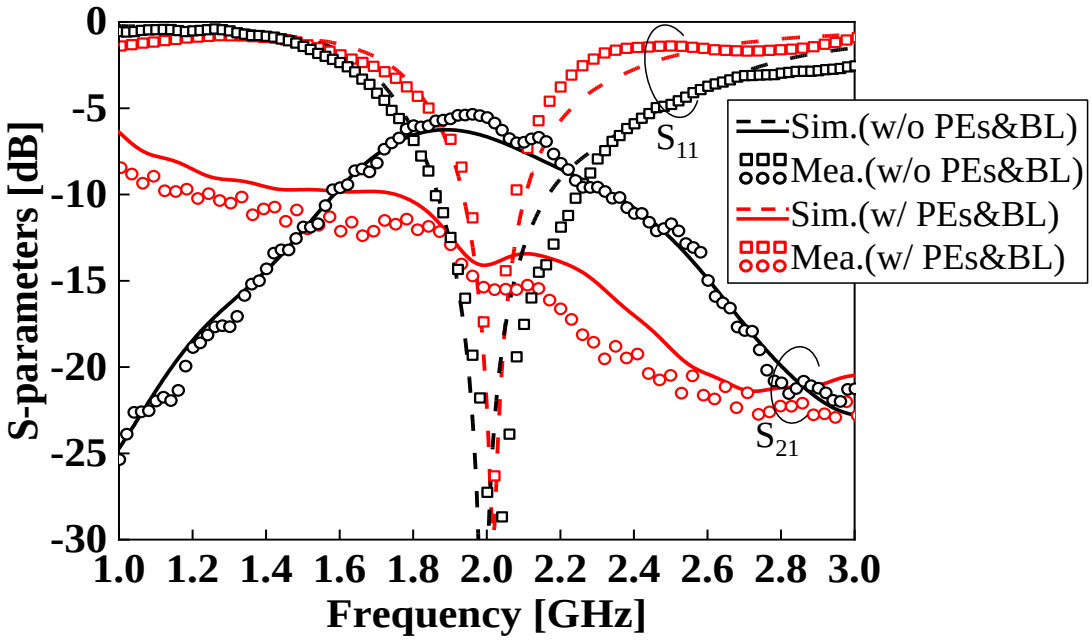

Figure 2.24: Simulation and measurement S-parameters results of two PIFAs with and without PEs and BL

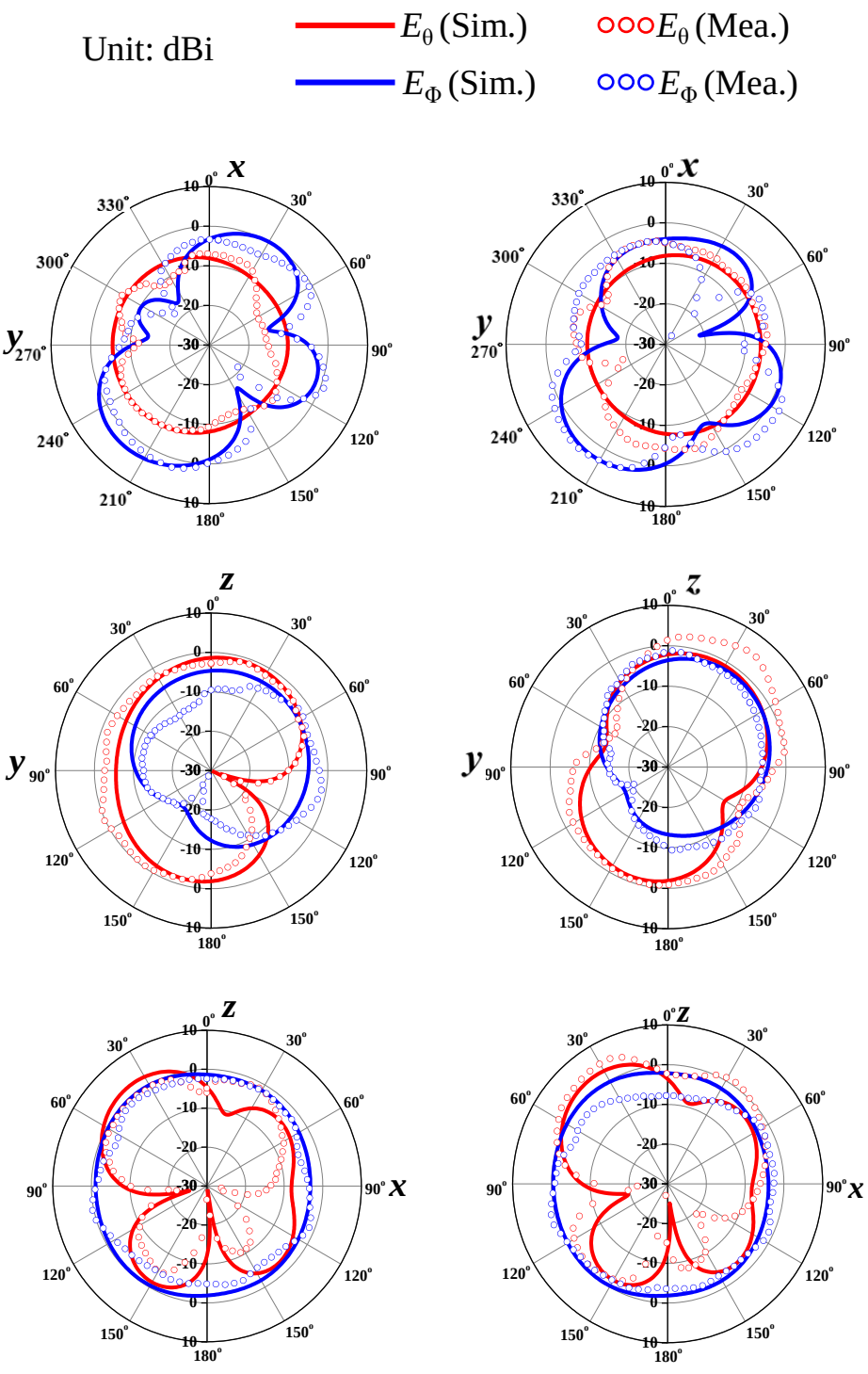

(a) without PEs and BL (b) with PEs and BL

Figure 2.25: Simulation and measurement radiation pattern results of PIFA1

2.7 Comparison with Other Previous Studies

This section compares the proposed method in this chapter with some other previous studies in term of the port-to-port distance, operating bandwidth, isolation, total antenna efficiency and ECC as shown in Table 2.3.

The proposed method and other previous methods can be compared as follows: 1) The proposed method is effective even when the port-to-port distance between two PIFAs is only 0.087λ, which is smaller than [4-8, 11, 13] and slightly larger than [15]; 2) The operating bandwidth of the two PIFAs proposed in this study is approximately equal to or wider than most other previous studies, except for [4]; 3) The isolation achieved in this study is only −14.1 dB, but the total antenna efficiency is better than [4-6, 13] and slightly lower than [15]. However, the proposed method does not require redesign or direct physical impact on the original antennas like the methods using neutralization line in [15]; 4) Like other methods, the ECC value obtained using the proposed method is extremely small and less than 0.05.

Table 2.3: Comparison with previous studies

Ref.	Decoupling method	Port-to-Port distance	Operating bandwidth [GHz] (S_{11}≤−10 dB)	Isolation [dB]	Total antenna efficiency [%]	ECC
[4]	Slot	0.28λ	1.7~2.7 (45.4%)	−10	87	-
[5]	Slot	0. 24λ	3.39~3.67 (7.93%)	−10	80	<0.05
[6]	Slot	0.15λ	2.4~2.5 (4.1%)	−35	70	-
[7]	EBG	0.37λ	2.3~2.61 (2.5%)	−30	-	-
[8]	EBG	0.5λ	8.2~9.1 (10.4%)	−35	-	-
[11]	Circuit	0.12λ	0.71~0.72 (1.4%)	−25	-	<0.05
[13]	Neutralization line	0.11λ	2.37~2.49 (5%)	−14.6	76	<0.05
[15]	Neutralization line	0.063λ	1.98~2.2 (10%)	−20.4	97	-
This study	**PEs&BL**	**0.087λ**	**1.9~2.1 (10%)**	**−14.1**	**94.6**	**<0.05**

λ: wavelength at the lowest resonant frequency; - : cannot found in source

2.8 Summary

In this chapter, the structure of the PIFA element and the ground plane were presented, and the characteristics of two PIFA elements were investigated when they are mounted on the ground plane with different arrangement and different positions of feeding pin. The structure of Model A was considered as the original model of two PIFAs, and decoupling methods to reduce mutual coupling between them was investigated.

The original two PIFAs were directly connected by a BL to confirm the effect of BL to their resonant frequency. It was confirmed that, when the two PIFAs were directly connected by the BL, the mutual coupling between them could be reduced but the resonance shifted to other frequencies. Therefore, the antenna size must be adjusted to shift the resonant frequency toward the desired frequency.

A decoupling method using PEs and BL was proposed for two PIFAs without having to redesign the original antenna sizes and structure. Instead of directly connecting the antennas, the BL was used to connect the PEs, which were then loaded onto the PIFAs. By using the proposed decoupling method, the mutual coupling decreased from −6.6 to −14.1 dB, and good impedance matching was maintained simultaneously at the desired resonant frequency of 2.0 GHz. Therefore, the total antenna efficiency improved from 77.4% to 94.6%. Moreover, the decoupling principle of the PEs and BL was quantitatively discussed using CMA. As a result, by loading the PEs and a BL onto the two PIFAs, the total inner product value changed from −0.43 to −0.11. This shows that the total inner product value changes close to zero after loading PEs and a BL onto the PIFAs, indicating that the currents excited by Port1 and Port2 are orthogonal to each other. For this reason, the interplay between them becomes weaker, and thus, mutual coupling is reduced.

A good agreement is observed between the simulation and measurement results; hence, the proposed decoupling method is validated.

Chapter 3
Dual-band Design and Decoupling Method for Two PIFAs

3.1 Introduction

In Chapter 2, a decoupling method was proposed for the two PIFAs. However, this proposed method was effective at only single band. Because the improvement in transmission efficiency by the MIMO technique also depends on the number of operating bands that can be covered, there are cases wherein antennas are required to have broadband or multi-band characteristics. Therefore, efficient decoupling methods for broadband or multi-band are also required. However, the decoupling for broadband or multi-band antennas has more challenges than single band antennas. This is because in most cases, the coupling mechanism works differently in different frequency bands.

Numerous decoupling methods have been proposed to meet the above requirements. These decoupling methods can be divided into two groups. In the first group, a certain decoupling method is often used for array antennas, which already have broadband or multi-band characteristics [32-42]. In this case, decoupling methods are typically accomplished by placing the antennas orthogonally [32,33], using a grounding branch [34], etching slots on the ground plane [35-38], adding a parasitic element (PE) [39], using a decoupling network [40], using a metasurface [41], or connecting the antennas with a bridge line [42]. In the second group, an array antenna that initially operates at a narrow single band is often selected for performance enhancement by applying the multi-band design method and decoupling method simultaneously as in [11] and [43-46]. The number of reported studies in the second group is significantly lower than that in the first group. For example, the decoupling method using short stub and branch element was reported in [43]; however, it also required the use of many electronic components to form the matching circuit. In [44], a slot was etched on the antenna patch and a PE was included to increase the operating frequency and improve the bandwidth, and then a characteristic mode analysis was conducted to determine the position of the antennas on the ground plane, such that the mutual coupling exhibited a minimum level. However, this required a large distance between the antennas. An L-shaped slot was

etched on an antenna to design a multi-band, while a T-shaped slot was etched on the ground plane as a decoupling solution [45]. In addition, the use of L-shaped stubs connected to the ground plane and the use of a bridge line to connect the stubs has been proposed as an effective method for multi-band design and decoupling, respectively [46]. Another method has been proposed in [47], which required etching a slot into the ground plane and adding several branch elements to the antennas. However, one common aspect of the proposed methods in [43-47] is that it is necessary to redesign the original antenna structure or connect the original antenna directly with additional elements. Therefore, to easily design the multi-band and decoupling under design conditions that hinder the implementation, an approach that does not require the redesign of the original antenna structure or its direct connection with additional elements is required.

In this chapter, the PEs and BL will be developed to allow two PIFAs to expand the operating band from single to dual bands and simultaneously decouple the two PIFAs in dual band. Section 3.2 first describes the structure and characteristic of 1-element PIFA, then shows the dual-band design process for 1-element PIFA. In Section 3.3, a decoupling method for the two PIFAs in dual band will be presented. Section 3.4 shows the fabrication prototypes and examines the agreement between simulation and measurement results to confirm the validity of the proposed decoupling method. Furthermore, in order to verify the versatility, the proposed method is applied to the dual-band design and decoupling at other frequencies as a concrete design example. This design example will be shown in Section 3.5. Section 3.6 compares the proposed method with other methods proposed in previous studies. Finally, Section 3.7 gives a summary of this chapter.

3.2 Dual-band Design for 1-element PIFA

3.2.1 Antenna Structure and Characteristics

Figure 3.1 depicts the structure of the original 1-element PIFA mounted on a ground plane. The structure and size of the PIFA element and ground plane are the same as shown in Fig. 2.1. Figure 3.2 depicts the characteristics of the 1-element PIFA. Figure 3.2(a) shows that the resonant frequency is 2.05 GHz with a good impedance matching. Figures 3.2(b) and (c) illustrate the current and electric field distributions at the resonant frequency, respectively. As shown in Fig. 3.2(b), the current flows strongly on the entire lower surface of the PIFA patch and on the ground plane, which is below the PIFA patch. On the upper surface, the current flows quite strongly only in some locations near the edge of the PIFA patch. In addition, the electric field distribution shows a strong coupling between the ground plane and PIFA patch, particularly near the edges of the PIFA patch.

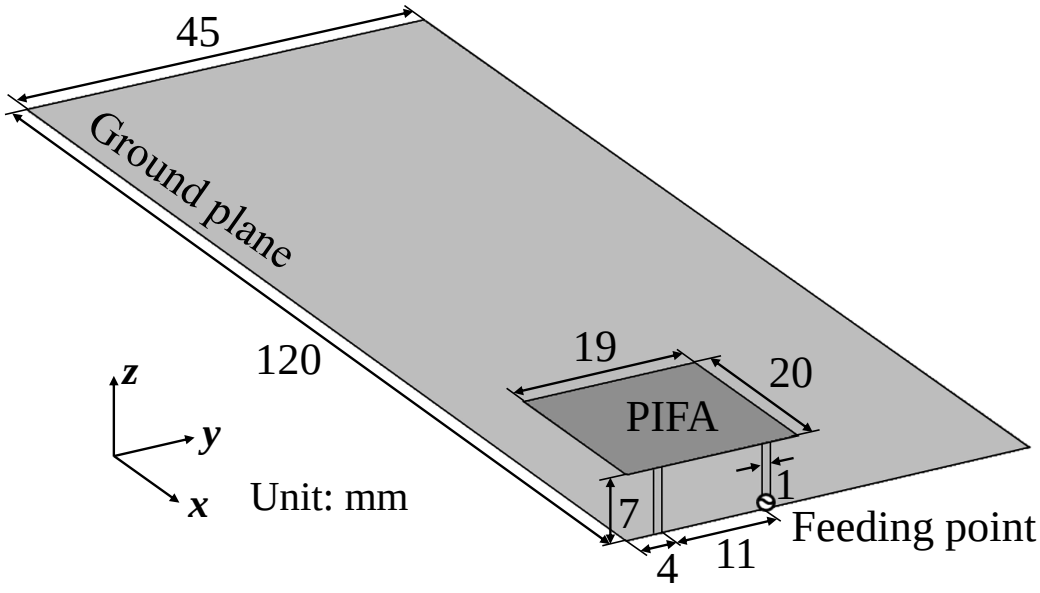

Figure 3.1: Structure of 1-element PIFA

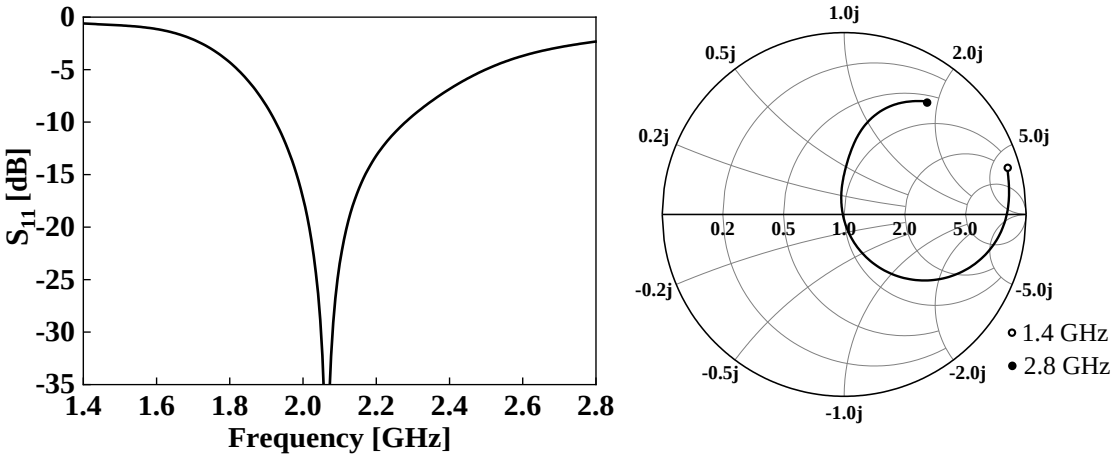

(a) Impedance characteristic

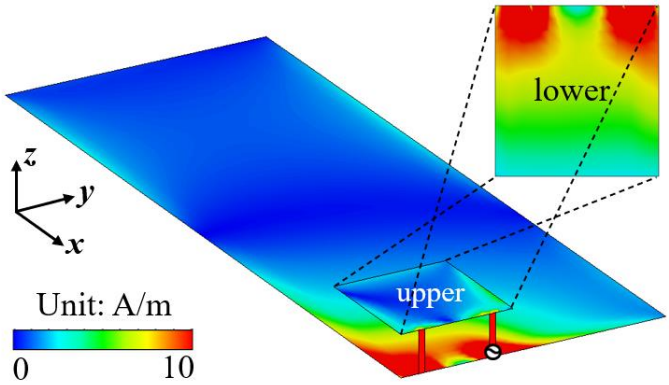

(b) Current distribution (2.05 GHz)

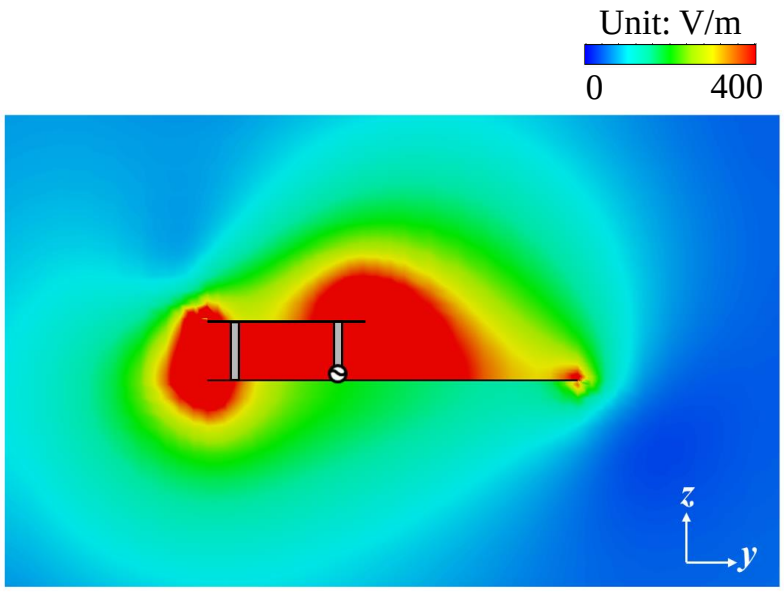

(c) Electric field distribution (2.05 GHz)

Figure 3.2: Characteristics of 1-element PIFA

3.2.2 Dual-band Design

In order to increase the operating frequency band of the PIFA from single band to dual bands without the need to redesign the original PIFA size or structure or directly connect any additional element to the PIFA, using a PE is considered as an effective method. In addition, the PE needs to be closely coupled with the main resonator to create a new resonance. Therefore, the locations near the edges of the PIFA would be most suitable for PE placement.

In Chapter 2, the PEs are placed above the feeding pins where the electric field is strong. However, as shown in Fig. 3.2(c), the electric field is strongly distributed not only on the feeding pin side, but also on the shorting pin side. Therefore, in order to use the PE more effectively, it is considered necessary to load it on the shorting pin side as well. Furthermore, in Chapter 2, it is clear that the length of the PE is the most important parameter for the frequency characteristics of the PIFA. Therefore, if the length of plate-shaped PE shown in Chapter 2 is significantly extended, the PIFA can achieve the multi-band characteristic due to the generation of higher-order modes. However, the volume of the PIFA including the PE will increases remarkably. Therefore, if it is desired to achieve multiband characteristic for PIFA in this way, the use of a linear-shaped PE seem to be more appropriate than a plate-shaped one. Moreover, to keep the volume of the PIFA including the PE as small as possible in the dual-band design, bent linear PE are considered as a suitable structure. In particular, it only needs to be placed close to the PIFA patch without having to connect directly to the PIFA.

In this chapter, 2.0 GHz and 2.4 GHz are chosen as the desired frequencies. Figure 3.3 depicts the dual-band design process using the PE. In STEP 1, a PE is loaded onto the PIFA patch with a small air gap (0.5 mm) and is bent along the three edges of the PIFA patch, where the electric field are strongly distributed. The length of the PE is 69 mm, which is approximately equal to the 2.4-GHz half wavelength, while the width is 1 mm. A part of the PE protrudes from the PIFA patch. Therefore, in STEP 2, the protruded part of the PE is bent orthogonal to the ground plane at a certain position.

Figure 3.4 depicts the impedance characteristics of 1-element PIFA with PE corresponding to the two steps. As shown, in both STEPs 1 and 2, two resonances are observed at approximately 2.0 and 2.4 GHz. Moreover, an antiresonance is also observed at 2.35 GHz. For convenience, these resonances are referred to as the first and second

resonances, respectively. The bending of the protruded part of the PE causes a slight shift in the first resonant frequency, while the second is almost unchanged and the dual-band characteristic is maintained. Notably, it is not necessary to bend the protruded part of the PE (e.g., STEP 2), if practical design conditions do not allow, for example, when there is a certain electric component under the PIFA patch that prevents the bending of the PE.

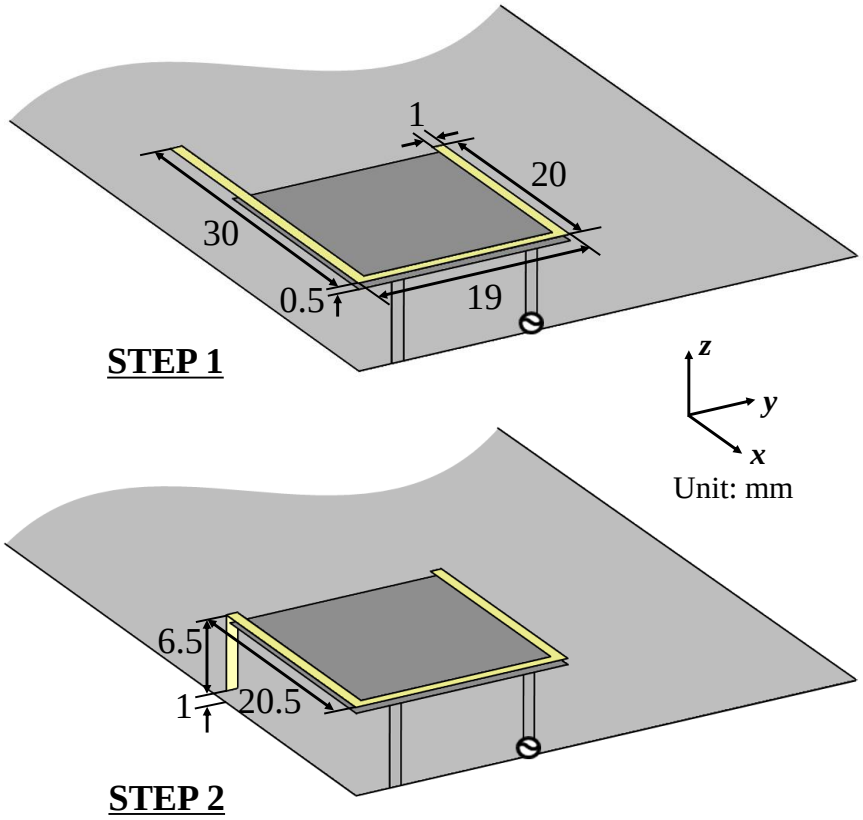

Figure 3.3: Dual-band design process using PE

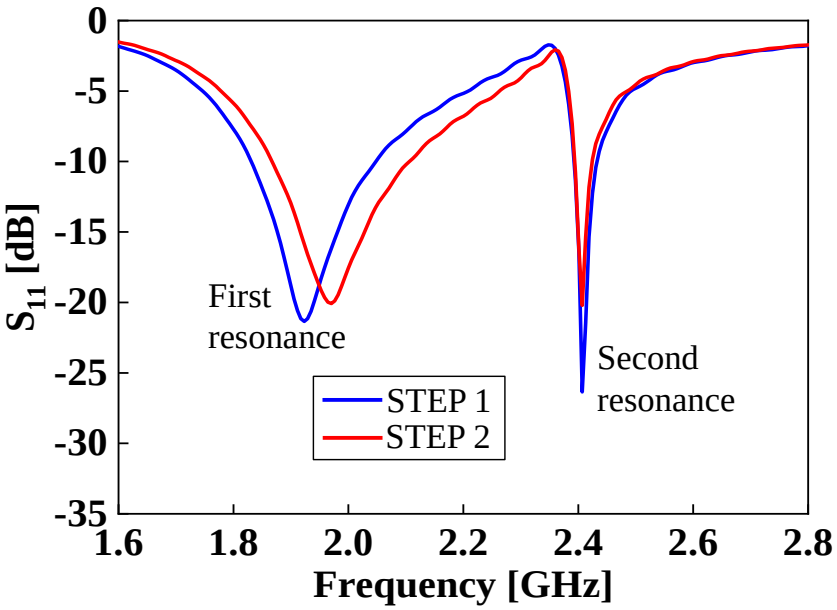

(a) S_{11}

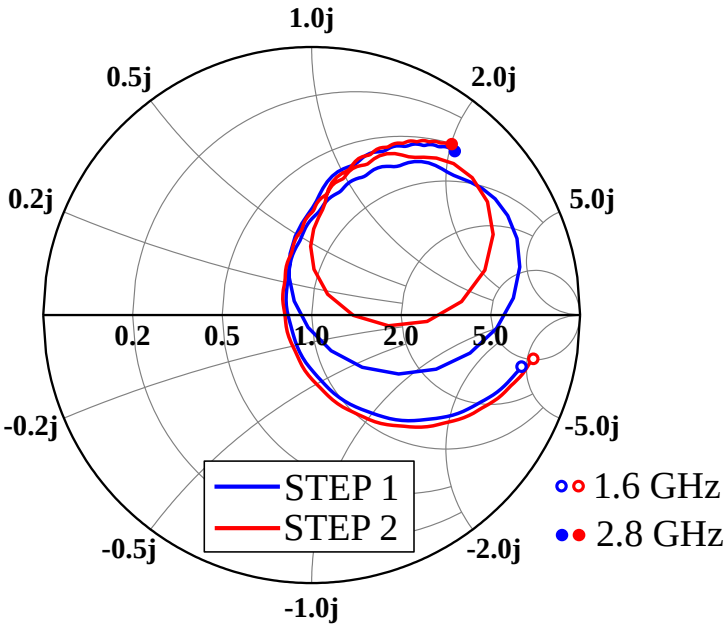

(b) Smith chart

Figure 3.4: Impedance characteristic of 1-element PIFA with PE

To clarify the operating principle of the PE, the current distributions at the two resonant frequencies of the 1-element PIFA loading the PE are compared, as shown in Fig. 3.5. At 2.0 GHz, almost the same current distribution as that of the PIFA without PE (Fig. 3.2(b)) is observed. Moreover, the current flowing on the PE is relatively weak. Therefore, the first resonance depends on the PIFA and is less affected by the PE. The current distribution at 2.4 GHz shows a different operating principle. The current mainly flows on the PE and edges of the PIFA patch where the PE is loaded. In addition, the current flowing on the ground plane is relatively weak compared to that in the 2.0-GHz case. Thus, it can be assumed that the second resonance appears because of the strong coupling between the PE and PIFA patches. In other words, the PE excites a new current mode on the upper surface of the PIFA patches to generate a new resonance at 2.4 GHz. In addition, as depicted in Fig. 3.5, the current on a part of the PE, located above the feeding pin side, is extremely weak in the 2.0-GHz case, while it flows strongly in the 2.4-GHz case. Therefore, it can be assumed that the second resonant frequency can be adjusted independently by varying a certain parameter of this part.

The changes in S_{11} according to the length l and width w of this part are illustrated in Fig. 3.6, respectively. These results indicate that the second resonant frequency can be tuned independently between 2.3 GHz to 2.6 GHz, and the first resonant frequency can be maintained at 2.0 GHz by varying the length l or width w. Therefore, if the desired frequency of the second resonance is set to a certain frequency between 2.3 GHz and 2.6 GHz, the use of PE is still an efficient method.

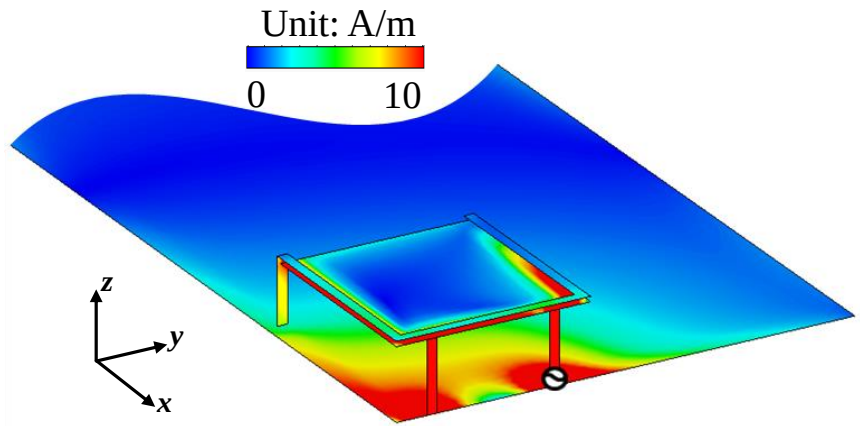

(a) 2.0 GHz

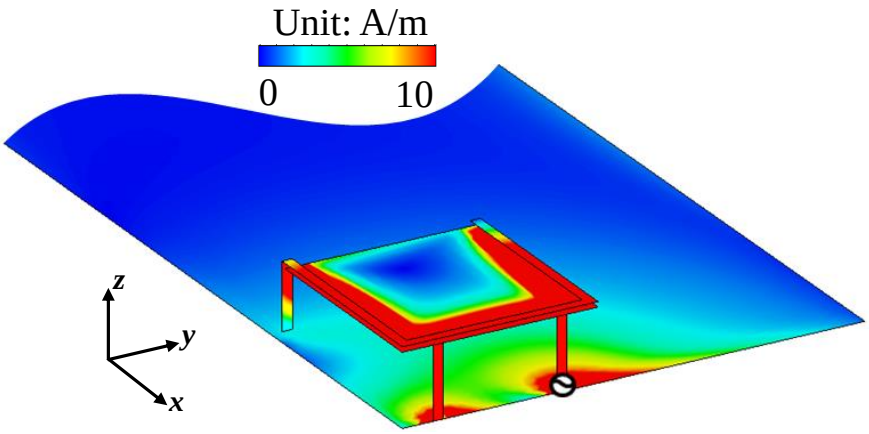

(b) 2.4 GHz

Figure 3.5: Current distribution of 1-element PIFA loading PE

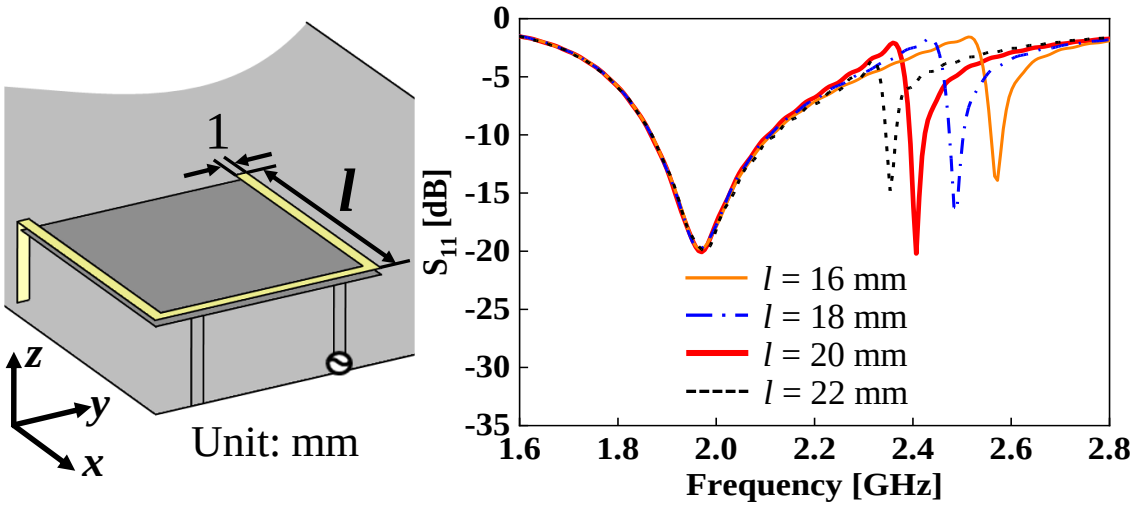

(a) Different length *l*

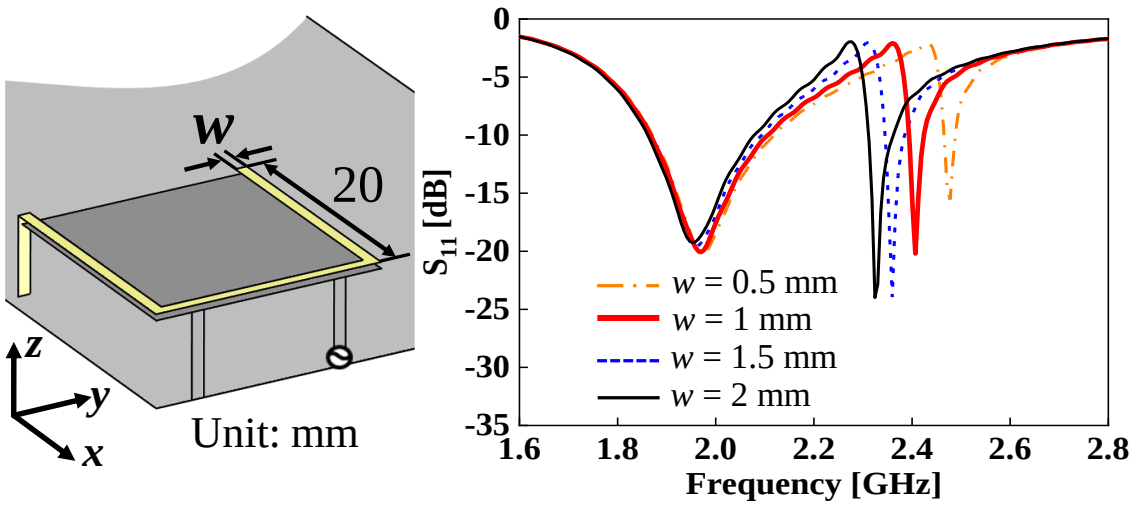

(b) Different width *w*

Figure 3.6: The S_{11} with different length *l* and width *w*

3.3 Decoupling for Two PIFAs in Dual Band

In this section, a simple method to decouple two PIFAs in the dual band without having to redesign the original antenna structure or directly connect it with additional elements is investigated. To this end, a method using a BL is utilized.

3.3.1 Proposed Decoupling Method

Figure 3.7(a), (b) and (c) depict the structure of the two PIFAs with different lengths of the BL. The structure of the two PIFAs is the same as shown in Fig. 2.1. The PEs designed in previous section are loaded onto each PIFA and connected by the BL. The BL is a thin copper wire with a width of 0.5 mm. In order to determine the optimal length of the BL (l_B) that enables decoupling in dual band, l_B is varied as 18 mm, 29 mm, and 41 mm. Figure 3.8 illustrates the change in S-parameters when l_B is varied. As shown in Fig. 3.8(a), when l_B = 18 mm or 41 mm, a good impedance matching is obtained at approximately 2.0 GHz, but there is an impedance mismatch at approximately 2.5 GHz. Furthermore, as shown in Fig. 3.8(b), when l_B = 18 mm or 41 mm, the mutual coupling reduces for less than −10 dB at 2.0 GHz, but significantly increases at 2.5 GHz. The increasing of mutual coupling at 2.5 GHz is considered as one of the causes of the impedance mismatch at this frequency. Meanwhile, when the l_B = 29 mm, two resonances with improved impedance matching can be obtained at 2.0 and 2.5 GHz. Furthermore, the mutual coupling is reduced remarkably at the resonant frequencies compared to the cases when l_B = 18 mm or 41 mm. Thus, the use of PEs and BL with l_B = 29 mm is effective in simultaneously improving the impedance mismatch and reducing the mutual coupling in dual band, even if it is not directly connected to the antenna. However, it also changes the second resonance to a higher frequency of 2.5 GHz. Therefore, it is necessary to shift the second resonance back to the desired frequency of 2.4 GHz without changing the first resonance at 2.0 GHz.

As shown in Fig. 3.6, increasing the length or width of the part of the PEs, located above the feeding pins side can widen the current path on the PE, causing the second resonance to shift to lower frequencies. Meanwhile, the first resonant frequency can be maintained at 2.0 GHz because the current on this part is extremely weak. Therefore, in order to shift the second resonance from 2.5 GHz to 2.4 GHz and maintain the first resonance at 2.0 GHz, the size of this part should be increased.

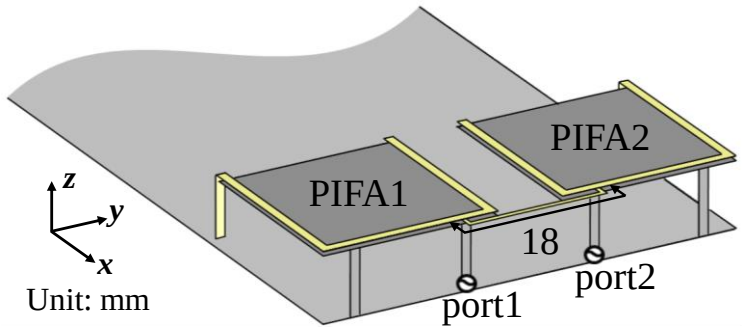

(a) l_B = 18 mm

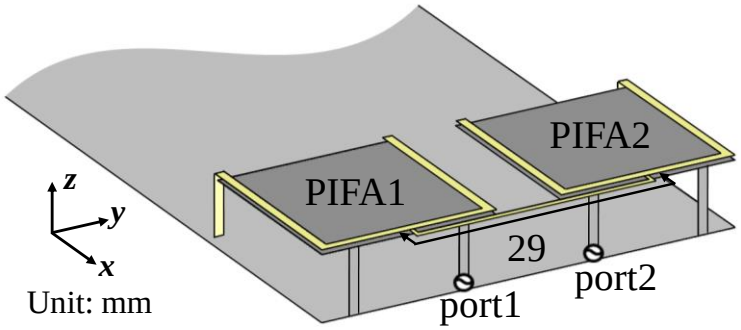

(b) l_B = 29 mm

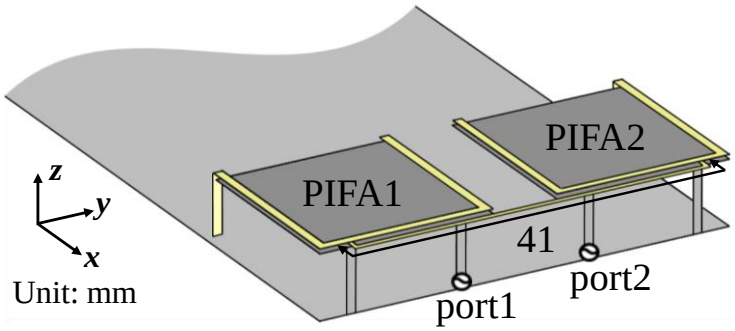

(c) l_B = 41 mm

Figure 3.7: Antenna structure with different lengths of BL (l_B)

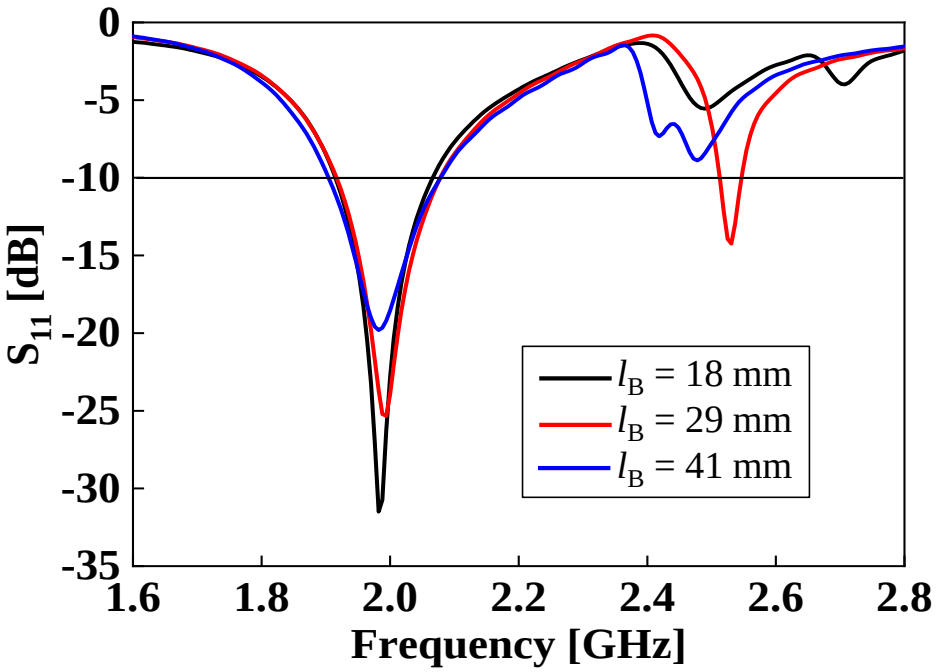

(a) S_{11}

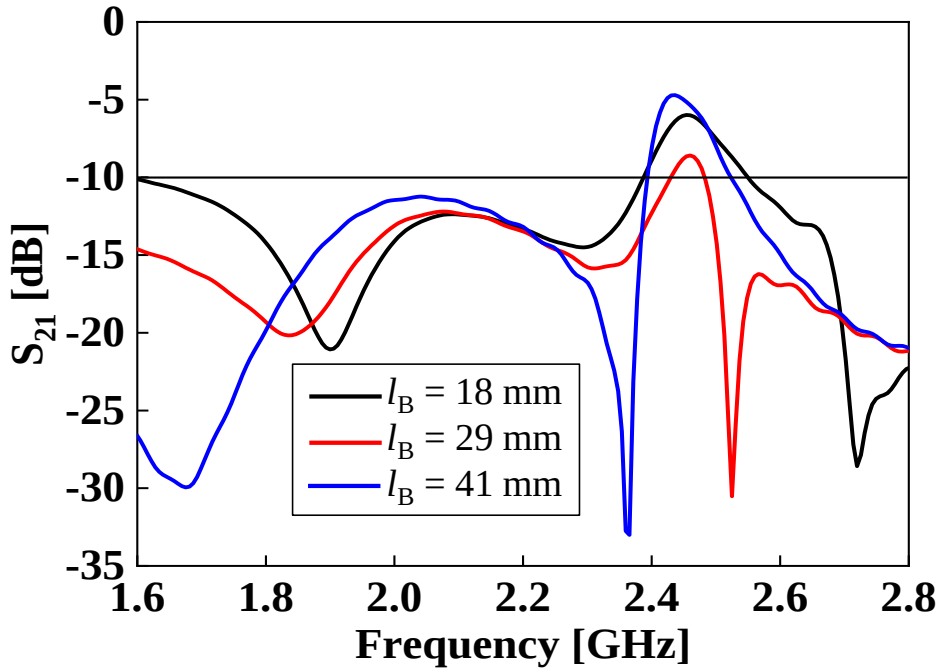

(a) S_{21}

Figure 3.8: S-parameters with different lengths of BL (l_B)

Figure 3.9(a) shows the structure of two PIFAs with PEs and BL when the width w of the part of the PEs located above the feeding pin side is widened from 1 to 2 mm. The other parameters are the same as those shown in Fig. 3.7(b). Figure 3.9(b) shows the S-parameters when w = 1 mm and 2 mm, respectively. As can be seen, when w is widened from 1 to 2 mm, the first resonance is maintained at 2.0 GHz and the second shifts from 2.5 GHz to 2.4 GHz. A good impedance matching is observed, and the mutual coupling is reduced for less than −10 dB at both desired resonant frequencies.

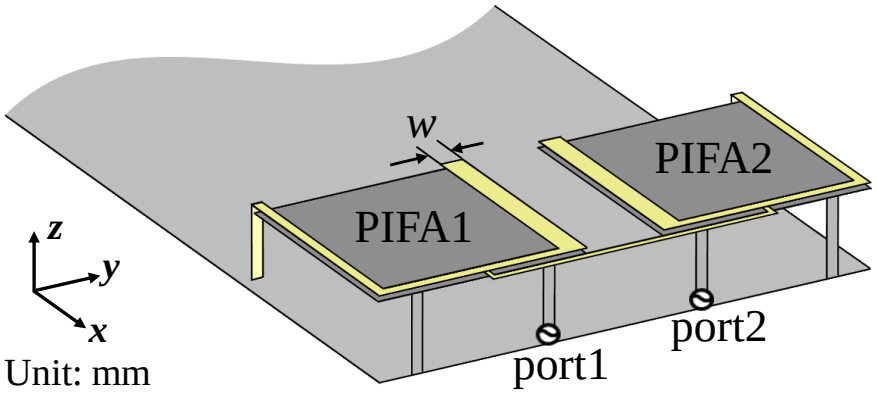

(a) Antenna structure

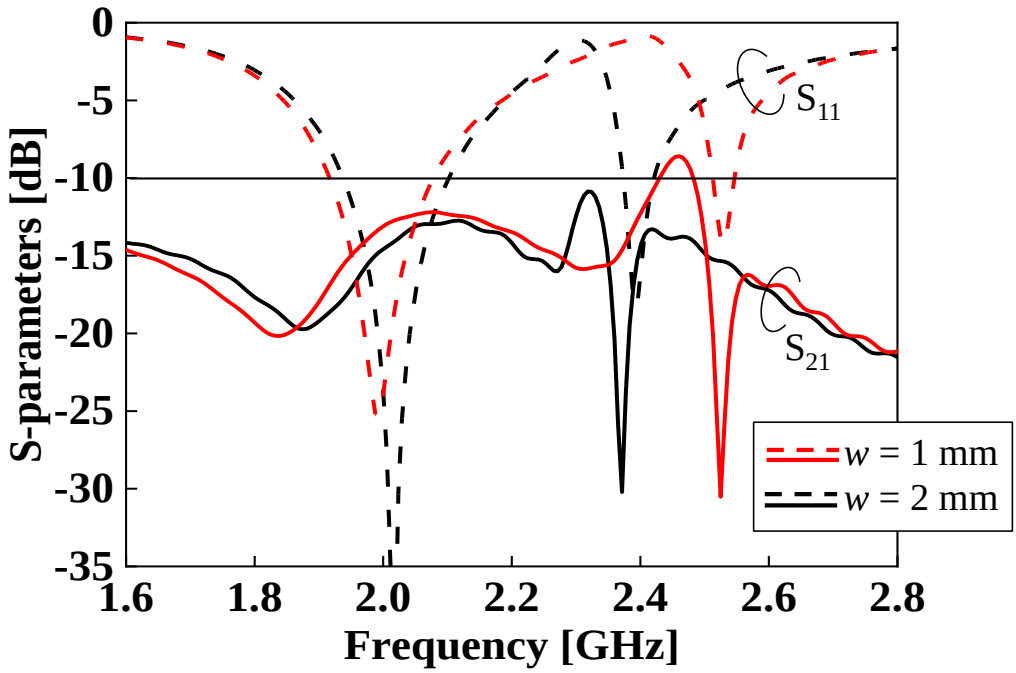

(b) S-parameters

Figure 3.9: Adjustment of the second resonant frequency

3.3.2 Comparison of Characteristics

Figure 3.10 shows the S-parameters of two PIFAs with and without PEs and BL. As shown, in the case of two PIFAs without PEs and BL, only one resonance can be obtained at 2.0 GHz, and the mutual coupling between the two PIFAs is −6.6 dB and −10.7 dB at 2.0 GHz and 2.4 GHz, respectively. However, by loading the proposed PEs and BL onto the two PIFAs, two resonances with good impedance matching can be obtained at 2.0 and 2.4 GHz. Moreover, the mutual coupling at these frequencies is reduced to −14.6 dB and −14.4 dB, respectively. Figure 3.11 shows the total antenna efficiency between PIFAs with and without PEs and BL. As can be seen in the figure, loading the proposed PEs and BL onto the two PIFAs can improve the total antenna efficiency from 77.4% to 95.2% at 2.0 GHz, and from 66.9% to 90.0 % at 2.4 GHz. Figure 3.12 shows the ECC of PIFAs with and without PEs and BL. The ECC is calculated from the far-field pattern [48]. As shown, loading PEs and BL reduces the ECC to be less than 0.05 at both desire frequencies. Because of the impedance mismatching and increased mutual coupling, the antenna efficiency and ECC change drastically at approximately 2.3 GHz.

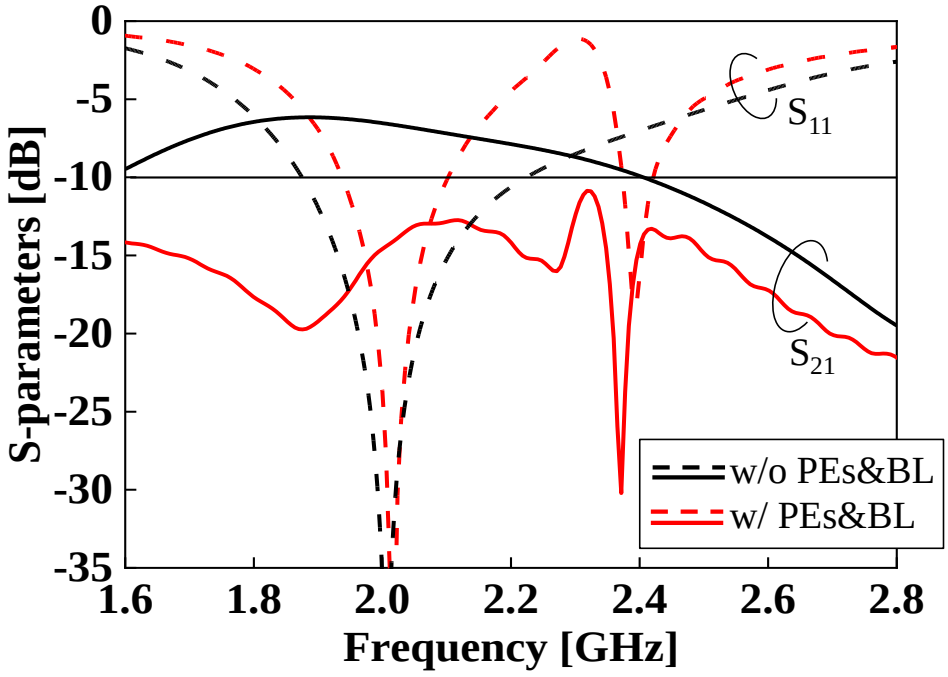

Figure 3.10: S-parameters of two PIFAs with and without PEs and BL

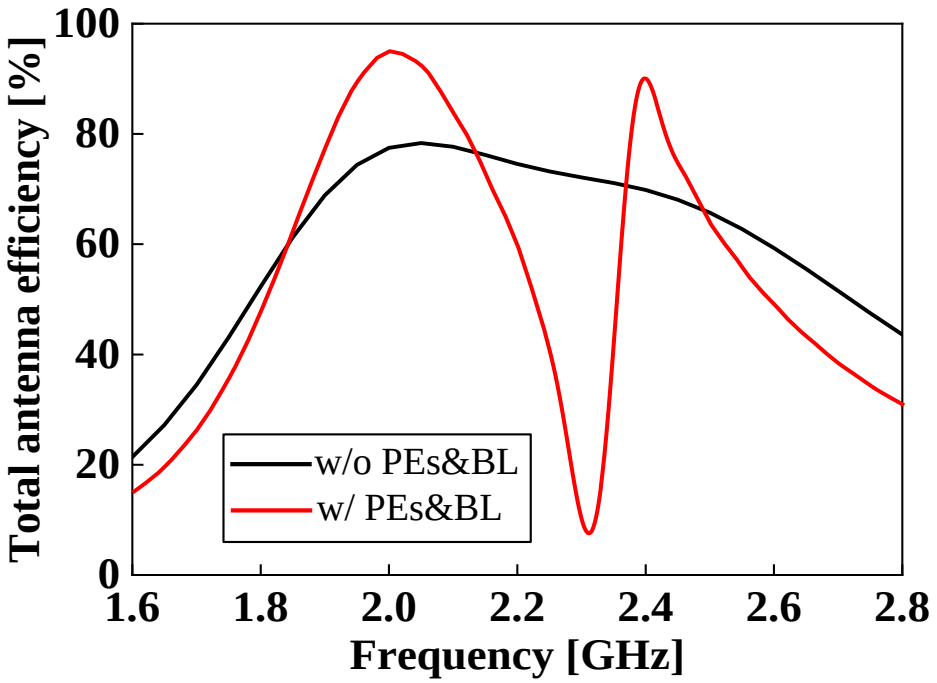

Figure 3.11: Total antenna efficiency of two PIFAs with and without PEs and BL

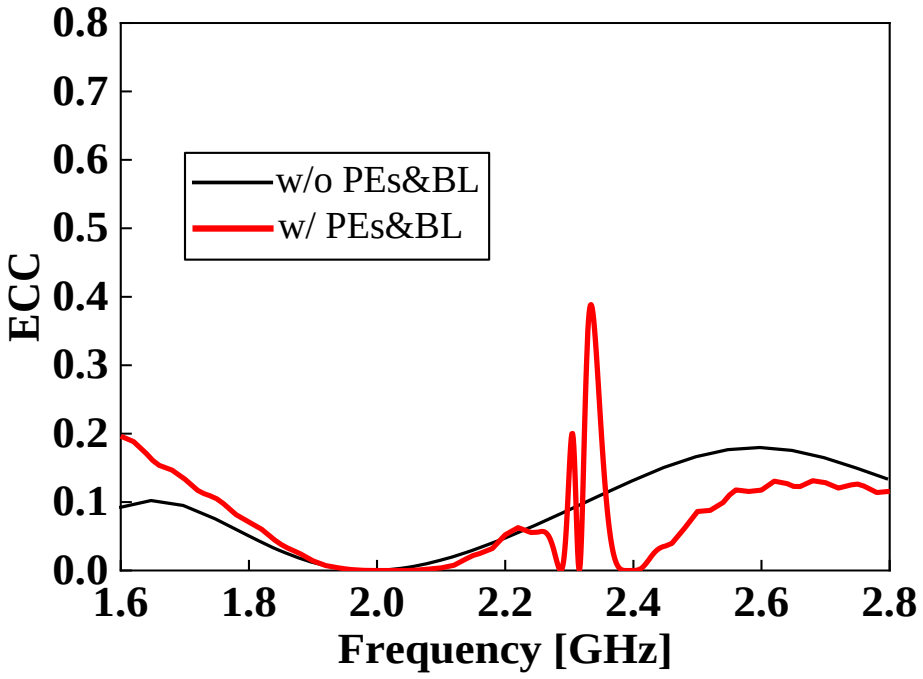

Figure 3.12: ECC of two PIFAs with and without PEs and BL

3.3.3 Discussion on Decoupling Principle

The operating principle of the proposed method is discussed by comparing the current distributions of each model. Figures 3.13(a) and (b) depict the current distributions of the PIFAs without PEs and BL at 2.0 and 2.4 GHz, respectively. In all cases, Port1 is excited and Port2 is terminated by a 50-Ω load.

As shown in Fig. 3.13(a), when PIFA1 is excited, strong currents flow primarily on the side where PIFA1 is located. However, a portion of these currents flows through the ground plane, and then flows strongly into PIFA2, particularly on the feeding pin.

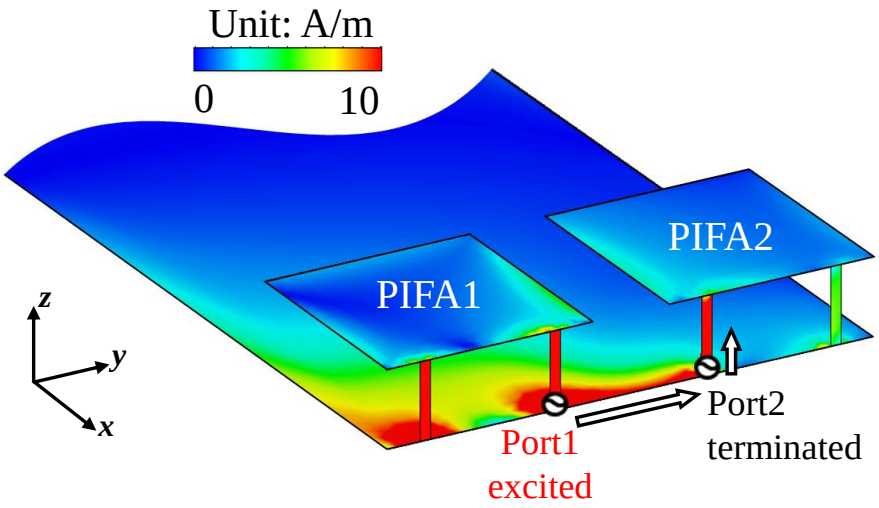

(a) 2.0 GHz

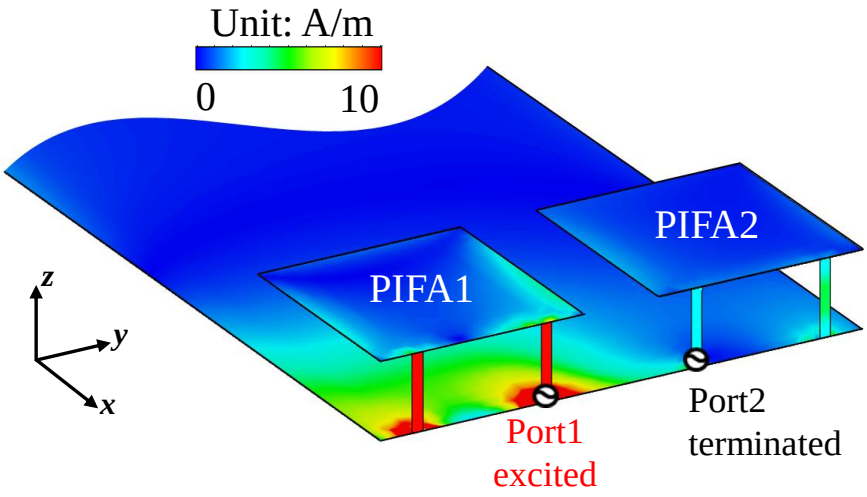

(b) 2.4 GHz

Figure 3.13: Current distribution of two PIFAs without PEs and BL

This current is considered to be the main contributor to the strong mutual coupling, referred to as the coupling current. As observed in Fig. 3.13(b), the current distribution is almost the same as shown in Fig. 3.13 (a), but the currents flowing on the PIFAs and ground plane are relatively weak, because of the impedance mismatching at 2.4 GHz.

Figures 3.14(a) and (b) depict the current distributions of the PIFAs with PEs and BL at 2.0 and 2.4 GHz, respectively. In all cases, Port1 is excited and Port2 is terminated by a 50-Ω load.

In the case of the PIFAs with PEs and BL, the decoupling principle at 2.0 GHz is explained as follows. When PIFA1 is excited, the PE on PIFA1 cause a portion of the current on the ground plane to change the direction toward the edge of the ground plane where PIFA1 is located, so that the current flowing from Port1 to Port2 is slightly reduced. Moreover, another portion of the current on PIFA1 is transmitted to PIFA2 via the BL, as shown in Fig. 3.14(a). The length of the current path through the PEs and BL, which is depicted by the black arrows in Fig. 3.14(a), is 77.5 mm and is approximately the half wavelength at 2.0 GHz. Therefore, even when the PIFAs are not directly connected to the BL, the proximity between the PEs and PIFA patch still enables the current on the PEs and BL to cancel the coupling current at the feeding pin of PIFA2 because of the opposite phase. For these two reasons, the mutual coupling at 2.0 GHz may be reduced.

Regarding the decoupling principle at 2.4 GHz, as mentioned before, the PEs excite a new current mode on the upper surface of PIFA patches, while the BL transmits a strong current from the PEs on PIFA1 toward the PIFA2 side as shown in Fig. 3.14(b). The length of the current path through the PEs and BL, indicated by the black arrows in Fig. 3.14(b), is 58 mm, which is the half wavelength at 2.4 GHz. Thus, the coupling current at 2.4 GHz is significantly canceled because of opposite phase and decoupling can be realized. In other words, the combination of PEs and BL acts as a self-decoupling structure at 2.4 GHz when they are loaded onto PIFA patches.

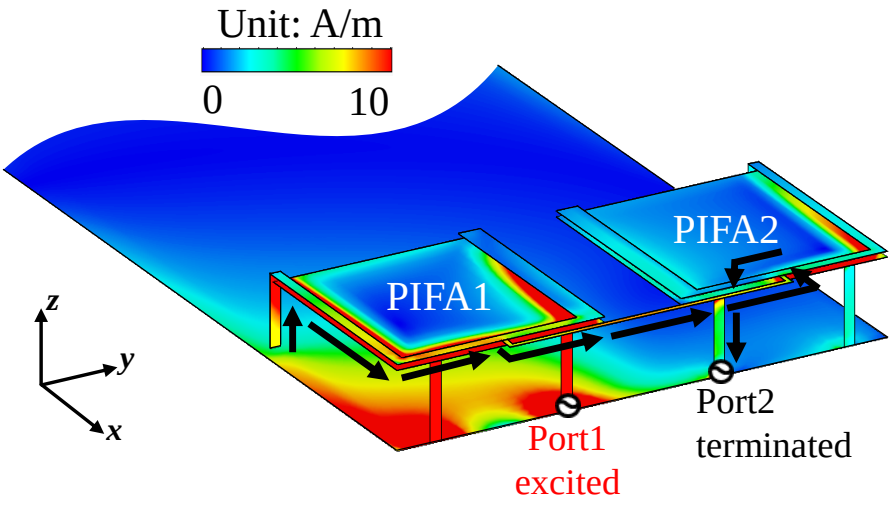

(b) 2.0 GHz

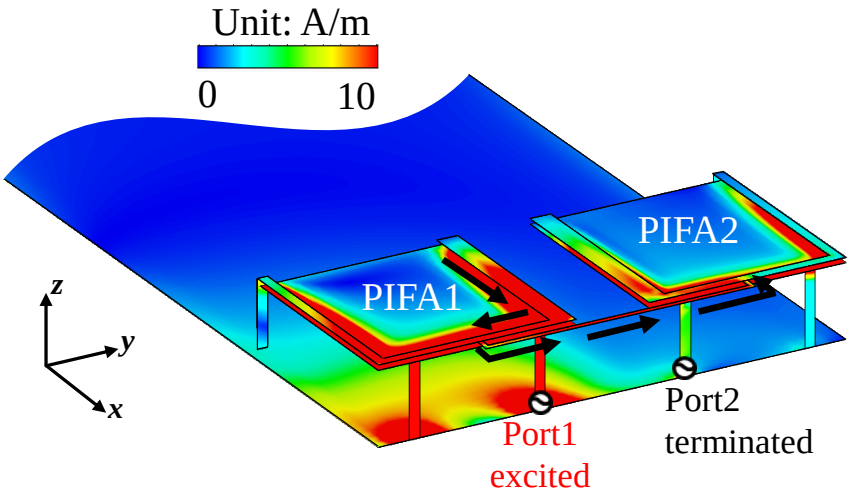

(b) 2.4 GHz

Figure 3.14: Current distribution of two PIFAs with PEs and BL

3.4 Fabrication and Measurement

In order to validate the simulation results, the two PIFAs with PEs and BL are fabricated and measured. Figure 3.15 shows photograph of the fabricated two PIFAs with PEs and BL. In this prototype, two pieces of Styrofoam with a thickness of 0.5 mm are inserted between the PIFAs and PEs to maintain an air gap between them.

Figure 3.16 shows the simulation and measurement S-parameters results of the PIFAs with PEs and BL. A good agreement is observed between the simulation and measurement results; hence, the proposed decoupling method is validated.

Figures 3.17(a) and (b) show the simulation and measurement radiation patterns of two PIFAs with PEs and BL at 2.0 and 2.4 GHz, respectively. Only the radiation patterns of PIFA1 are shown owing to the symmetrical structure of the PIFAs. The results in Figs. 3.17(a) and (b) indicate that almost the same radiation pattern can be obtained at 2.0 GHz and 2.4 GHz. Furthermore, the maximum gain in the main-lobe direction at 2.0 GHz is 3.5 dBi (*xy* plane). Meanwhile, the maximum gain in the main-lobe direction at 2.4 GHz is 2.38 dBi. The simulation results are validated by their consistency with the measurement results.

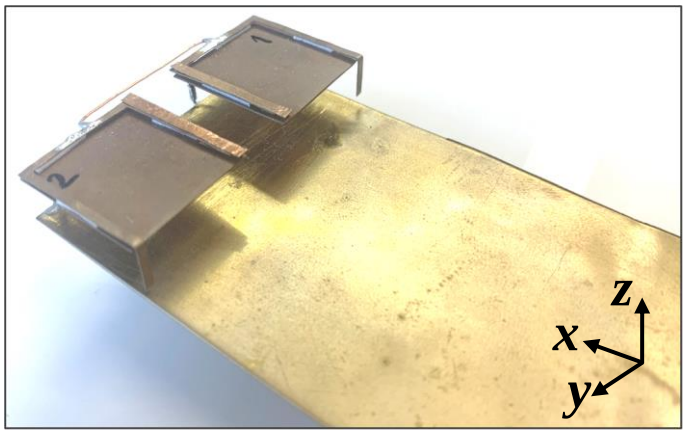

Figure 3.15: Fabricated prototype

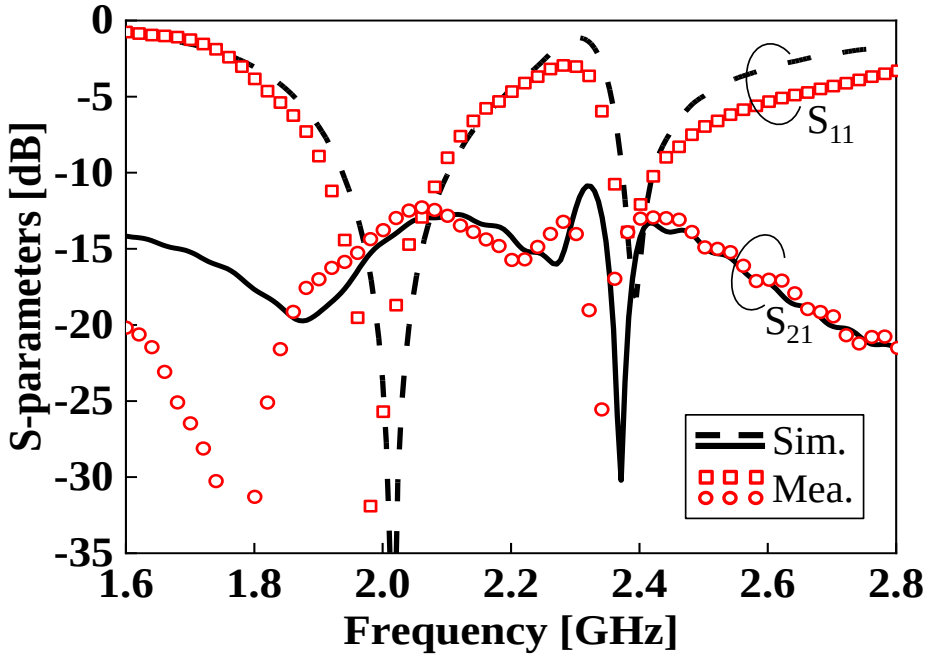

Figure 3.16: Simulation and measurement S-parameters results of two PIFAs with PEs and BL

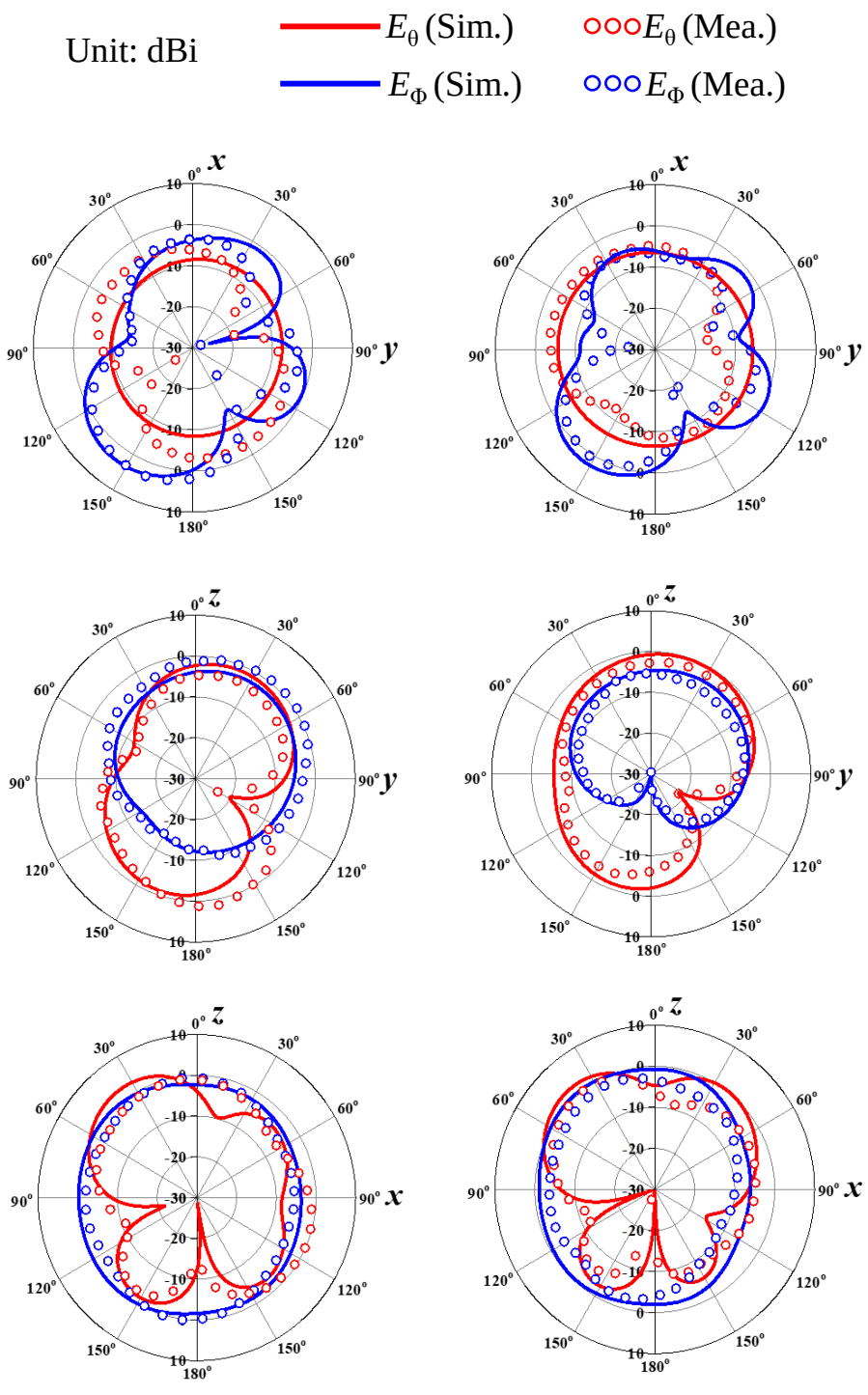

(a) at 2.0 GHz (b) at 2.4 GHz

Figure 3.17: Simulation and measurement radiation pattern of PIFA1 with PEs and BL

3.5 Versatility of Proposed Decoupling Method

To verify the versatility of the proposed method, the proposed method is applied to the dual-band design and decoupling at other frequencies as a concrete design example. The original antenna used here consists of two elements of PIFA and initially operates at a single band of 2.4 GHz (WLAN band) with a strong mutual coupling between the two PIFA elements. The proposed method is applied to increase their operating frequency band to 2.4 and 3.5 GHz (WiMAX band) and simultaneously decouple them by applying the proposed method.

Figures 3.18(a) and (b) depict the antenna structures without and with PEs and BL, respectively. As shown in Fig. 3.18(a), the two PIFAs are mounted on an 80 × 39 mm ground plane, which corresponds to the size of the shield plate for a small mobile terminal. The PIFA patch size is optimized by a size of 17 × 13 mm to operate at 2.4 GHz. The structure and size of the PEs and BL are shown in Fig. 3.18(b). Figure 3.19 shows photographs of the fabricated protype and Fig. 3.20 compares the S-parameters between PIFAs with and without PEs and BL. As shown in Fig. 3.20(b), although the bandwidth in the higher band is narrow, the PIFAs can operate at both desired frequency bands at 2.4 and 3.5 GHz after loading the PEs and BL. Therefore, the proposed method can be applied to mobile devices that do not require broadband. Furthermore, loading the PEs and BL in this case can reduce the mutual coupling from −6.7 dB to −11.1 dB at 2.4 GHz, and from −20.3 dB to −27.6 dB at 3.5 GHz. A quite good agreement is observed between the simulation and measurement S-parameters results. Therefore, the versatility of the proposed method is verified through this design example.

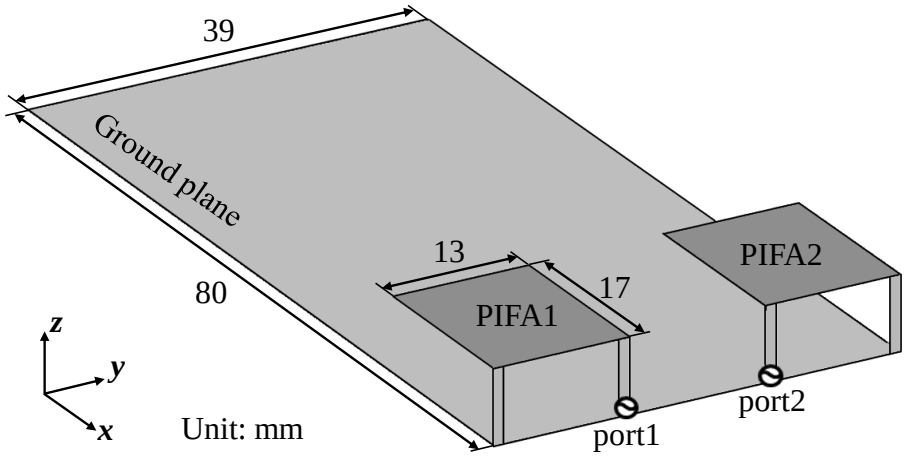

(a) without PEs and BL

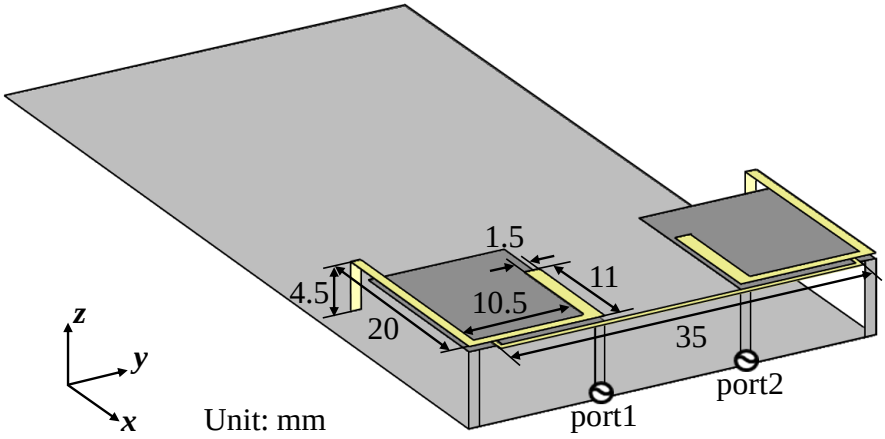

(b) with PEs and BL

Figure 3.18: Structure of two PIFAs with and without PEs and BL

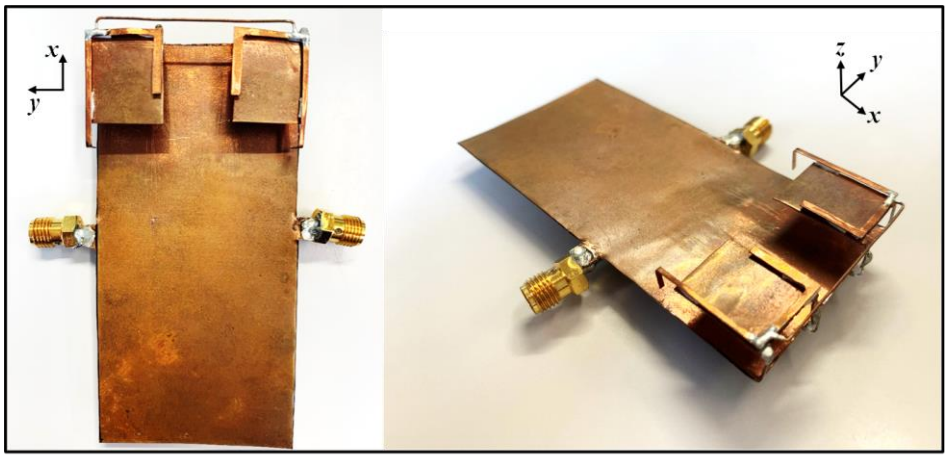

Figure 3.19: Fabricated prototype

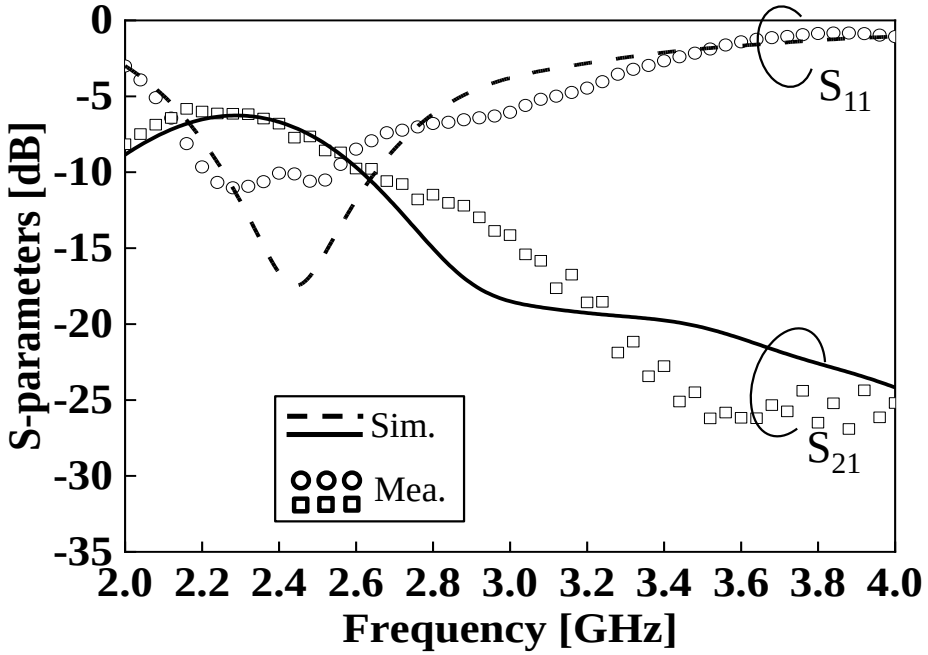

(a) without PEs and BL

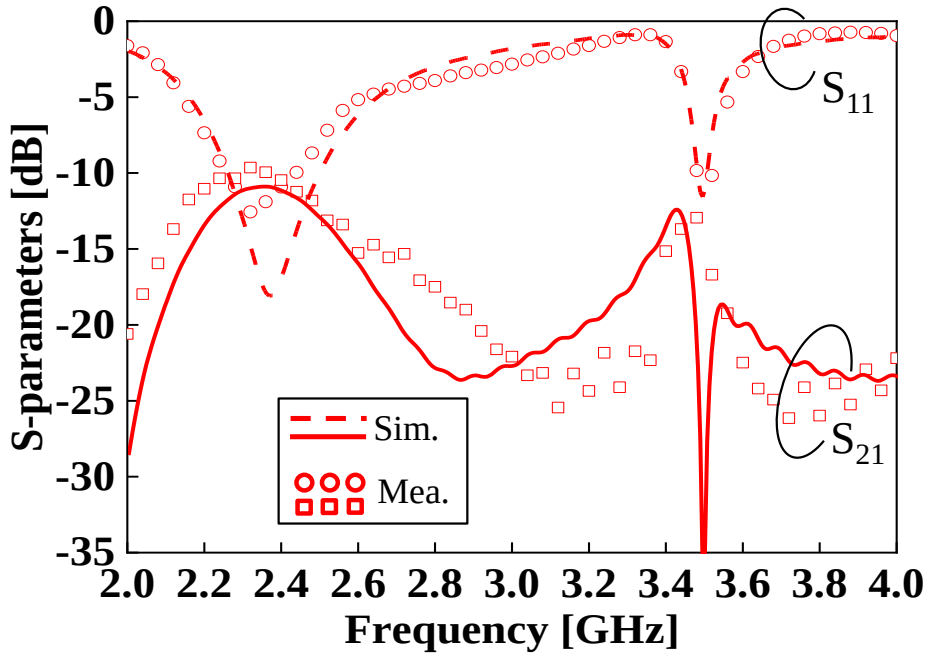

(b) with PEs and BL

Figure 3.20: Simulation and measurement S-parameters results of two PIFAs

3.6 Comparison with Other Previous Studies

This section compares the proposed method in this chapter with some other previous studies in term of the requirement of redesign or direct physical impact on original antennas, port-to-port distance, operating bandwidth, isolation and ECC as shown in Table 3.1.

The proposed method and other previous methods can be compared as follows: 1) The proposed method does not require redesign or direct physical impact on the original antennas. Whereas all other methods require it. It can also be emphasized again that this advantage is very useful in cases where the original size of the antenna is fixed or the redesign conditions are difficult; 2) The proposed method is effective even when the port-to-port distance between two PIFAs is only 0.087λ, which is smaller than [44-47] and slightly larger than [43]. However, the total isolation achieved in dual band according to the proposed method is better than [43]; 3) Like other methods, the ECC value obtained at both desired resonant frequencies using the proposed method is extremely small and less than 0.05; 4) The operating bandwidth in the 2.4 GHz band is relatively narrow compared to other methods, so bandwidth enhancement should be considered in the future.

Table 3.1: Comparison with previous studies

Ref.	Multi-band design method	Decoupling method	Requirement of redesign or direct physical impact on original antennas	Port-to-Port distance	Operating bandwidth [GHz] (S_{11}≤−10 dB)	Isolation [dB]	ECC
[43]	Matching circuit	Short Stub and Branch Element	Yes	0.054λ	-	−10.2 (1.8 GHz) −15.5 (2.1 GHz)	-
[44]	Slotting antennas and grounding PEs	Using CMA to define the best antenna location	Yes	0.887λ	2.5~2.7 (7.7%) 3.34~4.5 (29.6%)	−20 (2.5 GHz) −60 (3.5 GHz)	<0.05 (2.5 GHz)
[45]	Slotting antennas	Slotting GND	Yes	0.144λ	2.4~2.48 (1.6%) 3.4~3.6 (5.7%)	−19.2 (2.4 GHz) −22.8 (3.5 GHz)	-
[46]	Grounding PEs	BL	Yes	0.2λ	2.3~2.61 (12.2%) 3.2~4.1 (24.7%) 5.6~6.1 (8.5%)	−18 (2.4 GHz) −21 (3.5 GHz) −31 (5.8 GHz)	<0.1 (in all bands)
[47]	Branch element	Slotting GND	Yes	0.343λ	2.6~3.08 (16%) 5.48~6.12(13.1%)	−21.18 (2.9 GHz) −23 (5.8 GHz)	<0.08 (2.9 GHz) <0.1 (5.8 GHz)
This study	**Non-contact PEs**	**PEs&BL**	**No**	**0.087λ**	**1.94~2.1 (7.9%)** **2.37~2.42 (2.09%)**	**−14.6 (2.0 GHz)** **−14.4 (2.4 GHz)**	**<0.05** **(in all bands)**

λ: wavelength at the lowest resonant frequency; - : cannot found in source

3.7 Summary

In this chapter, a method using a combination of PEs and BL was proposed to increase the operating frequency band and decouple two PIFAs, which initially operate at a single band of 2.0 GHz, without having to redesign the original sizes or structure or directly connect any additional element to the PIFAs. The PEs excite a new current mode on the upper surface of PIFA patches, to help PIFAs operate at the 2.4-GHz band. For the decoupling principle at the 2.0-GHz band, the PEs reduce a portion of the current flowing from Port1 to Port2, while the BL transmits a strong current to cancel the coupling current flowing on the feeding pin of PIFA2. For the 2.4-GHz case, the combination of PEs and BL acts as a self-decoupling structure when they are loaded onto PIFA patches. Thus, decoupling can be realized in the dual band simultaneously. The two PIFAs with PEs and BL were fabricated and measured. A good agreement was observed between the simulation and measurement results of S-parameters and radiation patterns; hence, the proposed decoupling method was validated. Moreover, the versatility of the proposed method was verified by applying it to other frequency bands.

Chapter 4
Decoupling Method for Four PIFAs

4.1 Introduction

In Chapter 2, a decoupling method was proposed to improve the performance of the two PIFAs. However, to further enhance the transmission rate and channel capacity of MIMO antennas, the number of antenna elements should be greater than two. Therefore, efficient decoupling methods are required for MIMO antennas when the number of antenna element is greater than two. As the number of antennas increases, one problem that can be mentioned is that decoupling them becomes considerably more complicated and requires considerable effort from the antenna designer.

Several studies have proposed a MIMO configuration composed of four elements with four separated ground planes, as in [49,50]. In addition, two separate ground planes were used for two antenna pairs in [51]. By totally separating the ground plane, such as in these studies, there is no coupling current through them, resulting in a reduction in mutual coupling. However, as mentioned in [52], separating ground planes cannot ensure that all antenna elements operate as expected because, in practice, the supposition of having all ground planes with the same voltage level is invalid. Thus, the design of MIMO antenna structures with multiple ground planes should be avoided.

Recently, several representative MIMO configurations consisting of four or eight antenna elements sharing the same ground plane have been proposed. The related studies can be divided into two groups. In the first group, the authors usually arrange the antenna elements orthogonal to each other or use self-decoupled antenna structures to configure a MIMO antenna. Thus, a low level of mutual coupling can be achieved without the need for any decoupling structure. However, a relatively large spacing is still required between them [53-57]. Therefore, these methods are not suitable for application to compact MIMO systems. Some previous studies have proposed compact and wideband MIMO antenna [58,59]. However, the center-to-center distance of the adjacent radiating elements as shown in [58] is large, and a feeding network with balun structures as shown in [59] is extremely complex. In the second group, additional decoupling structures are usually added to reduce mutual coupling. For example, in [60,61], a pair of antenna elements is

decoupled first, and then several decoupled antenna pairs are arranged to compose a MIMO antenna. Although the spacing between antenna elements in the same pair is extremely close, the pair-to-pair spacing is still large. The method using a defected ground structure is regarded in [62,63] as a simple method that does not increase the size of the antenna; however, this method reduces the space for mounting electronic components on the ground plane. A decoupling surface was used in [64] to reduce the mutual coupling of multiple patch antennas. However, because the decoupling surface must be loaded onto the antenna at a large distance from it, the profile of the antenna, including the decoupling surface, significantly increases. An extremely close four-element MIMO antenna was proposed in [65] with a decoupling method using a metal wall that can reduce their mutual coupling from approximately −7.0 dB to −20.0 dB. However, the antenna efficiency was slightly degraded even when the isolation was improved. This indicates that higher isolation does not result in better efficiency.

One common feature of the aforementioned methods is that they require redesign or a direct physical impact on the original antennas, and the spacing between the antennas is large. In this chapter, the method using PEs and BLs is further developed to decouple the four PIFAs, which are mounted on a ground plane with close spacing to each other. Section 4.2 will examine the decoupling effectiveness of the PEs and BLs, which are proposed in Chapter 2, when they are applied to the case of four PIFAs. Then, the PEs and BLs will be functionally developed to reduce the mutual coupling between four PIFAs in Section 4.3. Section 4.4 compares the characteristics of the four PIFAs with and without PEs and BLs, and then discusses the decoupling principle of the proposed method by comparing the current distributions. Section 4.5 shows the fabrication prototypes and examines the agreement between simulation and measurement results to confirm the validity of the proposed decoupling method. Section 4.6 compares the proposed method with other methods proposed in previous studies. Finally, Section 4.7 gives a summary of this chapter.

4.2 Effects of Previously Proposed PEs and BLs on Four PIFAs

In this section, the structure and S-parameters of four PIFAs will be presented first. Then, the decoupling efficiency of PE and BL, proposed in Chapter 2, will be examined when they are applied to the case of four PIFAs.

4.2.1 Structure and Characteristic of Four PIFAs

Figure 4.1 shows the original structure of the four PIFAs mounted on a rectangular ground plane measuring 120 mm × 97 mm. The ground plane is represented as a shielding plate in mobile devices such as small tablets. For such mobile devices, the antennas should be placed at the edge of the ground plane in order to increase the space for mounting other electronic components. Therefore, the four PIFAs are arranged in a horizontal row at one edge of the ground plane. The structure and size of each PIFA element are the same as those shown in Fig. 2.1. The edge-to-edge and center-to-center spacings of adjacent PIFA elements are maintained at only 7 mm ($0.05\lambda_0$ at 2.0 GHz) and 26 mm ($0.17\lambda_0$ at 2.0 GHz), respectively.

Figure 4.2 shows the S-parameters of the original four PIFAs. Owing to the symmetry of the antenna, only the typical S-parameters of PIFA1-PIFA4 are presented. In the case of two PIFAs, as shown in Chapter 2, good impedance matching can easily be obtained for both PIFAs. However, as shown in Fig. 4.2, S_{11} is less than −10 dB, whereas S_{22} is only −7.1 dB at 2.0 GHz. Therefore, when the number of PIFAs is increased from two to four, an impedance mismatch appears at the PIFAs arranged at the center of the ground plane (PIFA2 and PIFA3). Moreover, the mutual coupling between adjacent PIFA elements with the feeding pins facing each other is extremely strong (S_{21} = −5.3 dB). This indicates that when the number of PIFA elements increases to four, the mutual coupling between adjacent PIFA elements with the feeding pins facing each other becomes stronger than is the case of two PIFAs as shown in Chapter 2. However, the mutual coupling is relatively weak for the PIFAs with the feeding pins not facing each other (S_{32} = −9.7 dB). In addition, the mutual coupling between non-adjacent PIFAs is extremely weak (S_{31} = S_{41} = −16.5 dB). Therefore, the mutual coupling between PIFA1-2 and PIFA3-4 must be reduced, and simultaneously the impedance matching of PIFA2 and PIFA3 must be improved to enhance the performance of the four PIFAs.

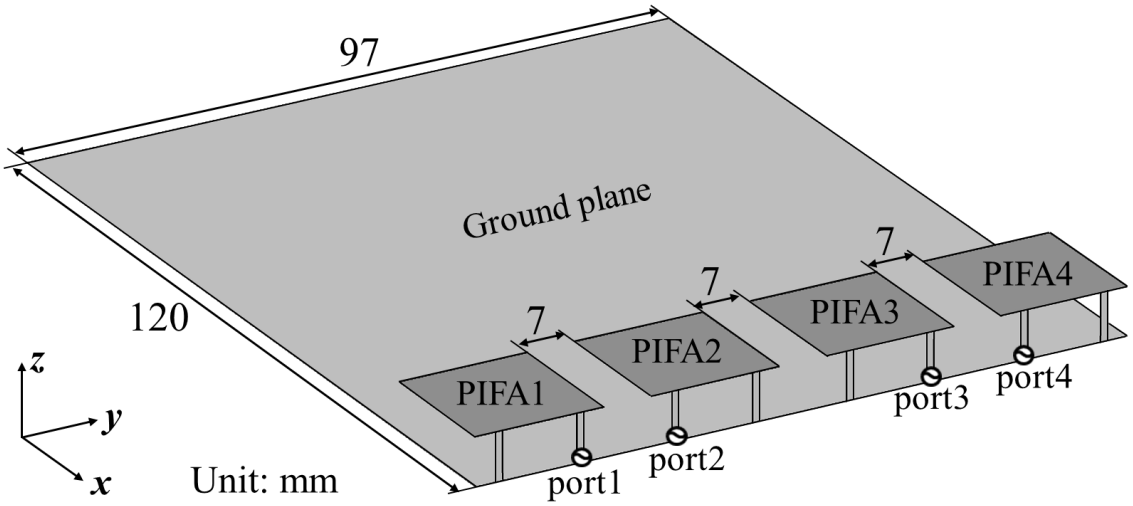

(a) Antenna structure

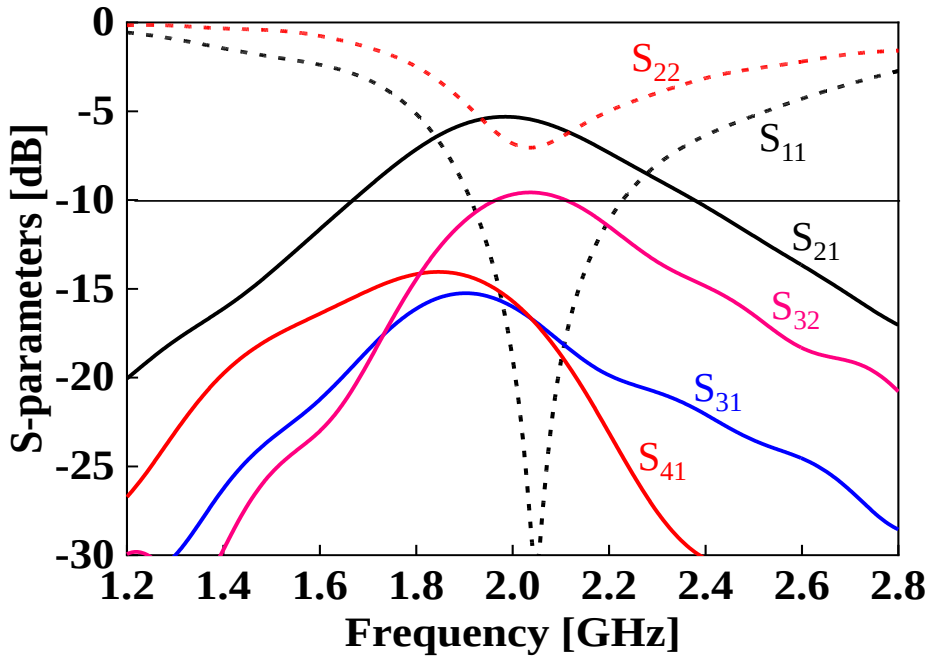

(b) S-parameters

Figure 4.1: Structure and S-parameters of original four PIFAs

4.2.2 Effects of Previously Proposed PEs and BLs

Figure 4.2 shows the structure and S-parameters of four PIFAs with previously proposed PEs and BLs. Four PEs with a width of 9.5 mm are loaded onto four PIFAs with a spacing of 0.5 mm. The PE1-PE2 and PE3-PE4 pairs are connected by BL1 and BL2, respectively,

which are depicted by the red parts. The width of PEs, the spacing between PEs and PIFAs, and the total length of BLs are the same as those shown in Chapter 2. However, to obtain a resonance at 2.0 GHz in the case of four PIFAs, the length of PEs is set to 28 mm. As shown in Fig. 4.2(b), when the PEs and BLs are loaded onto the four PIFAs, the resonant frequency is maintained at 2.0 GHz and the mutual coupling (S_{21} and S_{32}) at 2.0 GHz is reduced compared to the four PIFAs without PEs and BLs. However, S_{21} at 2.0 GHz is still for beyond −10 dB, whereas, with the same PEs and BL structure, S_{21} was

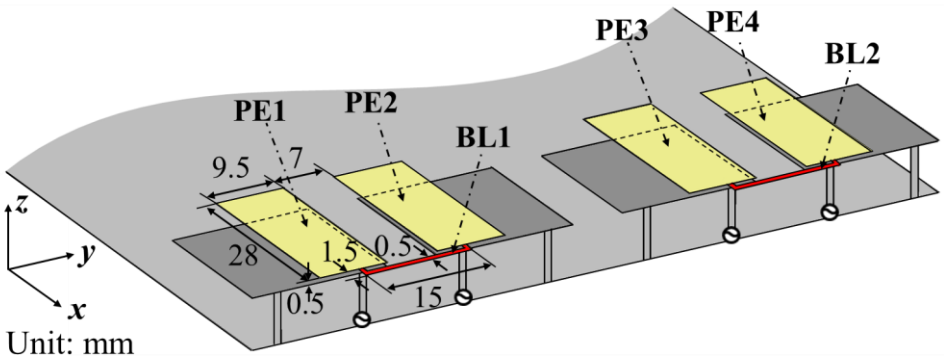

(a) Antenna structure

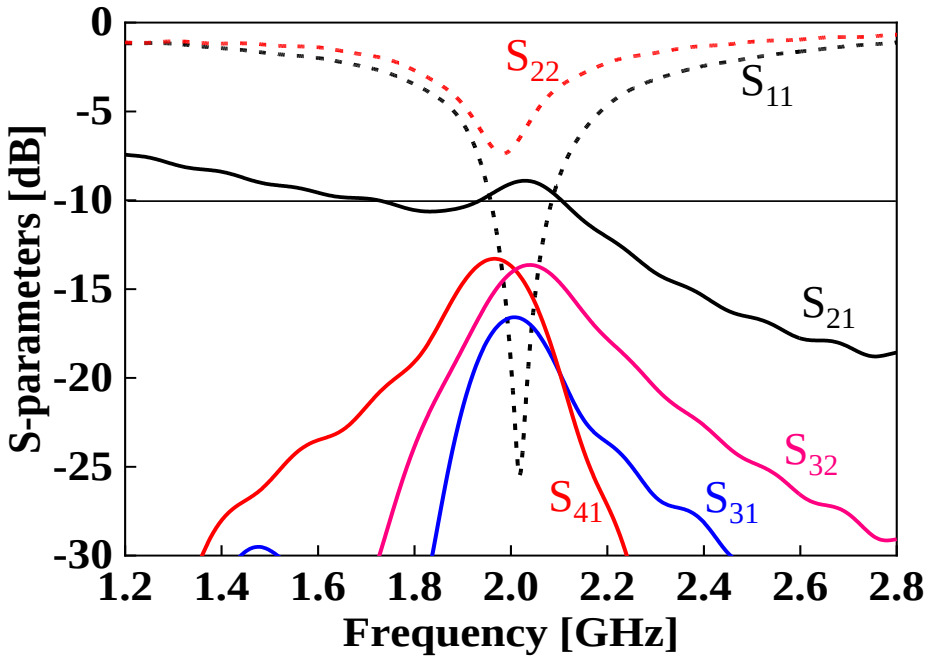

(b) S-parameters

Figure 4.2: Structure and S-parameters of four PIFAs with previously proposed PEs and BLs

easily reduced for less than −10 dB in the case of two PIFAs as shown in Chapter 2. Therefore, it is clear that the previously proposed method is still effective even when it is applied to the case of four PIFAs, but its decoupling effectiveness is partially attenuated.

The reason for the attenuation of the decoupling effectiveness can be explained by comparing the current distribution of the two PIFAs and the four PIFAs. Figures 4.3(a) and (b) depict the current distributions of the two PIFAs and the four PIFAs when PIFA1 is excited, respectively. In all case, when Port1 is excited, the others are terminated by 50-Ω loads. As can be seen, in both cases, a coupling current flows from PIFA1 through the ground plane to PIFA2. However, since the ground plane in the case of four PIFAs is large, the current path on the ground plane increases, resulting in an increase in coupling current flowing from PIFA1 to PIFA2. For this reason, the previously proposed PEs and BLs cannot completely suppress the coupling current in the case of four PIFAs.

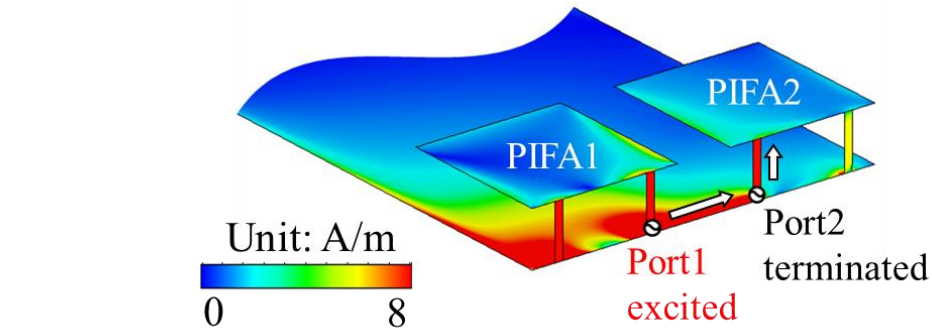

(a) Two PIFAs

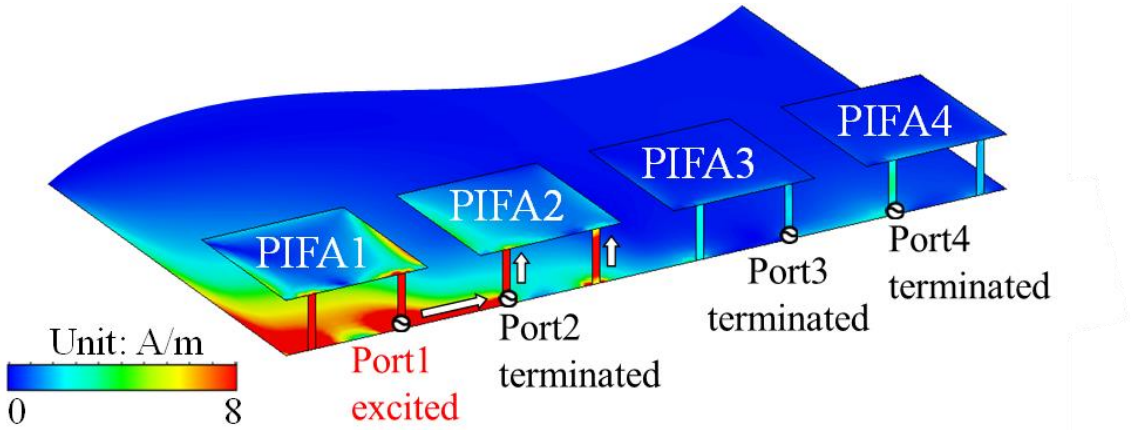

(b) Four PIFAs

Figure 4.3: Current distribution when PIFA1 is excited (2.0 GHz)

4.3 Proposed Decoupling Method Using PEs and BLs for Four PIFAs

In this section, the PEs and BLs will be functionally developed to reduce the mutual coupling between four PIFAs. As mentioned in the previous section, in the case of four PIFAs, the mutual coupling becomes stronger due to the increased coupling current on the ground plane. Therefore, to be able to completely suppress the coupling current in this case, it is necessary to increase the opposite-phase current flowing on the PEs and BLs. A simple idea to do this is to increase the size of PEs and BLs.

4.3.1 Structure and Effects of PEs and BLs

Figure 4.4 shows the structure and S-parameters of the four PIFAs with PEs and BLs. Four PEs with a width of 19 mm are loaded onto four PIFAs with a spacing of 0.5 mm. To obtain a resonance at 2.0 GHz, the lengths of PE1 and PE4 are set to 28.5 mm, whereas those of PE2 and PE3 are set to 27 mm. The PE1-PE2 and PE3-PE4 pairs are connected by BL1 and BL2, which are depicted by the red parts in Fig. 4.4 (a), respectively. The lengths of BL1 and BL2 are 45 mm, whereas width w_B is varied from 3 mm to 11 mm to define their optimal size. The changes in the S-parameters when w_B is varied are shown in Fig. 4.4(b). Notably, although certain attenuation is observed in the operating bandwidth after loading PEs and BLs onto the four PIFAs, S_{11} at 2.0 GHz is still maintained for less than −10 dB for any value of w_B. Evidently, S_{21} is reduced if w_B is increased. In particular, S_{21} could reach less than −10 dB at 2.0 GHz when w_B = 11 mm. In the case of S_{31} and S_{41}, which are initially weak because of the large distance between the non-adjacent PIFAs, mutual coupling is constantly maintained for less than −10 dB

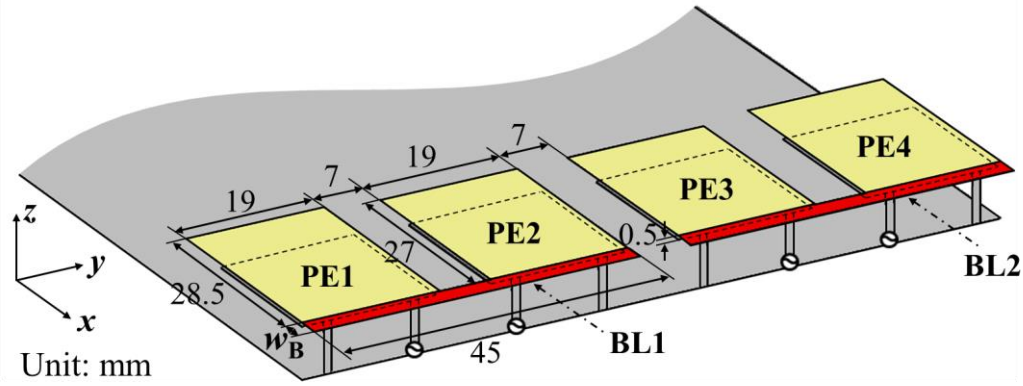

(a) Antenna structure

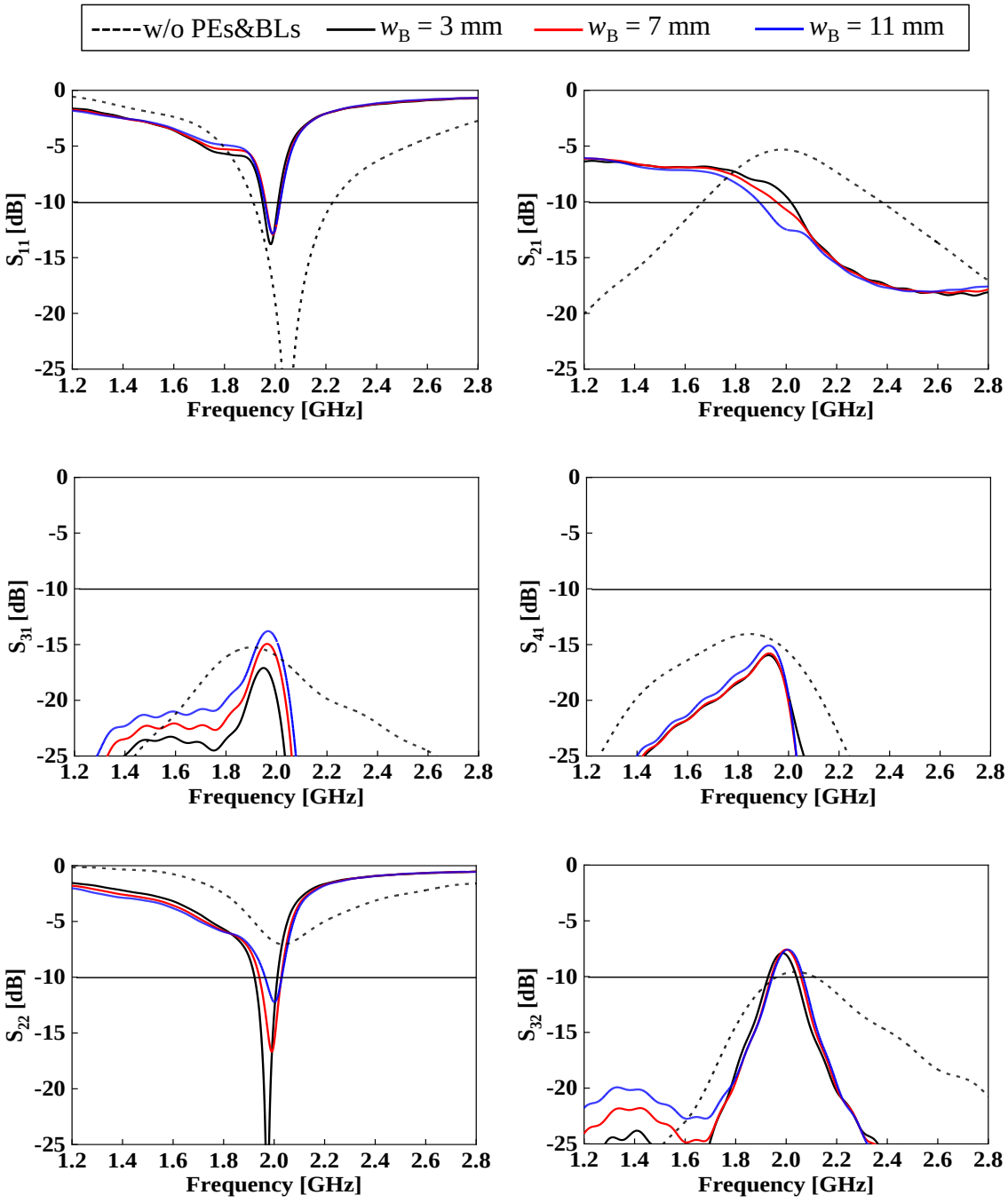

(b) S-parameters when w_B is varied

Figure 4.4: Decoupling of four PIFAs using PEs and BLs

for any value of w_B. This indicated that w_B did not affect the mutual coupling between the PIFA elements that are not adjacent to each other. For S_{22}, an improvement in impedance matching could be observed compared to the case of the four PIFAs without PEs and BLs. Certain degradation in impedance matching appeared when w_B increased to 11 mm, but S_{22} is still maintained for less than −10 dB at 2.0 GHz. In the case of the four PIFAs without PEs and BLs, S_{32} is only −9.1 dB, which is a relatively weak mutual coupling level. However, as shown in Fig. 4.4(b), the loading of PEs and BLs increased it to −7.5 dB, meaning that the mutual coupling between PIFA2 and PIFA3 become stronger. It can be explained that when the PEs and BLs are loaded onto the four PIFAs, the improved impedance matching of PIFA2 and PIFA3 causes a greater power to be transmitted between them, resulting in a stronger mutual coupling compared to the case without PEs and BLs. Therefore, the loading of PEs and BLs with w_B = 11 mm could reduce S_{21} and S_{43} for less than −10 dB, simultaneously improve the impedance matching of PIFA2 and PIFA3. However, this also increased the mutual coupling between PIFA2 and PIFA3; thus, this aspect also must be considered.

A simple idea to reduce S_{32} is to widen the spacing between PE2 and PE3 to restrict the interaction between them as much as possible. As shown in Fig. 4.5(a), the widths of PE2 and PE3 are reduced from 19 mm to 4 mm. Simultaneously, the widths of PE1 and PE4 are also reduced to 4 mm to maintain the distance between them and PE2 and PE3, as far as possible. The dimensions of the BLs are 45 mm × 11 mm. Figure 4.5(b) shows the S-parameters of the four PIFAs with PEs and BLs after adjusting the size of the PEs. Notably, S_{32} is reduced for less than −10 dB, and the other S-parameters are simultaneously maintained for less than −10 dB at 2.0 GHz.

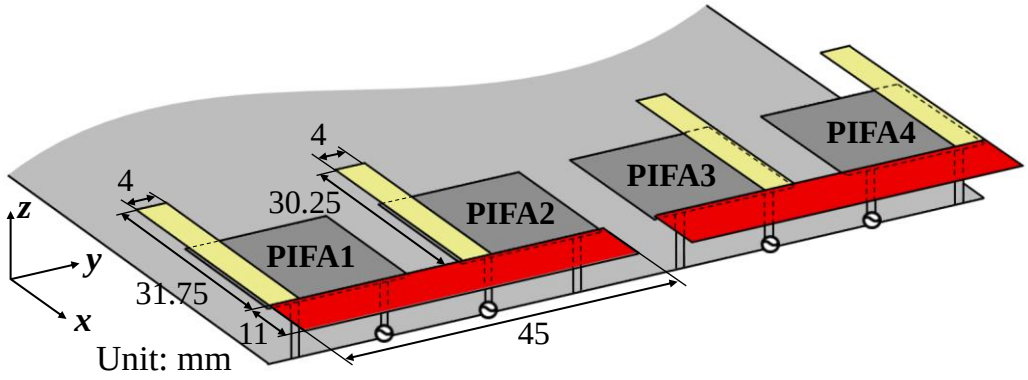

(a) Antenna structure

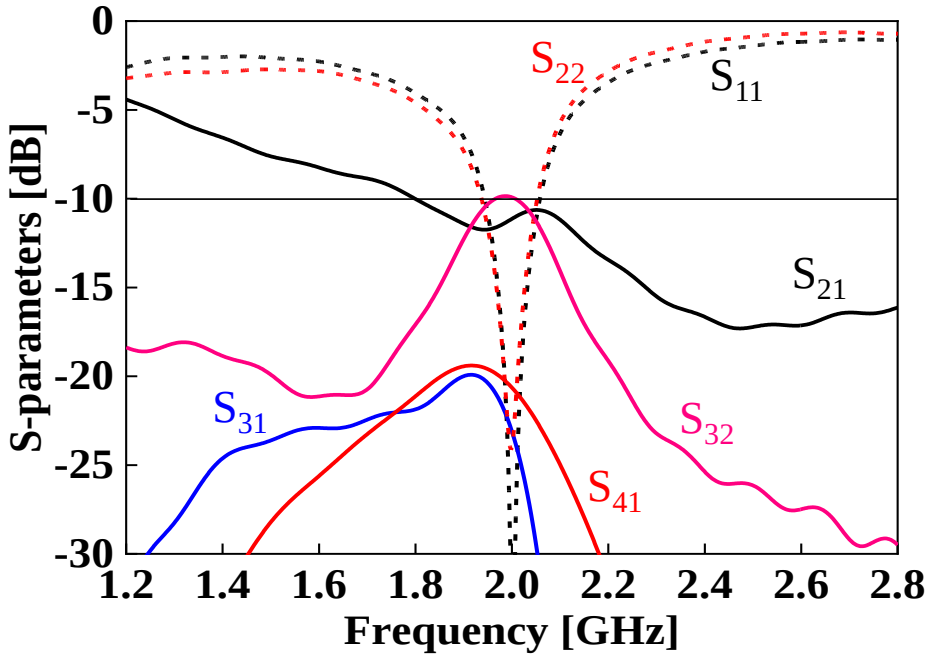

(b) S-parameters

Figure 4.5: Effects of adjusting the size of the PEs

4.3.2 Space-saving of BLs

By loading the PEs and BLs with the afore-determined parameters, a low level of mutual coupling and good impedance matching are obtained at 2.0 GHz. However, the volume of PIFAs, including PEs and BLs, increased. In particular, the BLs significantly protruded from the edge of the ground plane. Therefore, the space saving of the proposed structure must be considered. To achieve this, the BLs are bent at a certain position, as shown in Fig. 4.6(a), and the S-parameters after bending the BLs are shown in Fig. 4.6(b). The results demonstrate that the resonant frequency remained unchanged when the BLs are bent. In addition, the mutual coupling level remained at 2.0 GHz for less than −10 dB. Certain degradations in the impedance matching of PIFA2 and PIFA3 are also observed, but they are still maintained for less than −10 dB.

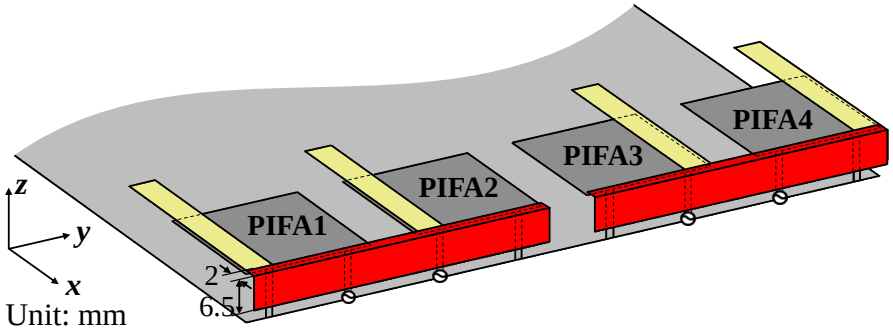

(a) Antenna structure

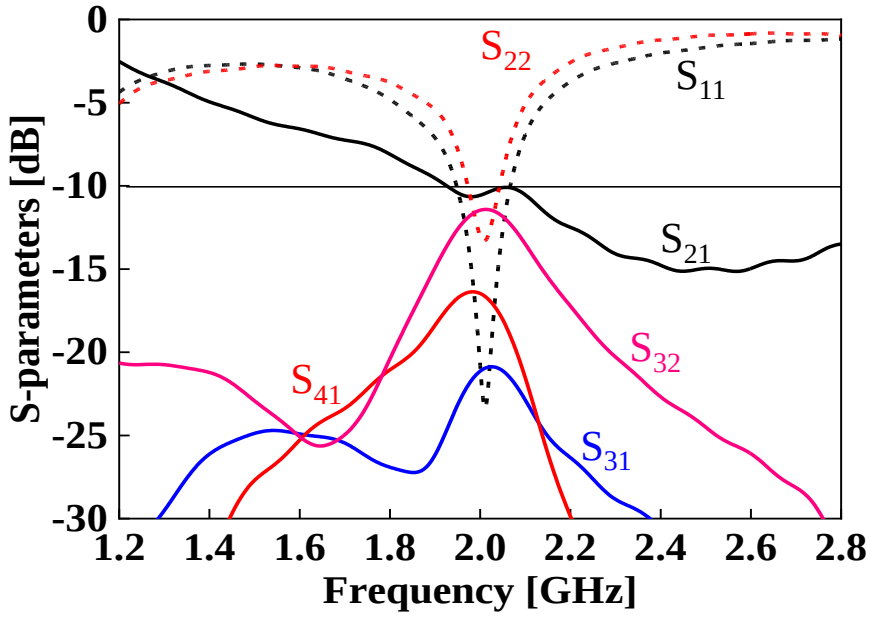

(b) S-parameters

Figure 4.6: Space-saving of BLs (proposed model)

4.4 Comparison of Characteristics and Discussion on Decoupling Principle

The decoupling effectiveness of the proposed PEs and BLs is studied by comparing several important characteristics such as the S-parameters, total antenna efficiency, ECC, and radiation pattern between the four PIFAs with and without PEs and BLs. The decoupling principle of the proposed method will be explained by comparing the changes in current distribution of the four PIFAs with and without PEs and BLs.

4.4.1 Comparison of Characteristics

Figure 4.7 shows the S-parameters of the four PIFAs with and without proposed PEs and BLs. From the S_{11} characteristic, it is clear that although the bandwidth is slightly narrower, the resonant frequency at 2.0 GHz with good impedance matching is maintained. Besides, the mutual couplings (S_{21}, S_{31}, S_{41} and S_{32}) in the case with PEs and BLs are reduced as well as maintained for less than −10 dB compared to the case without PEs and BLs; therefore, the decoupling effectiveness of the proposed method is confirmed. Moreover, the S_{22} is improved to less than −10 dB after loading PEs and BLs onto the four PIFAs. Therefore, the proposed method is not only effective in decoupling, but also effective in improving the impedance matching of PIFA2 and PIFA3.

Figure 4.8 shows the total antenna efficiency of the four PIFAs with and without PEs and BLs. By loading the PEs and BLs onto the four PIFAs, the antenna efficiency of PIFA1 and PIFA4 at 2.0 GHz can be improved from 64.2% to 84.8%, whereas that of PIFA2 and PIFA3 can be significantly improved from 35.9% to 74.2%. The antenna efficiency of PIFA2 and PIFA3 significantly improved because the proposed PEs and BLs can reduce mutual coupling between them and simultaneously improve their impedance matching at 2.0 GHz.

Figures 4.9(a) and (b) illustrate the simulated ECC for the four PIFAs with and without the proposed PEs and BLs. Owing to the symmetry of the antenna, only the representative ECC between PIFA1-2, PIFA1-3, PIFA1-4, and PIFA2-3 has been provided. The ECC was calculated from the far-field patterns. In the case of four PIFAs without PEs and BLs, the ECC between PIFA1-2 or PIFA2-3 is better than 0.2 at 2.0 GHz, indicating a rather high level of ECC between the adjacent PIFAs. However, for the pair PIFA1-3 or PIFA1-4, the ECC is initially low (< 0.05) owing to the large spacing between

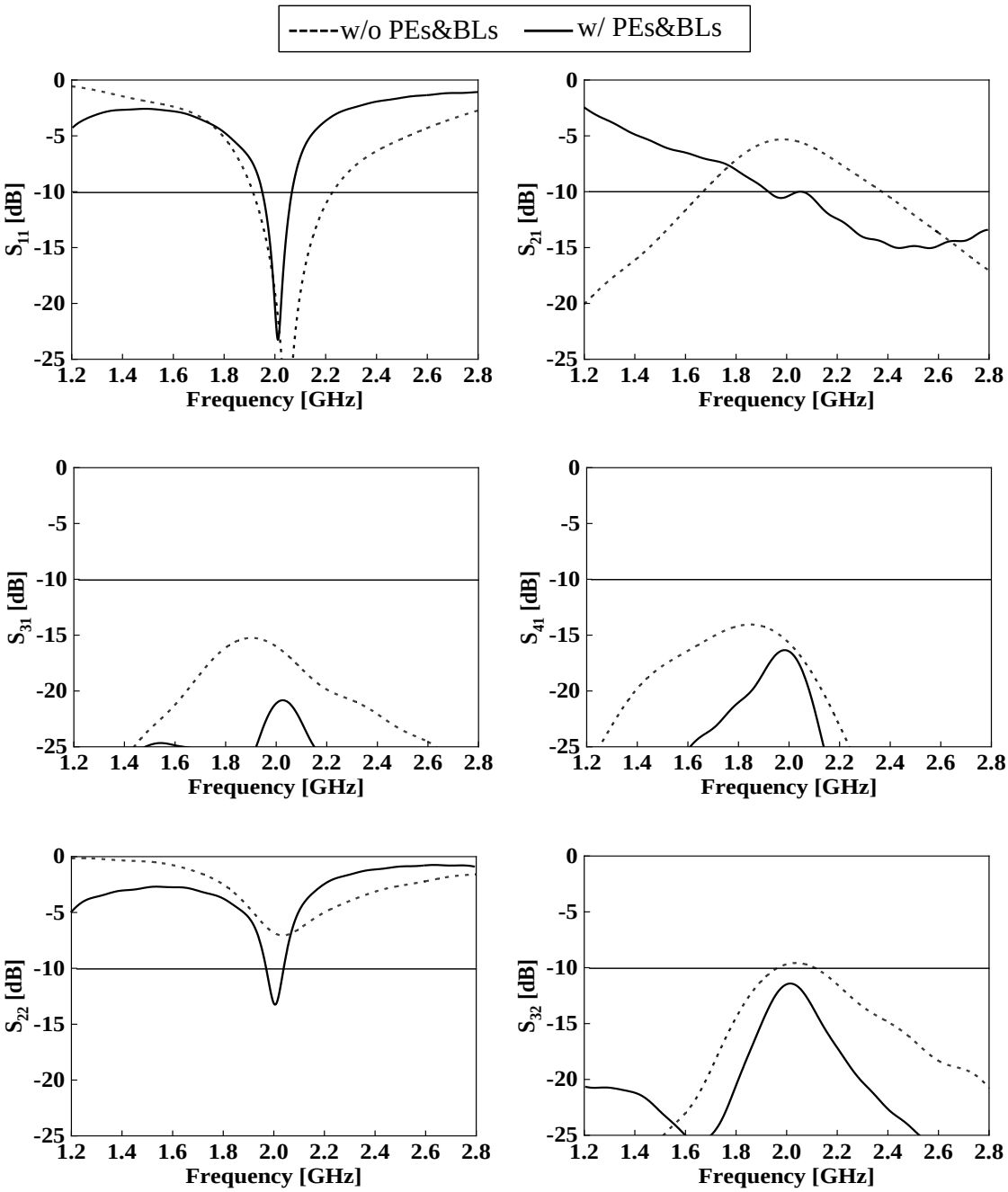

Figure 4.7: S-parameters of four PIFAs with and without PEs and BLs

them. In the case of four PIFAs with PEs and BLs, the ECC between PIFA1-PIFA2 or PIFA2-PIFA3 is significantly reduced at 2.0 GHz. In addition, the ECC between PIFA1-PIFA3 or PIFA1-PIFA4 is also maintained at a low level. Therefore, a good MIMO performance of ECCs < 0.05 can be achieved for four PIFAs when the proposed PEs and BLs are loaded onto them.

Figures 4.10 and 4.11 show the simulation radiation patterns of PIFA1 with and without PEs and BLs, and PIFA2 with and without PEs and BLs at 2.0 GHz, respectively. The results in these figures indicate that the radiation pattern significantly changed after loading the PEs and BLs onto the four PIFAs, but the gains are still maintained in all planes. Moreover, because the proposed antenna is designed for mobile terminals, the change in the radiation pattern after loading PEs and BLs has almost no adverse effect on the radio transmission efficiency of the four PIFAs.

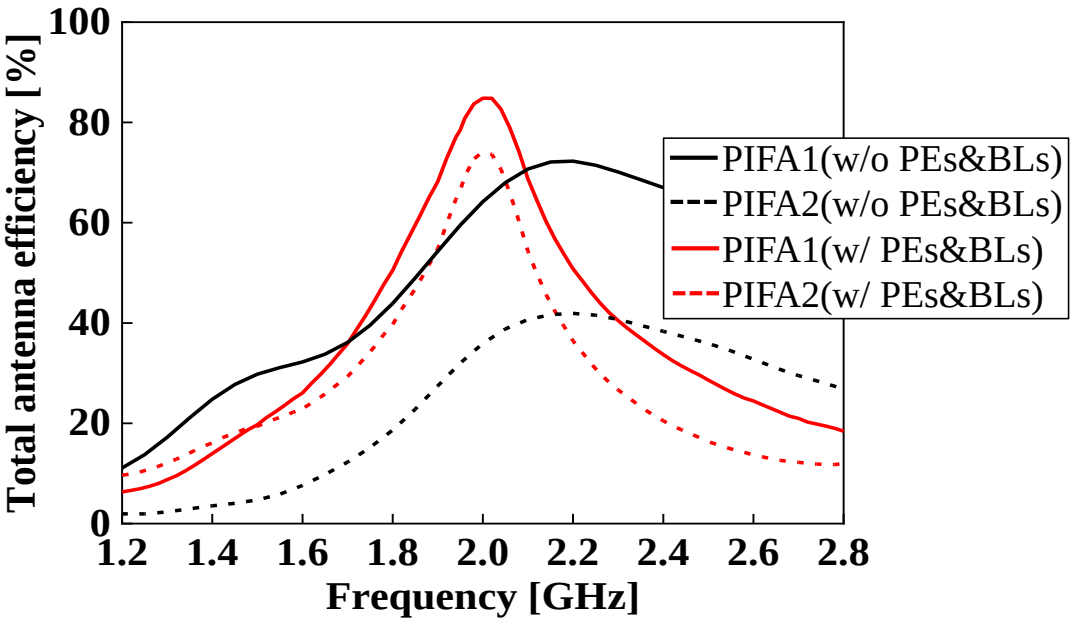

Figure 4.8: Total antenna efficiency of four PIFAs with and without PEs and BLs

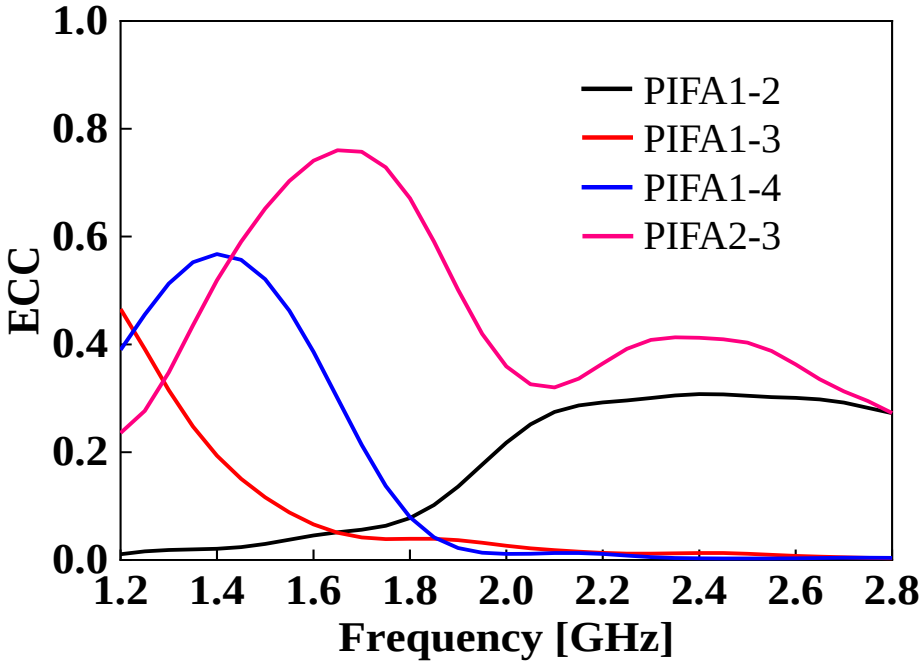

(a) without PEs and BLs

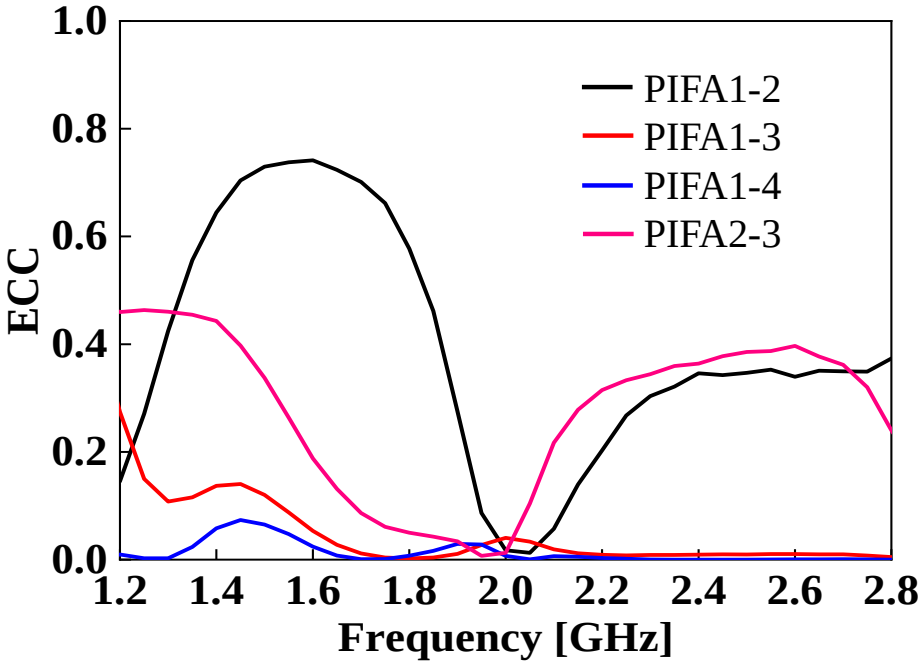

(b) with PEs and BLs

Figure 4.9: ECC of four PIFAs with and without PEs and BLs

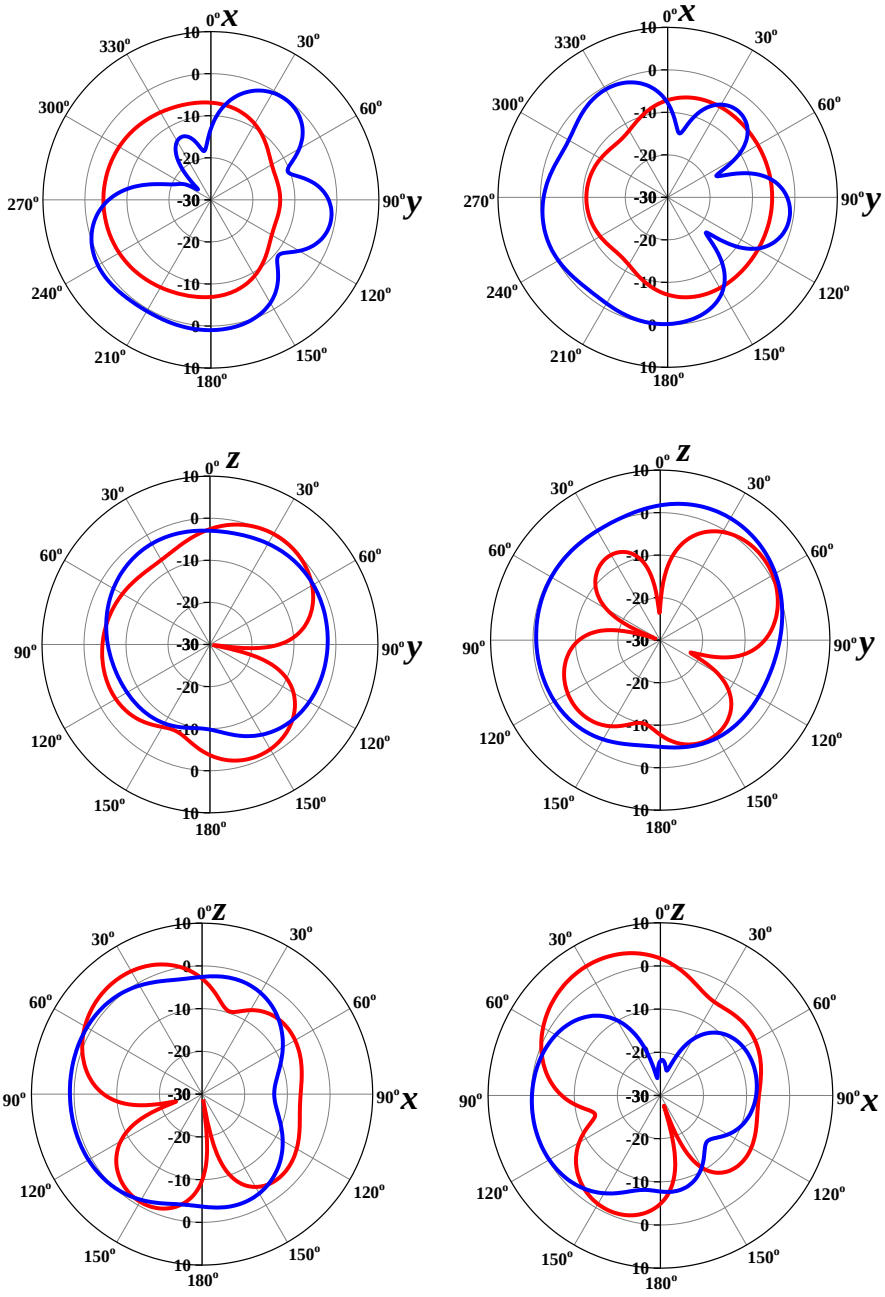

(a) without PEs and BLs (b) with PEs and BLs

Figure 4.10: Radiation pattern of PIFA1 (2.0 GHz)

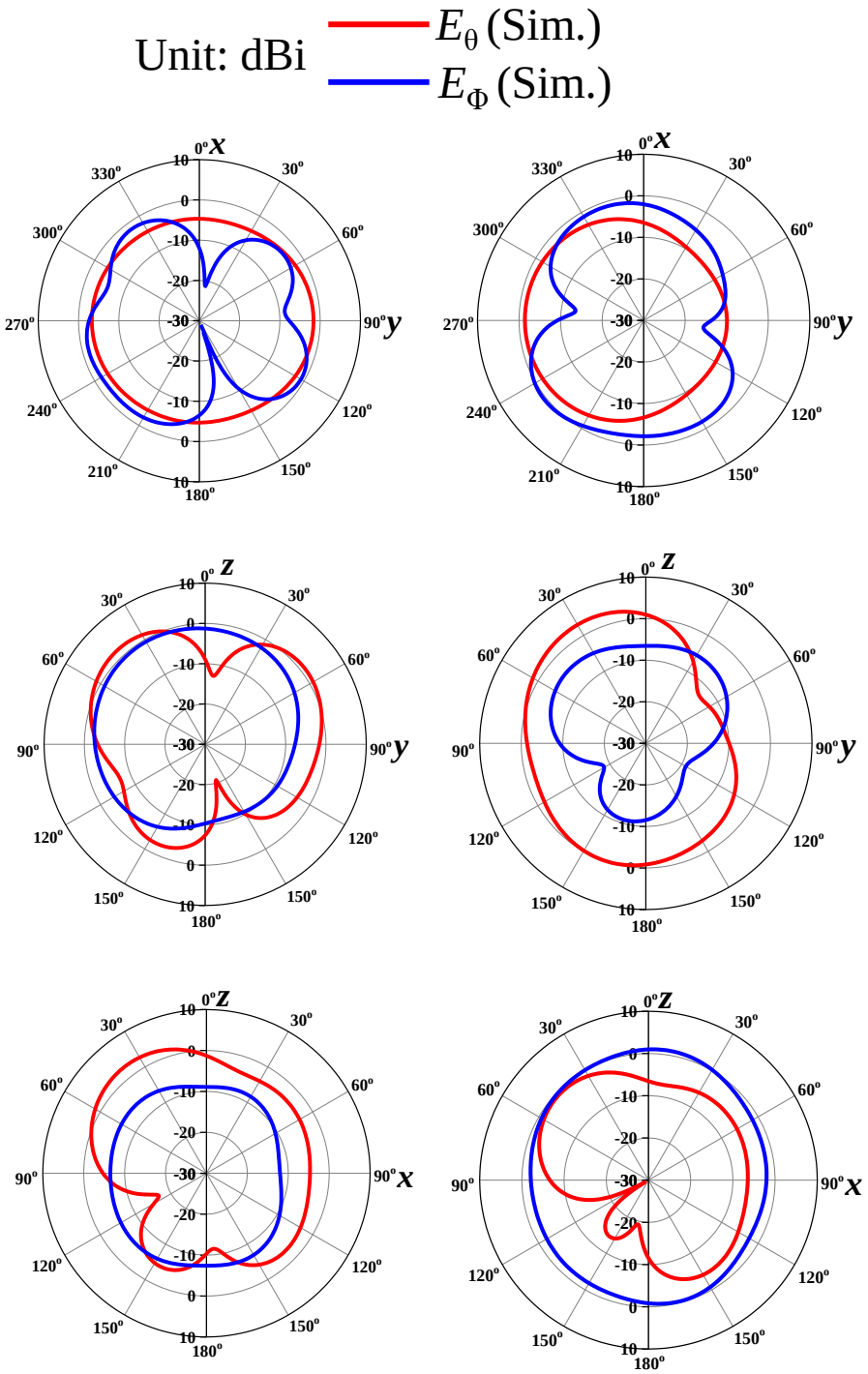

(a) without PEs and BLs (b) with PEs and BLs

Figure 4.11: Radiation pattern of PIFA2 (2.0 GHz)

4.4.2 Discussion on Decoupling Principle

In order to clarify the decoupling principle of the proposed method, the current distributions of the four PIFAs with and without PEs and BLs are compared. In all case, when one port is excited, the others are terminated by 50-Ω loads.

Figure 4.12(a) and (b) show the current distribution of the four PIFAs without PEs and BLs, when PIFA1 and PIFA2 is excited, respectively. As shown in Fig. 4.12(a), when PIFA1 is excited, the current from Port1 flows through the ground plane and then strongly flows into Port2. This current is considered to be the main contributor to the strong mutual coupling between PIFA1 and PIFA2, referred to as the coupling current (white arrows). However, the coupling currents that flow from Port1 into Port3 and Port4 are relatively weak due to the large distance between them. As shown in Fig. 4.12(b), when PIFA2 is excited, the coupling current from Port2 flows strongly into Port1. In addition, another coupling current flowing from Port2 into Port3 is also observed, but it is relatively weak compared with the coupling current flowing into Port1.

Figure 4.13(a) and (b) show the current distribution of the four PIFAs with PEs and BLs, when PIFA1 and PIFA2 is excited, respectively. The decoupling principle between PIFA1 and PIFA2 can be explained as following: when the PEs and BLs are loaded onto the four PIFAs, in addition to the coupling current flowing through the ground plane, a new current (black arrows) appears on the BL between PIFA1 and PIFA2 as shown in Fig. 4.13(a). These two currents cancel each other at the feeding pin of the PIFA2, due to opposite phase. In other words, the PE loaded onto PIFA1 creates an induced current and the BL acts like a transmission line to transmit that current toward PIFA2 to suppress the coupling current flowing through the ground plane. The same decoupling principle is also performed when PIFA2 excited, as shown in Fig. 4.13(b). For this reason, the mutual coupling between PIFA1 and PIFA2 can be reduced.

For the case of PIFA2 and PIFA3, a different decoupling principle can be explained. In most cases, when the impedance matching of the antennas is improved, the mutual coupling between them becomes stronger. However, by loading the PEs and BLs onto the four PIFAs, the mutual coupling between PIFA2 and PIFA3 is even reduced while their impedance matching is improved. There are two reason to explain it. The first reason is that when PIFA2 is excited as shown in Fig. 4.13(b), the coupling current between PIFA2 and PIFA3 is partially reduced because the shorting pin of PIFA3

interrupts the current path. Therefore, the coupling current from Port2 cannot flow directly to Port3 via ground plane. The second reason is due to the position of PEs on PIFA2 and PIFA3. The position of the PEs is an important factor because it affects the direction of the coupling current when the PIFA is excited. As can be seen, these PEs are arranged along the non-adjacent edge of PIFA2 and PIFA3, so the distance between them is relatively far. By arranging the PEs like this way, the flow direction of the coupling current from Port2 is changed to flow along PE2 direction instead of towards Port3. Thus, coupling current flowing from Port2 to Port3 is further reduced. Although the coupling current still exists between Port2 and Port3 as shown in Fig. 4.13(b), it is relatively weak. Therefore, the level of mutual coupling between PIFA2 and PIFA3 remains low even when their impedance matching is improved.

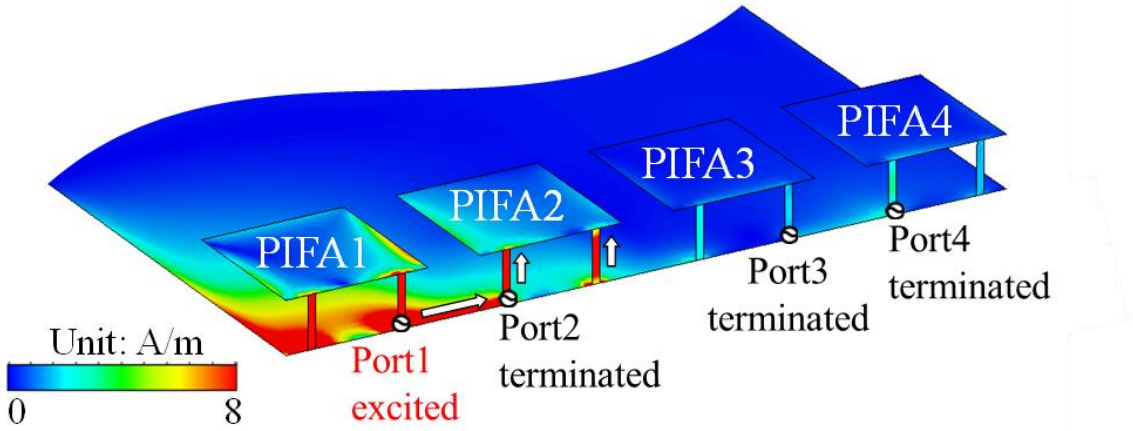

(a) PIFA1 excited

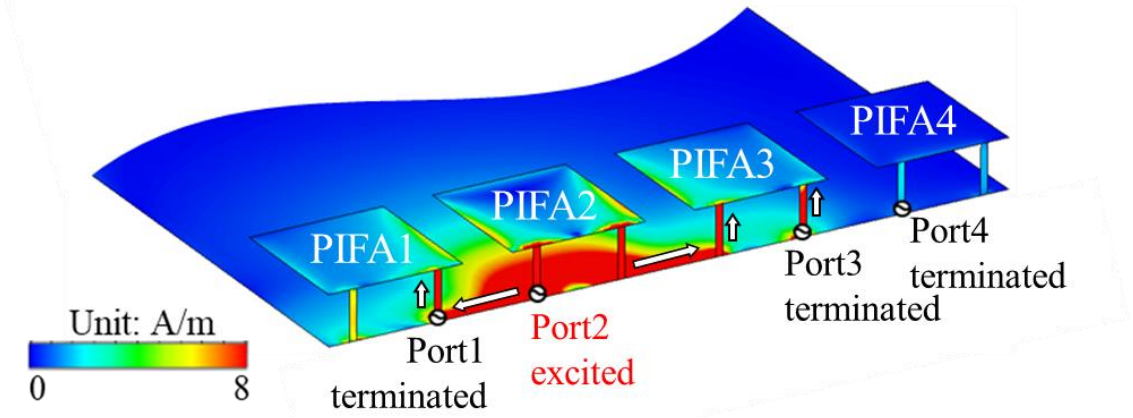

(b) PIFA2 excited

Figure 4.12: Current distribution of four PIFAs without PEs and BLs (2.0 GHz)

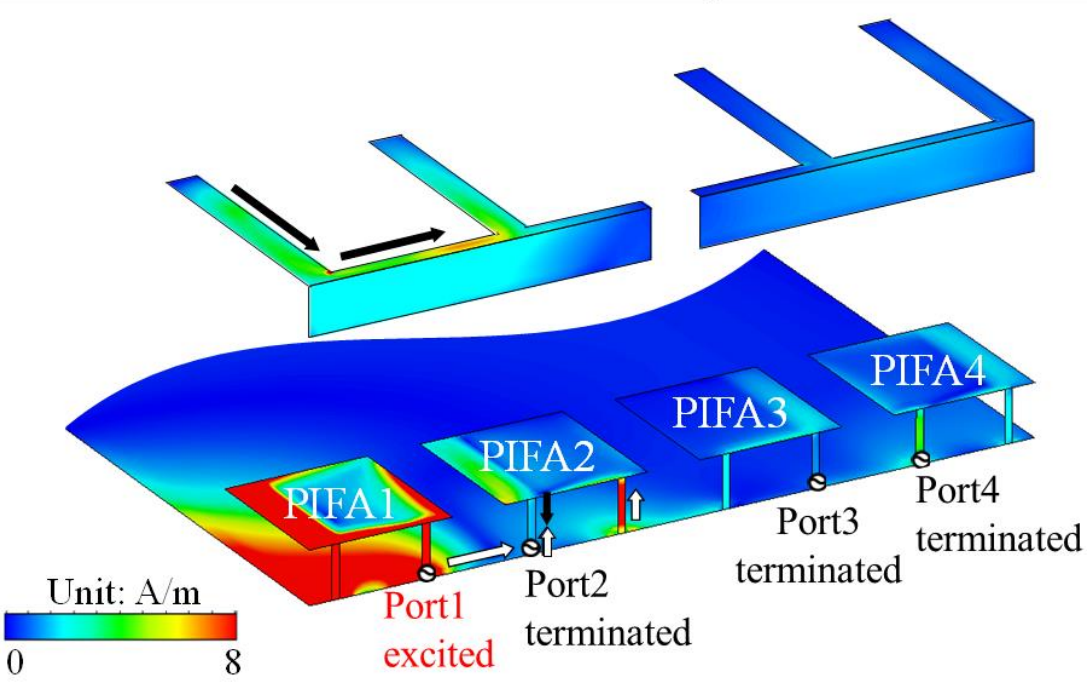

(a) PIFA1 excited

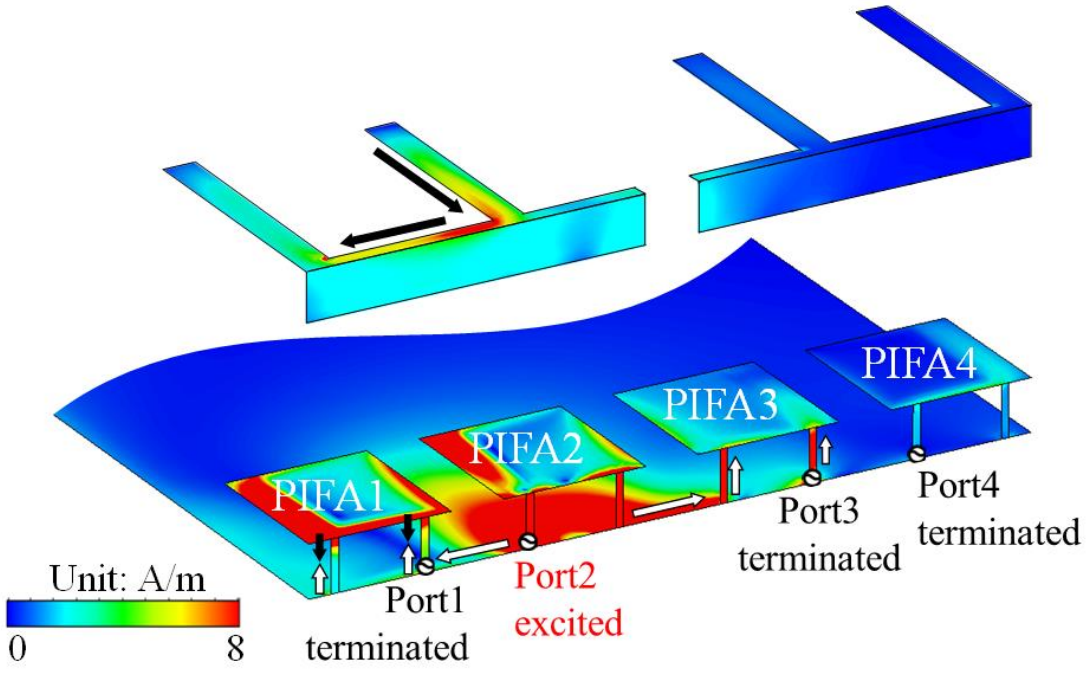

(b) PIFA2 excited

Figure 4.13: Current distribution of four PIFAs with PEs and BLs (2.0 GHz)

4.5 Fabrication and Measurement

To validate the simulation results shown in the previous section, a prototype of four PIFAs with PEs and BLs was fabricated and measured, as shown in Fig. 4.14. In this prototype, several pieces of Styrofoam with a thickness of 0.5 mm are inserted between the PIFAs and PEs to maintain an air gap between them. The simulation and measurement S-parameters and radiation patterns results are shown in Fig. 4.15 and Fig. 4.16, respectively. Notably, a good agreement is observed between the simulation and measurement results of S-parameters and radiation patterns; hence, the simulation results is validated.

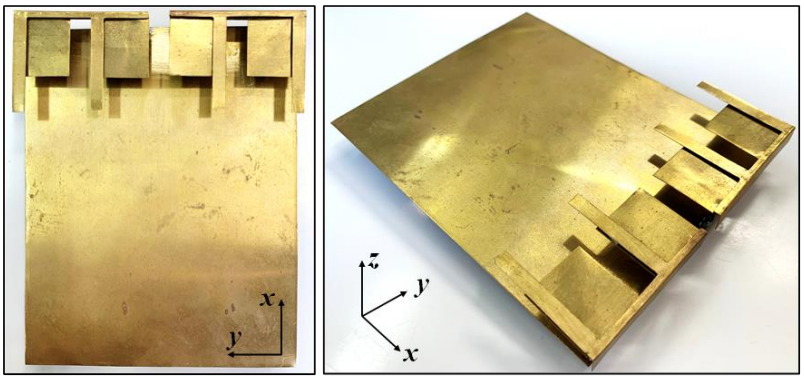

Figure 4.14: Fabricated prototype of four PIFAs with PEs and BLs

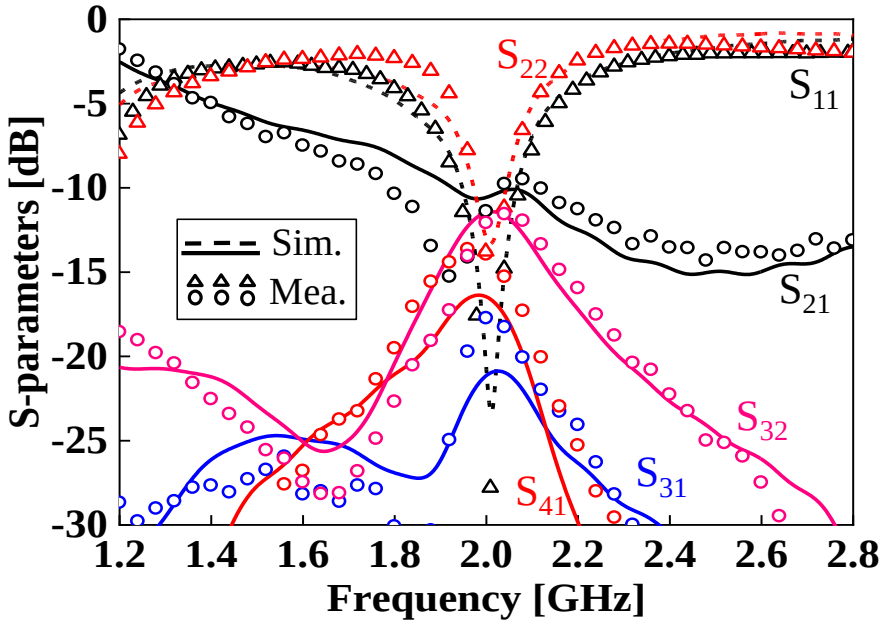

Figure 4.15: Simulation and measurement S-parameters results of four PIFAs with PEs and BLs

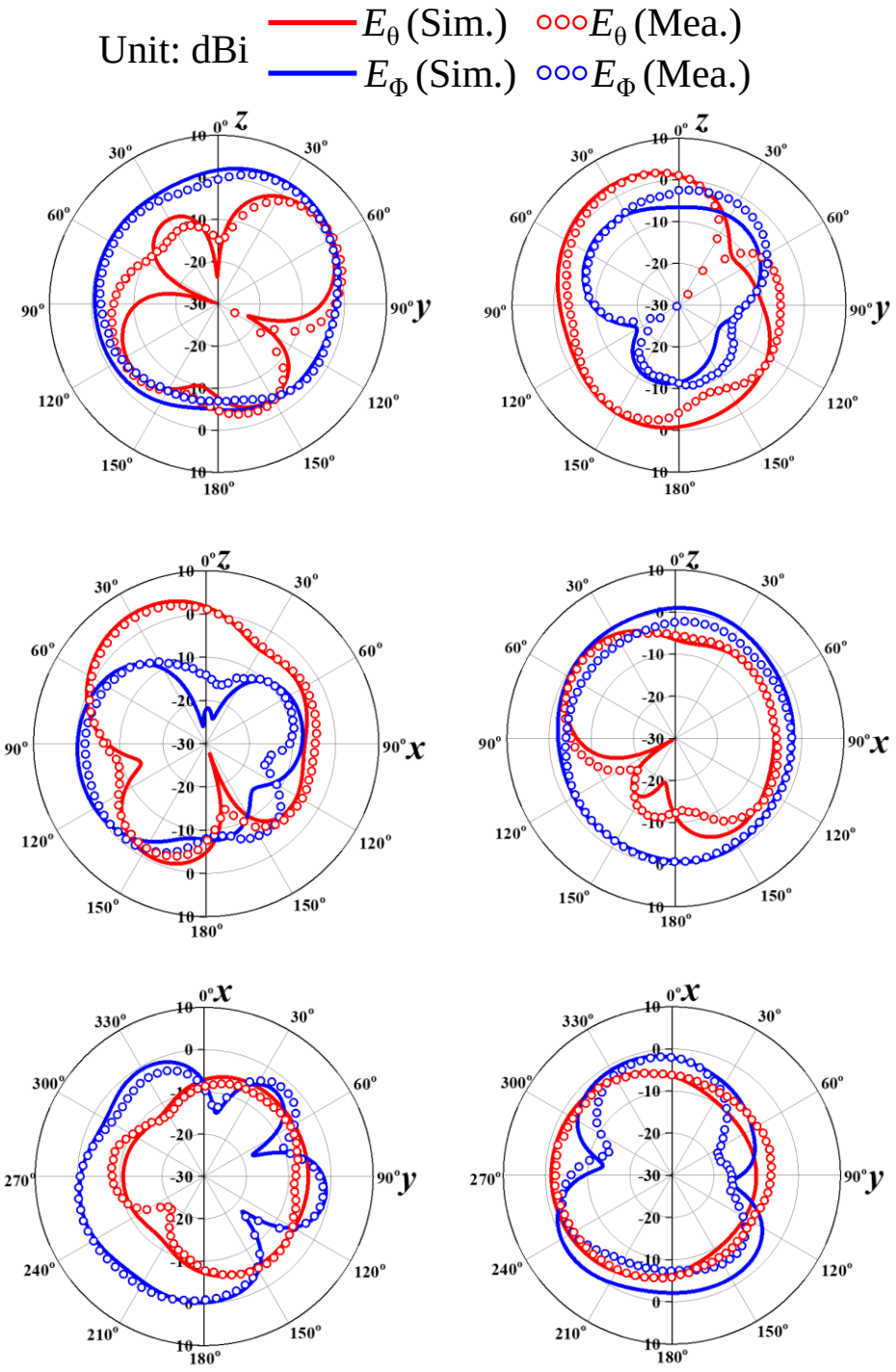

(a) PIFA1 (b) PIFA2

Figure 4.16: Simulation and measurement radiation pattern of PIFA1 and PIFA2 with PEs and BLs

4.6 Comparison with Other Previous Studies

This section compares the proposed method with other previous studies in terms of the edge-to-edge and center-to-center spacing of adjacent elements, isolation, total antenna efficiency, and ECC, as shown in Table 4.1.

The proposed method and other previous methods can be compared as follows: 1) The proposed method is effective even when the edge-to-edge and center-to-center spacings of adjacent elements are only $0.05\lambda_0$ and $0.17\lambda_0$, respectively. These spacings are smaller than those in [53,54,56,58,60-63] and slightly larger than those in [65]. 2) Although the maximum isolation achieved by the proposed method is only 10 dB, the total antenna efficiency at the desired frequency can be significantly improved to 84.8% for PIFA1 and PIFA4 and to 74.2% for PIFA2 and PIFA3. However, in other studies, such as [63,65], even if a good improvement in isolation is obtained, there is almost no improvement in the total antenna efficiency. 3) Similar to other methods, the ECC value at the desired resonant frequency after loading the proposed PEs and BLs is less than 0.05, which is an extremely small level.

Table 4.1: Comparison with previous studies

Ref.	Decoupling method	No. of port	Center frequency [GHz]	Edge-to-edge spacing of adjacent element	Center-to-center spacing of adjacent element	Isolation [dB]	Total antenna efficiency [%]	ECC
[53]	None	4	2.7	0.09λ	0.18λ	>11	-	<0.07
[54]	None	4	2.4 and 5.5	0.23λ	0.33λ	>13	-	<0.05
[56]	None	8	3.5	0.22λ	-	>17.5	76	<0.05
[58]	None	4	4.15	-	0.23λ	>15	>80	<0.03
[60]	None	4	3.5 and 4.9	0.85λ (ant.1 – ant.3)	-	>15	65 (3.5 GHz) 70 (4.9 GHz)	<0.1
[61]	Mode cancellation	8	3.75	0.44λ (ant.2 – ant.3)	-	>10.5	76	<0.08
[62]	Defected ground structure	8	6.85	0.23λ	0.33λ	>15	70	<0.2
[63]	Defected ground structure and metal wall	4	1.264	0.2λ	0.5λ	>16.2	85%	<0.005
[65]	Metal wall	4	2.7	0.02λ	0.17λ	>11	66 @3.5 GHz 68 @5.7 GHz	<0.08
This study	**PEs&BLs**	**4**	**2.0**	**0.05λ**	**0.17λ**	**>10**	**84.8 (PIFA1&4) 74.2 (PIFA2&3)**	**<0.05**

λ: wavelength at the lowest resonant frequency; - : cannot found in source

4.7 Summary

In this chapter, a decoupling method using PEs and BLs was proposed for four PIFAs that are closely arranged on a ground plane. As the number of PIFAs increases to four, decoupling becomes considerably more complicated, and impedance mismatch is also an issue to be considered. Therefore, PEs and BLs were functionally developed to simultaneously achieve low mutual coupling and improve impedance matching of the four PIFAs. The simulation results showed that the proposed method could reduce and maintain all mutual coupling for less than −10 dB, which is an acceptable level for MIMO antennas, and simultaneously improve the impedance matching at 2.0 GHz. Although the bandwidth is narrow, the antenna efficiency at 2.0 GHz could be significantly improved from 64.2% to 84.8% for PIFA1 and PIFA4 and from 35.9% to 74.2% for PIFA2 and PIFA3. Therefore, the proposed method can be applied to applications that do not require broadband. Moreover, the proposed PEs and BLs only need to be loaded onto the four PIFAs, so there is no need to redesign the original sizes and structure of the PIFAs. The four PIFAs with PEs and BLs were fabricated and measured, and a good agreement was observed between the simulation and measurement results of S-parameters and radiation patterns. Hence, the proposed method was validated.

Chapter 5
Conclusion

This dissertation proposed a novel decoupling method to improve the performance of multiple planar inverted-F antennas (PIFAs), which are closely spaced on a ground plane. The proposed decoupling method consisting of parasitic elements (PEs) and bridge line (BL), which are loaded onto the PIFAs. An attractive feature of the proposed method is that the PEs and BLs only need to be loaded onto the PIFAs, so there is no need to redesign the original sizes and structure of the PIFAs. This is useful in improving antenna performance when design conditions make it difficult to redesign the original antenna, for example, for small modular antennas. The design target of this dissertation is to reduce and maintain all the return loss and mutual coupling at 2.0 GHz for less than −10 dB, which are acceptable levels for MIMO antennas.

Below is a summary of the contents that were described from Chapter 1 to Chapter 5 of this dissertation.

In Chapter 1, the background, motivation, and objective of the study in this dissertation were presented.

In Chapter 2, the proposed method was investigated for two PIFAs with the feeding pins facing each other as a primary study. By using the proposed decoupling method, the mutual coupling decreased from −6.6 to −14.1 dB, and good impedance matching was maintained simultaneously at the desired resonant frequency of 2.0 GHz. Therefore, the total antenna efficiency improved from 77.4% to 94.6%. The decoupling principle of the proposed method was quantitatively discussed using Characteristic Mode Analysis (CMA). As a result, by loading the PEs and a BL onto the two PIFAs, the total inner product value changes from −0.43 to −0.11, indicating that the currents excited by Port1 and Port2 are orthogonal to each other. For this reason, the interplay between them becomes weaker, and thus, mutual coupling is reduced.

In Chapter 3, the PEs and BL proposed in Chapter 2 were developed to increase the operating frequency band and decouple the two PIFAs at these frequency bands. The dual-band design for 1-element PIFA using PE was performed firstly. The simulation results show that the PE excite a new current mode on the upper surface of PIFA patch to

help PIFA operate at the dual band of 2.0-GHz and 2.4-GHz band. Subsequently, the PEs were connected by a BL, then loaded onto the two PIFAs. By loading the proposed PEs and BL onto the two PIFAs, two resonances with good impedance matching can be obtained at 2.0 and 2.4 GHz. Moreover, the mutual coupling at these frequencies is reduced to −14.6 dB and −14.4 dB, respectively. Therefore, the total antenna efficiency was improved from 77.4% to 95.2% at 2.0 GHz, and from 66.9% to 90.0 % at 2.4 GHz. For the decoupling principle at the 2.0-GHz band, the PEs reduce a portion of the current flowing from Port1 to Port2, while the BL transmits a strong current to cancel the coupling current flowing on the feeding pin of PIFA2. For the 2.4-GHz case, the combination of PEs and BL acts as a self-decoupling structure when they are loaded onto PIFA patches. Moreover, the versatility of the proposed method was verified by applying it to other frequency bands.

In Chapter 4, the method using PEs and BLs was investigated to reduce the mutual coupling between four PIFAs. As the number of PIFAs increases to four, decoupling becomes considerably more complicated, and impedance mismatch is also an issue to be considered. Therefore, PEs and BLs were functionally developed to simultaneously achieve low mutual coupling and improve impedance matching of the four PIFAs. The simulation results show that the proposed method could reduce and maintain all mutual coupling for less than −10 dB, and simultaneously improve the impedance matching at 2.0 GHz. Although the bandwidth is narrow, the antenna efficiency at 2.0 GHz could be significantly improved from 64.2% to 84.8% for PIFA1 and PIFA4 and from 35.9% to 74.2% for PIFA2 and PIFA3.

From the results obtained above, it can be concluded that the design target of this dissertation has been achieved.

By loading the proposed PEs and BLs onto the PIFAs, the performances of the antenna are significantly improved. However, the PEs and BLs also increase the overall antenna size and make the structure more complex. Therefore, the space saving of PEs and BLs as well as the improvement of the bandwidth should also be considered in the future.

Appendices

A Decoupling Method for Two PIFAs Using CMA

From the results in Chapter 2 (Section 2.5), it is clarified that if the total inner product value is adjusted closer to zero, the mutual coupling can be reduced. Based on this principle, instead of PIFA elements, the current modes on the ground plane will be investigated to adjust the total inner product value close to zero and then another decoupling method will be proposed in this section.

A.1 Ground Plane Current Modes and Proposed Decoupling Method

In the case of the original two PIFAs (without PEs and BL), the total inner product value was −0.43, which is a negative value, as shown in Section 2.5. This means that the total amplitude of the MWC of all anti-phase modes is larger than that of all the in-phase modes. Therefore, to adjust the total inner product value close to zero, it is necessary to increase the amplitude of the MWC in the in-phase modes without changing the MWC in the anti-phase modes as much as possible. To achieve this, the current distribution on ground plane in each mode needs to be carefully considered. Figure A.1(a) depicts the specific current distribution on the ground plane in the in-phase and anti-phase modes, and Fig. A.1(b) depicts the schematic diagram of their strong current positions. In order to increase the amplitude of MWC in in-phase modes without changing the MWC in anti-phase modes as much as possible, four places where the in-phase mode current is strong should be selected as the design positions, as shown in Fig. A.1(b). In particular, this section will focus mainly on Mode 1 to increase its MWC amplitude because it is the dominant in-phase mode.

In order to increase the amplitude of the MWC in Mode 1, it is necessary to increase the current of the ground plane in Mode 1. By simulation, it has been studied that when a thin conductor is placed in a position on the ground plane where the current is strong, the current usually flows strongly on that thin conductor. Therefore, as shown in Fig. A.2, four inverted-L-shaped elements (ILSEs) are placed at selected design positions, where the in-phase mode current is strong. The total length of the ILSEs is set to 33 mm, and the width is 1 mm after performing a parametric study. Table A.1 shows the MWC in each mode and the total inner product value of the PIFAs with four ILSEs.

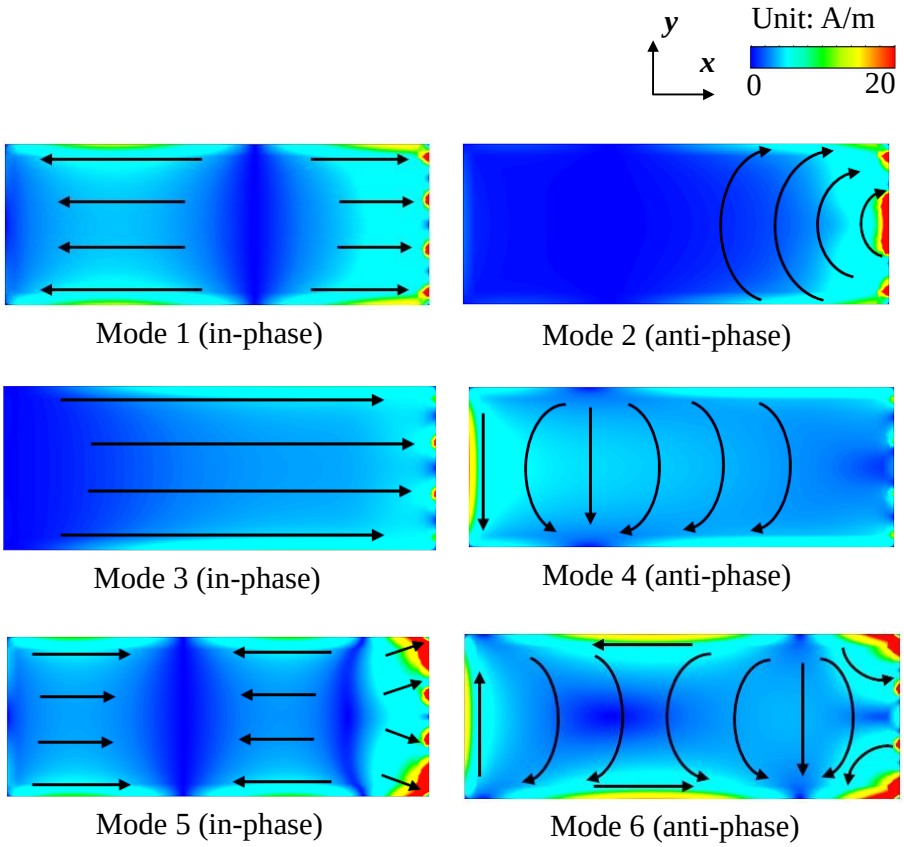

(a) Specific current distribution in each mode

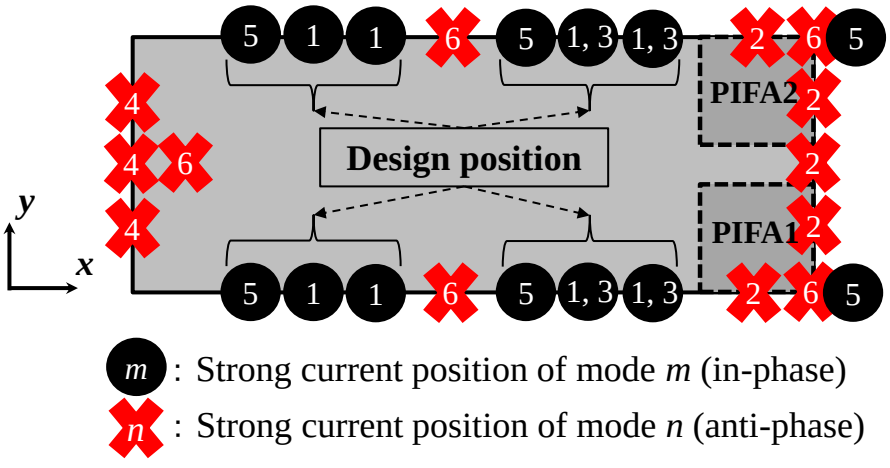

(b) Schematic diagram of strong current positions

Figure A.1: Current distribution on ground plane (2.0 GHz)

In the case of the original PIFAs, the amplitude of the MWC in Mode 1 is 0.47, as shown in Table 2.1 (Chapter 2). However, placing the ILSEs increased it to 0.64. Thus, the inner product of Mode 1 changes remarkably from 0.22 to 0.41. The amplitude of MWC in other modes also changes but is insignificant compared to Mode 1. Therefore, the total inner product value is adjusted to −0.3, and the correlation coefficient is −0.25, which is closer to zero than that in the case without the ILSEs.

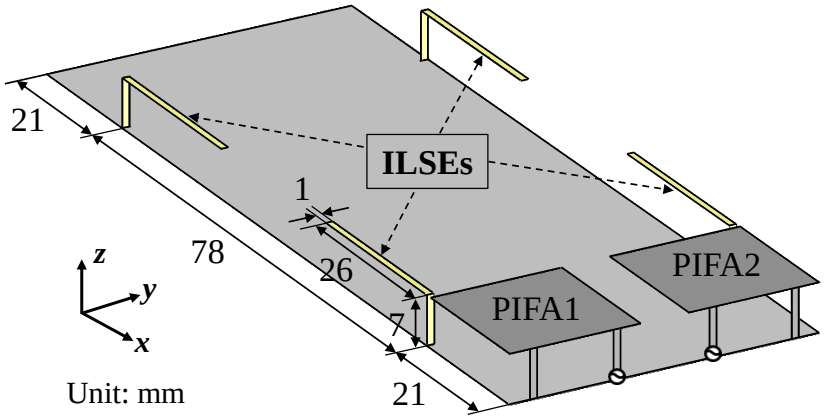

Figure A.2: Structure of PIFA with four ILSEs

Table A.1: MWC in each mode and total inner product value (with four ILSEs)

Mode	MWC (port1)		MWC (port2)				
	Amplitude	Phase (deg.)	Amplitude	Phase (deg.)	Phase difference (deg.)	Inner product of each mode	Total inner product
1	0.64	170.5	0.64	107.5	0	0.41	
2	0.8	-14.4	0.8	165.6	180	-0.64	
3	0.05	136.4	0.05	136.4	0	0	
4	0.16	38.3	0.16	-141.7	180	-0.03	**-0.3**
5	0.2	-108.2	0.2	-108.2	0	0.04	
6	0.28	-124.1	0.28	55.9	180	-0.08	

A.2 Comparison of Characteristics

In order to confirm the effectiveness of the proposed four ILSEs, several characteristics such as the S-parameters, total antenna efficiency, current distribution and radiation pattern are compared between the two PIFAs with and without four ILSEs.

Figure A.3 shows the S-parameters of the two PIFAs with and without the four ILSEs. As shown, when the four ILSEs are placed, the mutual coupling reduces appreciably from –6.6 to –10.2 dB at 2.0 GHz. Furthermore, although the bandwidth is slightly narrower, the resonant frequency at 2.0 GHz with good impedance matching is maintained to be less than –10 dB. Figure A.4 shows the total antenna efficiency of the two PIFAs with and without the four ILSEs. As shown, the use of four ILSEs can improve the total antenna efficiency improved significantly from 77.4% to 86.1% at the desired frequency of 2.0 GHz.

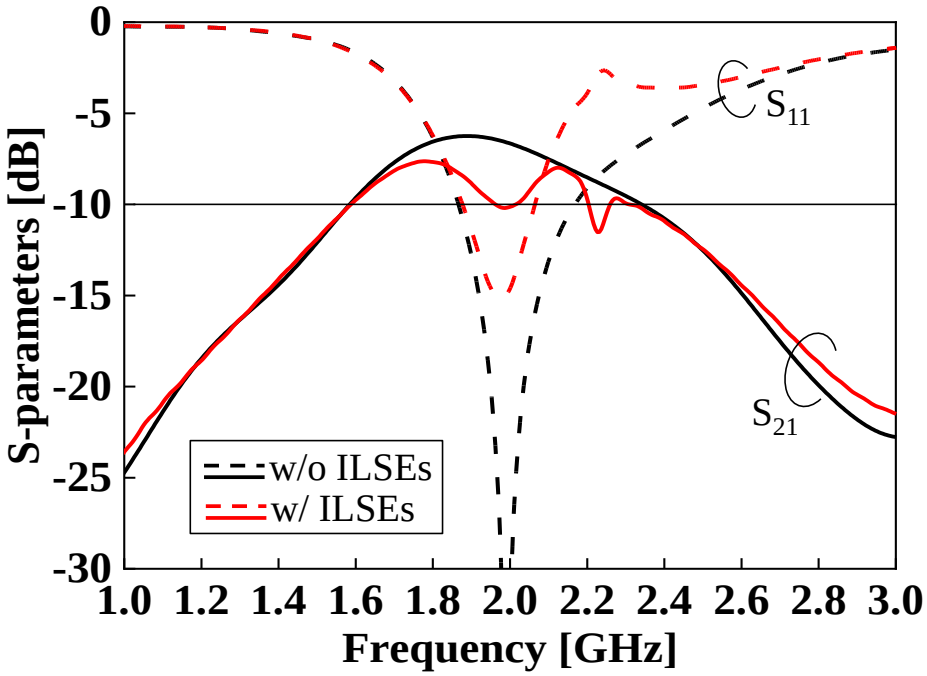

Figure A.3: S-parameters of two PIFAs with and without four ILSEs

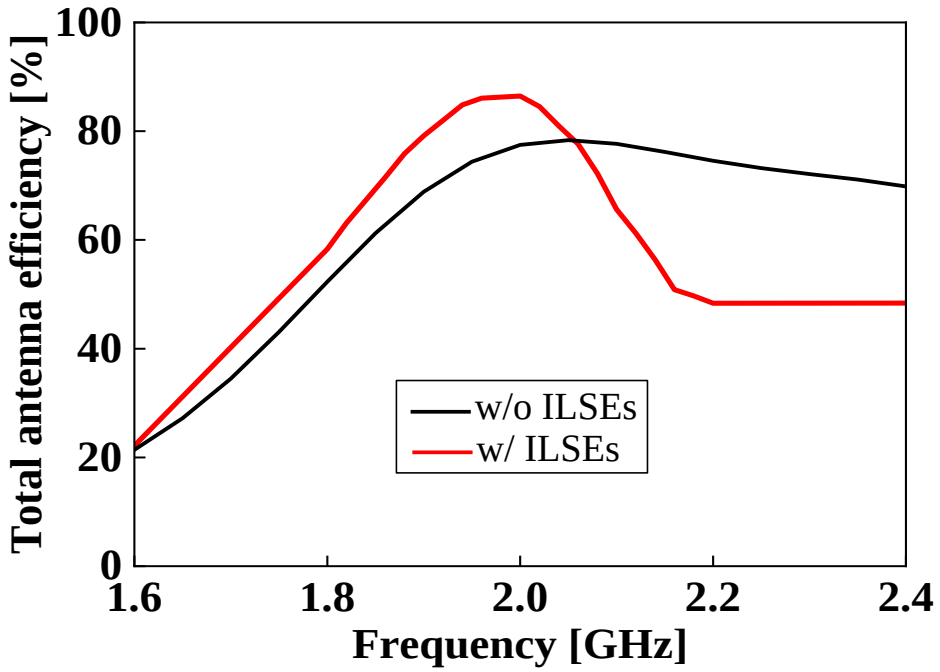

Figure A.4: Total antenna efficiency of two PIFAs with and without four ILSEs

Figures A.5(a) and (b) show the current distributions of the two PIFAs without and with four ILSEs at 2.0 GHz, respectively. In both cases, Port1 is excited and Port2 is terminated by a 50-Ω load. As shown, in the case with ILSEs, a strong current flow on the ILSEs, which are placed in PIFA1 side. Especially, it is observed that the coupling current flowing from Port1 to Port2 is reduced compared to the case without ILSEs. Therefore, the decoupling effectiveness of the proposed four ILSEs is confirmed.

The radiation patterns at 2.0 GHz of the PIFA1 without and with four ILSEs are shown in Figs. A.6(a) and (b), respectively. It is clear that the radiation pattern changes at some positions when the four ILSEs are placed, but the gains are still maintained in all planes. Therefore, it can be concluded that the four ILSEs do not significantly affect the radiation pattern of the two PIFAs.

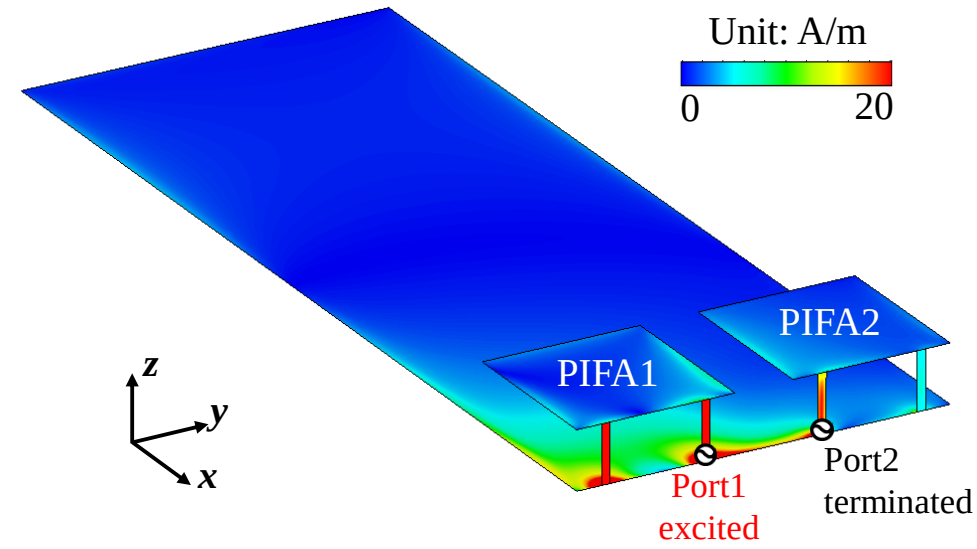

(a) without four ILSEs

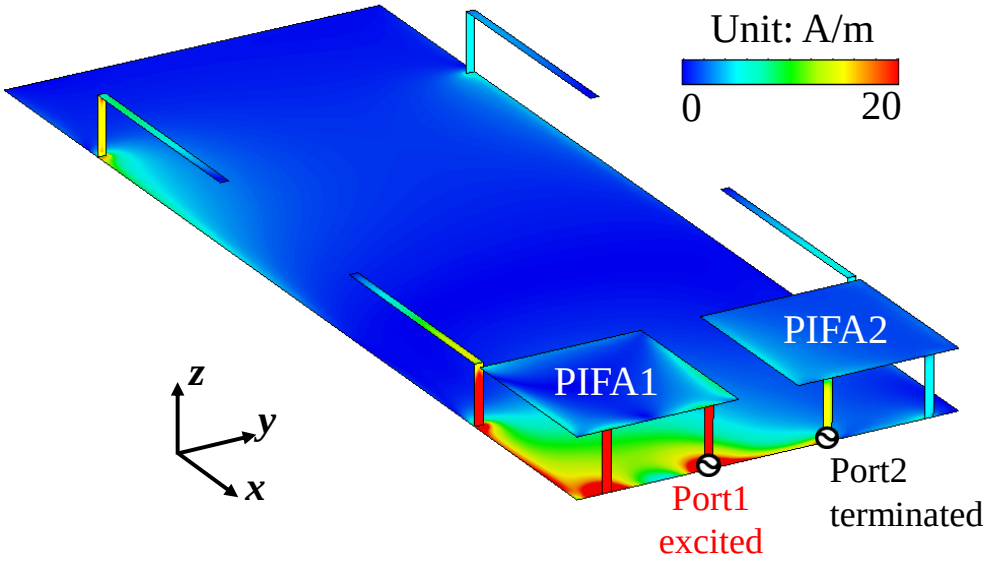

(b) with four ILSEs

Figure A.5: Current distribution of two PIFAs (2.0 GHz)

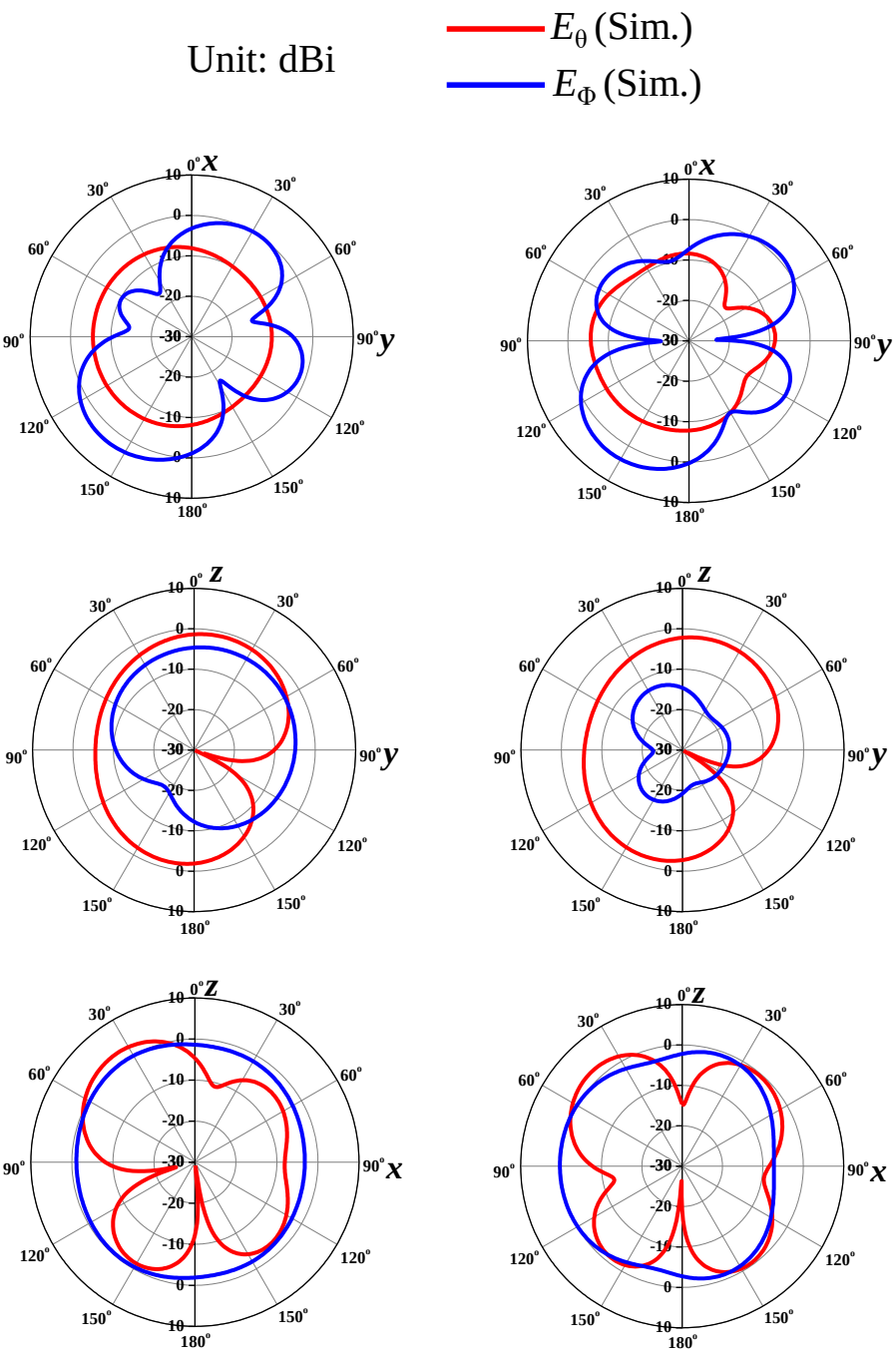

(a) without four ILSEs (b) with four ILSEs

Figure A.6: Radiation pattern of PIFA1

A.3 Fabrication and Measurement

Figures A.7 and A.8 show a photograph of the fabricated two PIFAs with four ILSEs, and their simulation and measurement S-parameters result, respectively. A good agreement is observed between the simulation and measurement S-parameters result as shown in Fig. A.8. The simulation and measurement radiation patterns at 2.0 GHz of the PIFAs with four ILSEs are shown in Fig. A.9. Only the radiation patterns of PIFA1 are shown owing to the symmetrical structure of the PIFAs. The simulation results are validated by their consistency with the measurement results.

Figure A.7: Fabricated PIFAs with four ILSEs

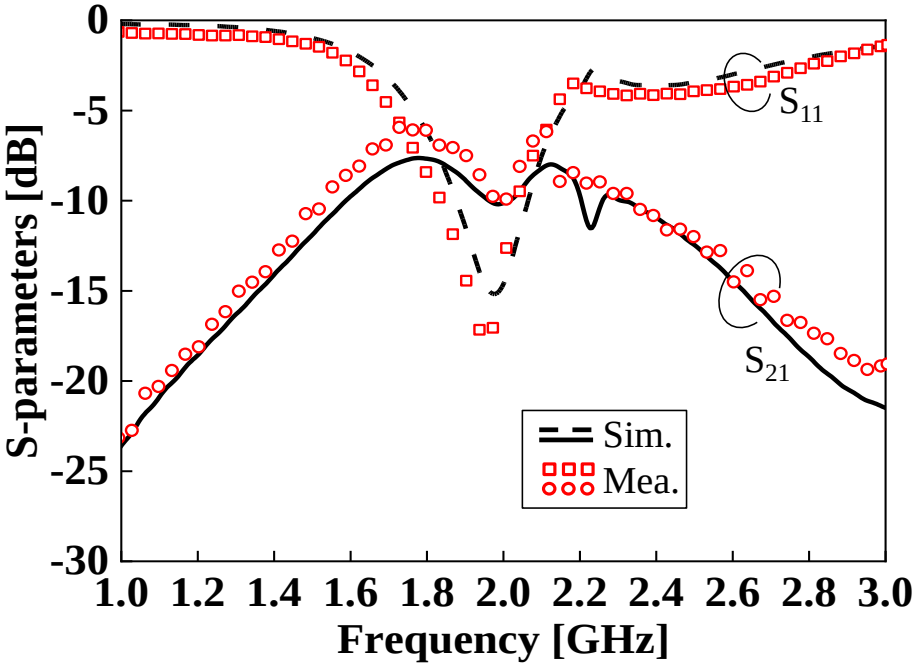

Figure A.8: Simulation and measurement S-parameters result of two PIFAs with four ILSEs

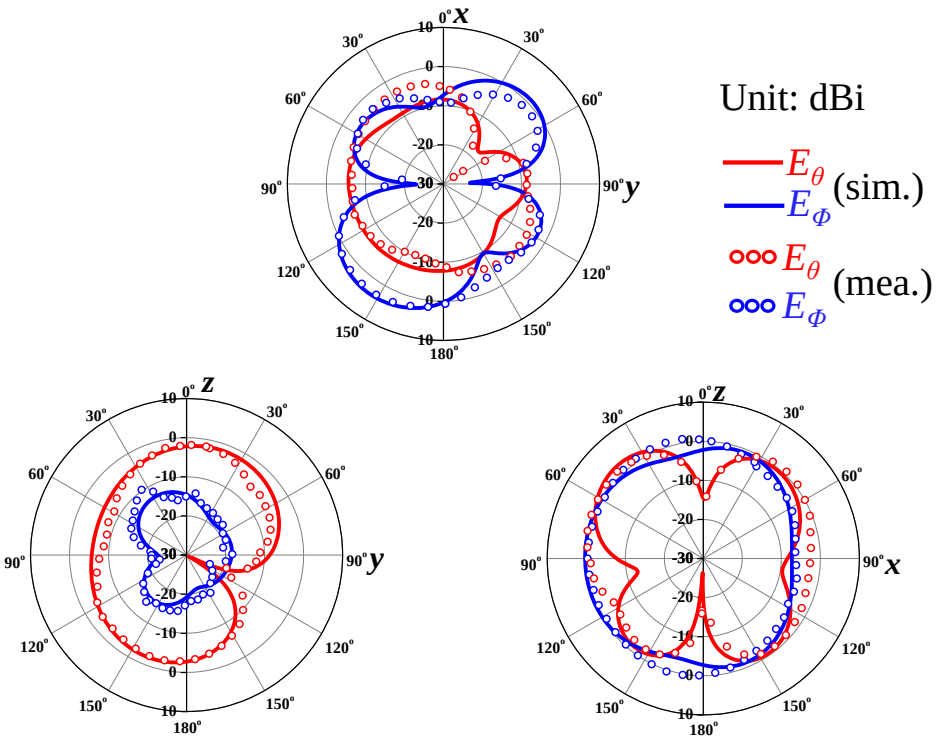

Figure A.9: Simulation and measurement radiation pattern of PIFA1 with four ILSEs

B Antenna Design for WiMAX Using CMA

To enhance the communication quality for wireless devices, the built-in antennas are required to cover a wider bandwidth with an even more compact design. Therefore, the design of antennas with broadband characteristics is one of the important concepts in the development of antennas for wireless devices. In [66], a U-shaped folded dipole antenna (UFDA) consisting of a UFDA element and a ground plane (GP) with small size have been proposed. The proposed antenna could be installed inside a wireless device for worldwide interoperability for microwave access (WiMAX). By using a suitable objective function in a particle swarm optimization (PSO), the designed UFDA covered dual frequency bands from 2.3 GHz to 2.7 GHz and from 3.4 GHz to 3.8 GHz for $S_{11} \leq -6$ dB. Furthermore, the occupancy area of the antenna was reduced to 23.1% of the previous optimized UFDA. Although the optimal sizes of the antenna could be only obtained by the PSO design, the physical mechanism of the antenna was not clear.

Therefore, in this section, the characteristic mode analysis (CMA) is utilized as an effective method for the broadband design while understanding the physical mechanism of each part of the UFDA element and the GP. First, the characteristic modes of the UFDA on the GP are analyzed. After considering the physical mechanism of each part of the UFDA element and the GP, the antenna is designed to cover completely dual frequency bands of the WiMAX.

B.1 Antenna structure and CMA result

Firstly, two parts of the antenna (UFDA element only and GP) are separated and analyzed independently. After determining the resonant frequencies and characteristics (broadband or narrowband) of modes of these separated parts, they are combined to return the initial model, then analyze with CMA.

Figure B.1(a) shows the GP with the overall length of 75 mm×31 mm and its MS. The modes are observed between 1.0 and 5.5 GHz including frequency bands of WiMAX. Two resonances appear at the frequency of 1.7 GHz (Mode 1) and 3.9 GHz (Mode 2) and both of them have wide bandwidth defined by MS > 0.707. The antenna element has a folded dipole antenna bent into U-shape with detailed dimensions and its MS are shown in Fig. B.1(b). As can be seen, three resonances at the frequency of 1.8 GHz (Mode 3), 2.8 GHz (Mode 4) and 5.1 GHz (Mode 5) appear after analyzing the UFDA element only.

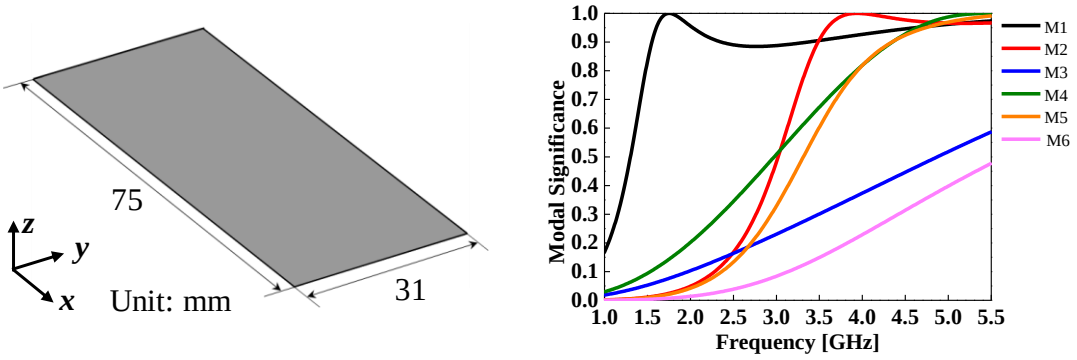

(a) GP only and its MS

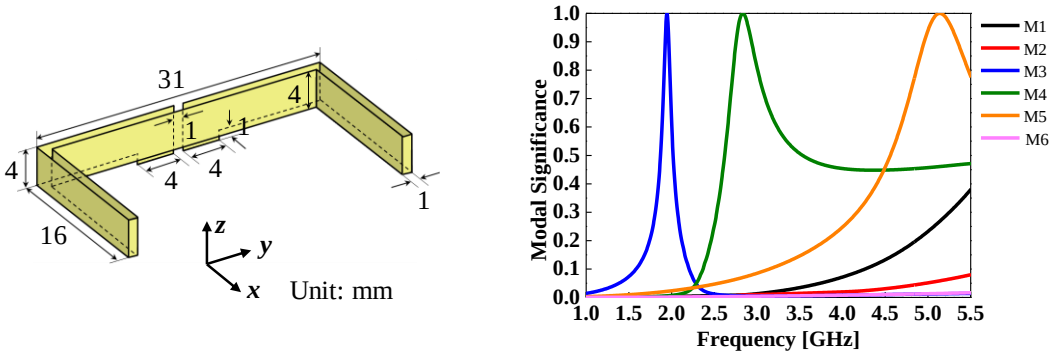

(b) UFDA element only and its MS

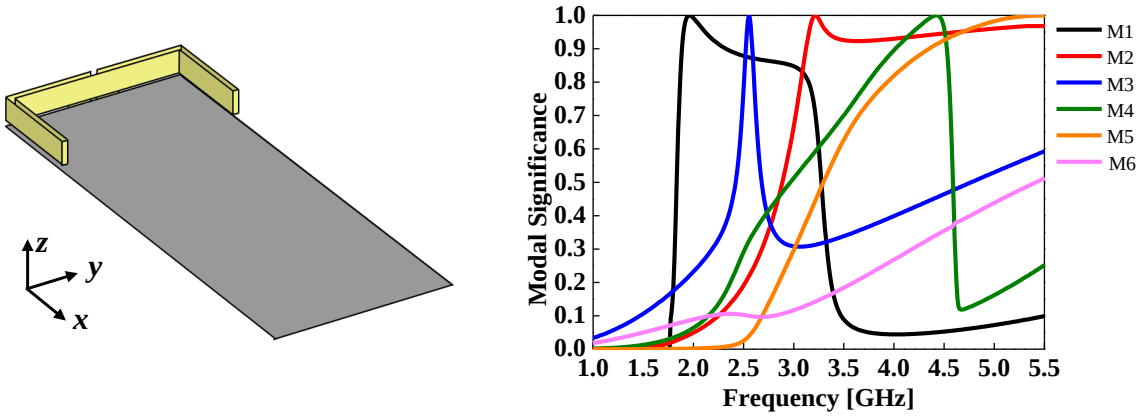

(c) The combined model and its MS

Figure B.1: The structure of UFDA and MS results

By comparing the bandwidth of mode between GP only and UFDA element only, it is obvious that the modes of UFDA element only have narrower bandwidth than the modes of the GP only. Figure B.1(c) shows the MS of the combined model of the GP and the

UFDA element without feeding. By analyzing the combined model, four modes are defined including 1.9 GHz (Mode 1), 3.2 GHz (Mode 2), 2.5 GHz (Mode 3) and 4.4 GHz (Mode 4). With the same way of examining the characteristics of each mode, it is clear that Modes 1 and 2 of the combined model have wide bandwidth, similar to Modes 1 and 2 of the GP only shown in Fig. B.1(a). Meanwhile, Mode 3 and Mode 4 of the combined have narrower bandwidth, similar to Mode 3 and Mode 4 of the UFDA element only shown in Fig. B.1(b).

By observing these bandwidth similarities in the aspect of modes, it is possible to recognize which separation part of the antenna affects which mode the most. However, the mode of each part shifted to different frequency when the UFDA element and the GP are combined. Thus, the validity of them is needed to be confirmed by comparing the surface current distribution at each resonant frequency of mode between separated parts and the combined model. Figure B.2(a) shows the surface current distribution of GP only at 1.7 GHz (Mode 1) and of the combined model at 1.9 GHz (Mode 1). Figure B.2(b) shows the surface current distribution of GP only at 3.9 GHz (Mode 2) and of the combined at 3.2 GHz (Mode 2). As shown, the locations of current maxima or minima are at the same position and the direction of the currents are also similar to both of GP. This verified that Modes 1 and 2 are the mode of the GP. Figure B.2(c) shows the surface current distribution of UFDA element only at 1.8 GHz (Mode 3) and of the combined model at 2.5 GHz (Mode 3). Figure B.2(d) shows the surface current distribution of UFDA only at 2.5 GHz (Mode 4) and of the combined model at 4.4 GHz (Mode 4). As shown, the surface current distributions are similar on the UFDA element, and the directions are in the same direction to each other. This verified that that Mode 3 and Mode 4 are the modes of the UFDA element.

The simulation S_{11} of the combined model after feeding is indicated as Fig. B.3. The UFDA element is fed by a 50-Ω source at feeding strip and connected to the GP at the shorting strip. As can be seen, three resonances appear at 1.8 GHz, 2.6 GHz, and 3.4 GHz, and they have the same resonant frequency of Mode 1, Mode 3 and Mode 2 in CMA result, respectively. Thus, the validity of CMA result was confirmed. For convenience, these resonances are called by the first, the second and the third resonance, respectively.

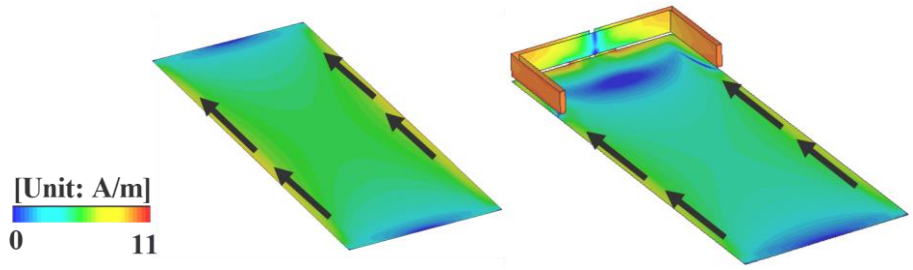

(a) GP only (1.7 GHz) and combined model (1.9 GHz)

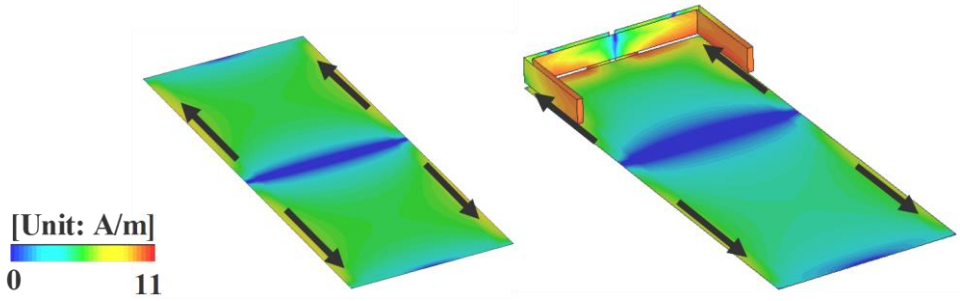

(b) GP only (3.9 GHz) and combined model (3.2 GHz)

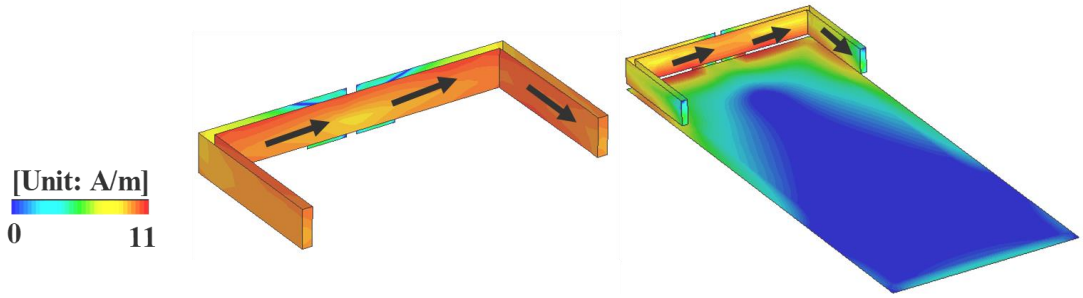

(c) UFDA element only (1.8 GHz) and combined model (2.5 GHz)

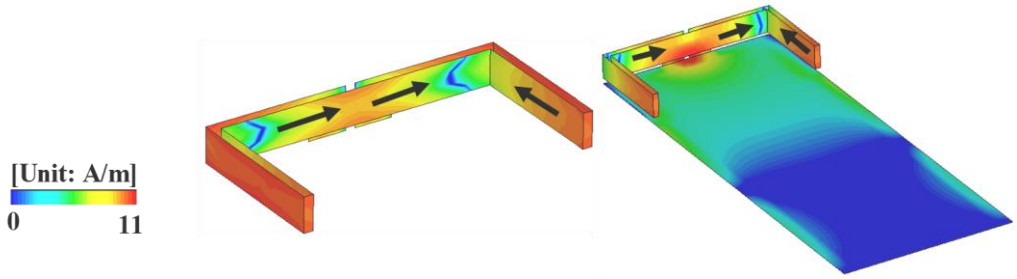

(d) UFDA element only (2.5 GHz) and combined model (4.4 GHz)

Figure B.2: The comparison of current contributions

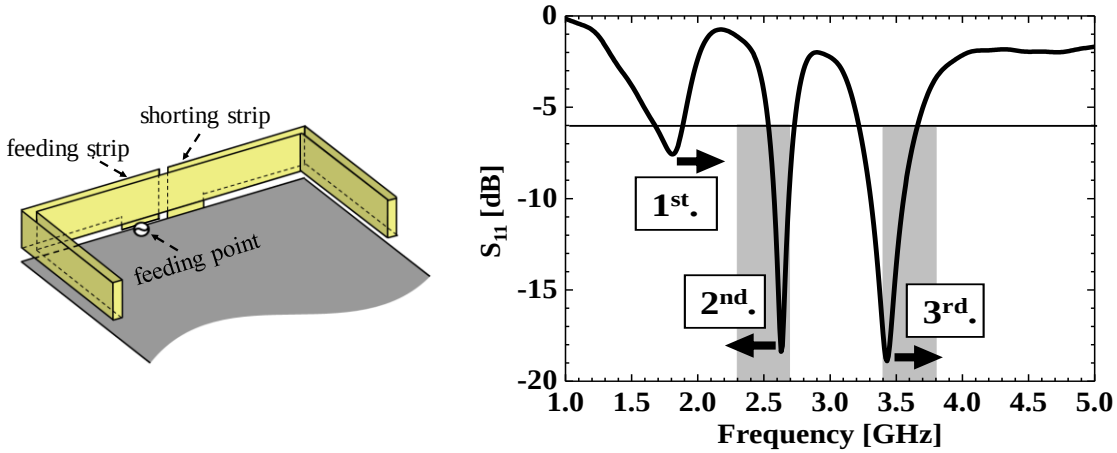

Figure B.3: Simulation S_{11} of combined model

By comparing with the result of CMA, it can be concluded that the first and third resonance are associated with Modes 1 and 2 of GP. Meanwhile, the second one is associated with Mode 3 of the UFDA element. Moreover, the gray ranges in Fig. B.3 present two frequency bandwidths of WiMAX and they are not covered completely for $S_{11} \leq -6$ dB. Therefore, in order to cover completely these frequency bandwidths, the shape of GP should be adjusted to the first and third resonance shifting to higher frequency, while the shape of UFDA element should be adjusted to the second resonance shifting to lower frequency.

B.2 Antenna Design

Figure B.4(a) shows the design for GP only, which mostly affected Modes 1 and 2 of CMA result. After observing the common position of maximum current distribution on the GP shown in Fig. B.2(a) and (b), two parts on the GP are trimmed with a dimension of 10 mm×5 mm. Therefore, resonant frequency of Modes 1 and 2 could be shifted to higher frequency. While, for the UFDA element only, resonant frequency of Mode 3 shift to lower frequency when a center part of the UFDA element is reduced from 4 mm to 2 mm, as shown in Fig. B.4(b). After obtaining two separated parts with desired design, the new UFDA is combined, and its CMA result is shown in Fig. B.4(c). As shown, the resonant frequencies of Modes 1 and 2 shift to higher frequency (2.1 GHz and 3.3 GHz, respectively), the resonant frequency of Mode 3 shifts to lower frequency (2.3 GHz) compared to the initial UFDA as shown in Fig. B.1(c).

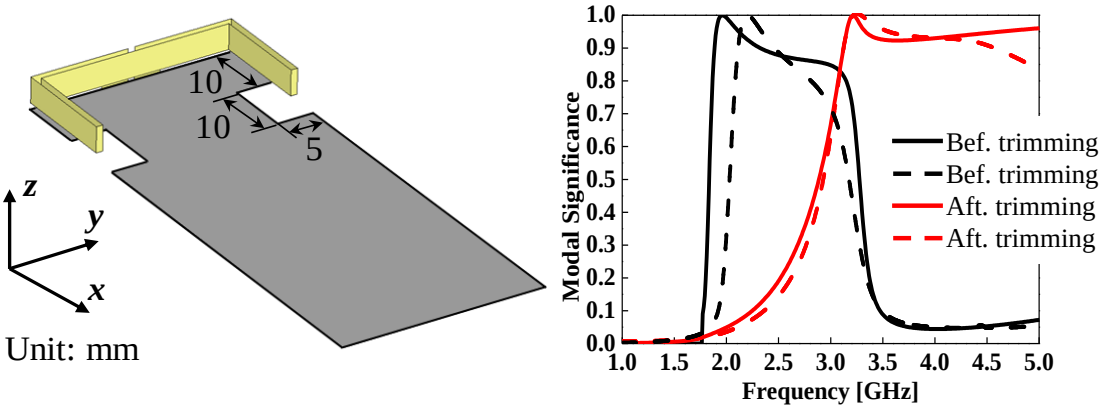

(a) Design for the GP only

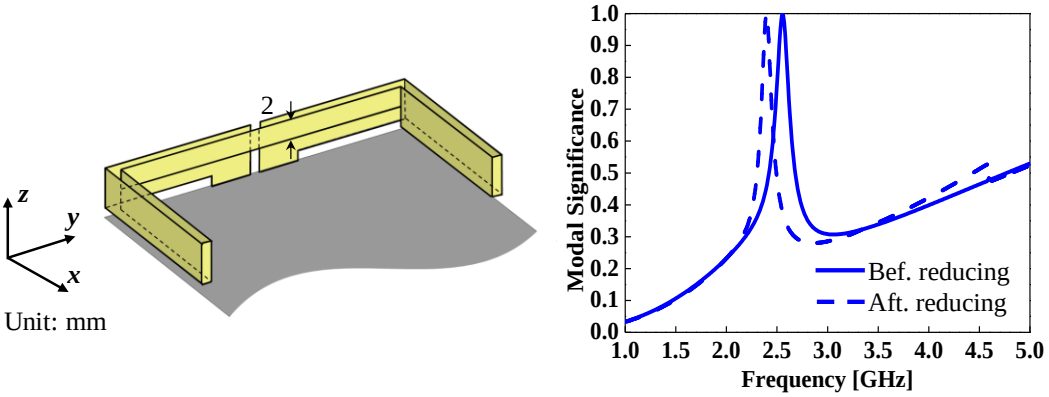

(b) Design for the UFDA element only

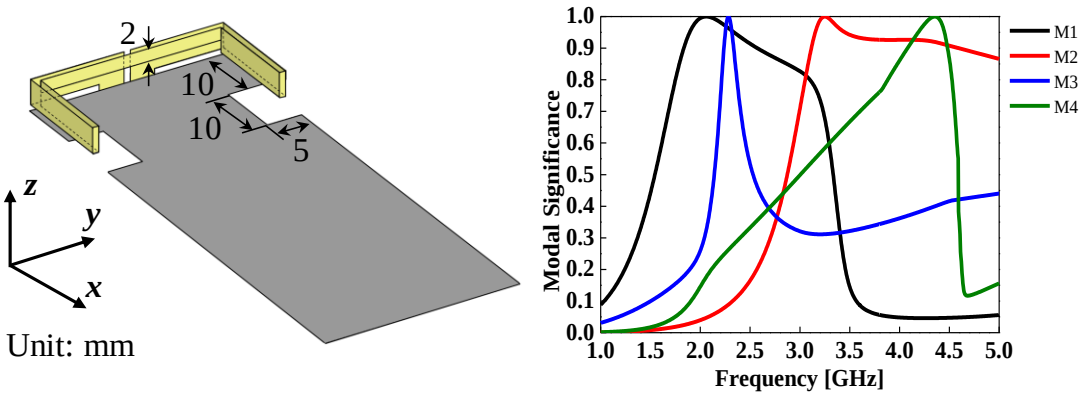

(c) Combined model of UFDA after designing (proposed model)

Figure B.4: Design for UFDA to cover WiMAX bandwidths

B.3 Fabrication and Measurement

Figures B.5 shows fabricated prototype, simulation and measurement results of S_{11} and radiation pattern of the proposed model, respectively. As shown, the bandwidth of the proposed model is wider than the initial model from 2 GHz to 2.7 GHz and from 3.3 GHz to 3.9 GHz, which could cover completely the WiMAX frequency bands. Moreover, a good agreement is observed between the simulation and measurement S_{11} and radiation pattern in the *yz* plane; hence, the simulation results is validated.

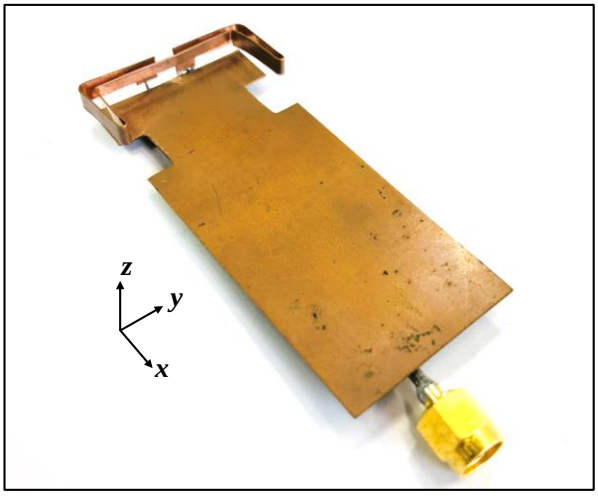

(a) Fabricated prototype of proposed model

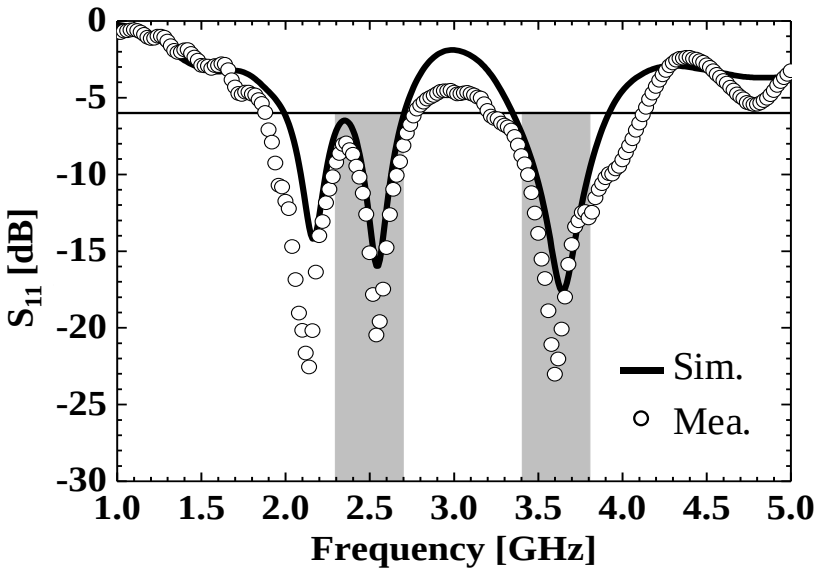

(b) Simulation and measurement S_{11}

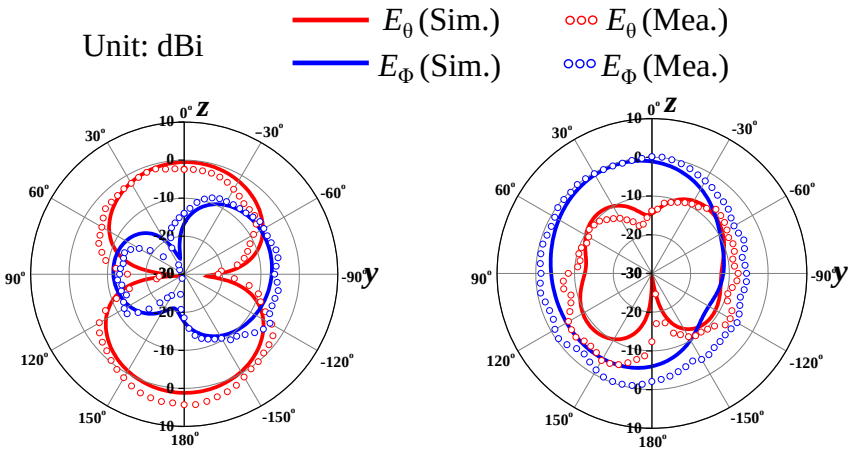

(c) Simulation and measurement radiation pattern of *yz* plane

Figure B.5: Fabricated prototype, simulation and measurement results of proposed model

Acknowledgements

First, I want to express my deepest appreciation to my direct supervisor, Professor Hisashi Morishita, who gave me many invaluable supports and advice to complete this dissertation. During my time at Morishita Lab., I have learned a lot of knowledge, thinking as well as effective working methods from him. Not only in my research work, but he also supported me in other aspects of life, and always encouraged me to be more motivated to do my research.

Next, I am truly thankful to Dr. Yoshio Koyanagi and Dr. Hiroshi Sato of *Panasonic System Networks R&D Lab*. for their helpful advice and comments that helped me get design ideas and discover the operating principle of the proposed decoupling methods in this dissertation. Through the meetings, I have received a large amount of knowledge in the field of antennas and propagation from them.

I would like to thank Professor Naobumi Michishita of *National Defense Academy*, Professor Hiroyuki Arai of *Yokohama National University* and Professor Masaharu Takahashi of *Chiba University* for giving me the kind guidance and constructive comments to configure this dissertation.

I also appreciate the sincere cooperation of my senior, peer, and junior colleagues who were with Morishita Lab. and Michishita Lab., including Dr. Tuan Hung Nguyen (*Le Quy Don Technical University*), Dr. Hiroshi Hashiguchi *(National Defense Academy)*, Dr. Yuka Akiyama (*Japan Air Self-Defense Force*), Mr. Naoki Akiyama (*Japan Air Self-Defense Force*), Dr. Kazuya Matsubayashi (*Acquisition, Technology & Logistics Agency*), Dr. Yuta Nakagawa (*Yazaki Corporation*), Mr. Kunihisa Gamo (*Japan Air Self-Defense Force*), Mr. Hikaru Takizawa (*Japan Air Self-Defense Force*), Mr. Tomokazu Mizutani (*Japan Ground Self-Defense Force*), Mr. Taiyo Kai (*Japan Ground Self-Defense Force*), Ms. Yukiko Wada (*Japan Air Self-Defense Force*), Mr. Cong Oai Nguyen (*Vietnam Army*), Mr. Thanh Binh Nguyen (*Vietnam Army*), Mr. Takahiro Hashimoto (*Japan Air Self-Defense Force*), Mr. Takumi Nishime (*Japan Ground Self-Defense Force*), and other bachelor students.

Finally, I want to thank all my family in Vietnam and my host family in Japan for their mental supports, all teachers, officers, assistant staffs, and students who met and helped me a lot all the time I have been in *National Defense Academy*.

References

[1] Ministry of Internal Affairs and Communications (in Japanese). Available: https://www.soumu.go.jp/johotsusintokei/whitepaper/ja/r03/html/nd105220.html

[2] Ministry of Internal Affairs and Communications (in Japanese). Available: https://www.soumu.go.jp/johotsusintokei/field/data/gt010602.pdf

[3] G.J. Foschini, and M.J. Gans, "On Limits of Wireless Communications in a Fading Environment when Using Multiple Antennas," *Wirel. Pers. Commun*., vol. 6, pp. 311-335, 1998.

[4] H. Huang, and J. Wu, "Decoupled Dual-Antenna With Three Slots and a Connecting Line for Mobile Terminals," *IEEE Antennas Wireless Propag. Lett*., vol. 14, pp. 1730-1733, Apr. 2015.

[5] Y. Li, C-Y-D. Sim, Y. Luo, and G. Yang, "High-Isolation 3.5 GHz Eight-Antenna MIMO Array Using Balanced Open-Slot Antenna Element for 5G Smartphones," *IEEE Trans. Antennas Propag*., vol. 67, no. 6, pp. 3820-3830, Jun. 2019.

[6] S. Zhang, B. K. Lau, A. Sunesson, and S. He, "Closely located dual PIFAs with T-slot induced high isolation for MIMO terminals," *2011 IEEE International Symposium on Antennas and Propagation* (APSURSI), Spokane, WA, USA, pp. 2205-2207, Aug. 2011.

[7] X. Yang, Y. Liu, Y-X. Xu, and S-x. Gong, "Isolation Enhancement in Patch Antenna Array With Fractal UC-EBG Structure and Cross Slot," *IEEE Antennas Wireless Propag. Lett*., vol. 16, pp. 2175-2178, May 2017.

[8] F. Caminita, S. Costanzo, G. Di Massa, G. Guarnieri, S. Maci, G. Mauriello, and I. Venneri, "Reduction of Patch Antenna Coupling by Using a Compact EBG Formed by Shorted Strips With Interlocked Branch-Stubs," *IEEE Antennas Wireless Propag. Lett*., vol. 8, pp. 811-814, Apr. 2009.

[9] S.C. Chen, Y.S. Wang, and S.J. Chung, "A Decoupling Technique for Increasing the Port Isolation Between Two Strongly Coupled Antennas," *IEEE Trans. Antennas Propag*., vol. 56, no. 12, pp. 3650-3658, Dec. 2008.

[10] S. Li, and N. Honma, "Decoupling Network Comprising Transmission Lines and Bridge Resistance for Two-Element Array Antenna," *IEICE Trans. Commun*., vol. E97-B, no. 7, pp. 1395-1402, July. 2014.

[11] R. A. Bhatti, S. Yi, and S-O. Park, "Compact Antenna Array With Port Decoupling for LTE-Standardized Mobile Phones," *IEEE Antennas Wireless Propag. Lett.,* vol. 8, pp. 1430-1433, Jan. 2010.

[12] A. Diallo, C. Luxey, P. Thuc, R. Staraj, and G. Kossiavas, "Study and Reduction of the Mutual Coupling Between Two Mobile Phone PIFAs Operating in the DCS1800 and UMTS Bands," *IEEE Trans. Antennas Propag*., vol. 54, no. 11, pp. 3063-3073, Nov. 2006.

[13] S-W. Su, C-T. Lee, and F-S. Chang, "Printed MIMO-Antenna System Using Neutralization-Line Technique for Wireless USB-Dongle Applications," *IEEE Trans. Antennas Propag*., vol .60, no. 2, pp. 456-463, Feb. 2012.

[14] J. Itoh, N.T. Hung, and H. Morishita, "The Mutual Coupling Reduction between Two J-Shaped Folded Monopole Antennas for Handset," *IEICE Trans. Commun*., vol. E94-B, no. 5, pp. 1161-1167, May 2011.

[15] Y. Kim, J. Itoh, and H. Morishita, "Decoupling method between two L-shaped folded monopole antennas for handsets using a bridge line," *IET Microw. Antennas Propag*., vol. 4, no. 7, pp. 863-870, Jul. 2010.

[16] S. Wang, and Z. Du, "Decoupled Dual-Antenna System Using Crossed Neutralization Lines for LTE/WWAN Smartphone Applications," *IEEE Antennas Wireless Propag. Lett*., vol. 14, pp. 523-526, Now. 2015.

[17] R. Waterhouse, "Printed Antennas for Wireless Communications," *John Wiley & Sons*, Hoboken, 2007.

[18] T. Taga, and K. Tsunoda, "Analysis of a Planar Inverted-F Antenna by Spatial Network Method," *IEICE Trans. Commun*., vol. J74-B2, no. 10, pp. 538-545, Oct. 1991. (in Japanese)

[19] J. Wang, and O. Fujiwara, "Electromagnetic Interaction between Built-in

Antennas and a Human Head for 1.5 GHz Portable Telephones," *IEICE Trans. Commun*., vol. J82-B, no. 7, pp. 1417-1419, Jul. 1999. (in Japanese)

[20] M. F. Abedin, and M. Ali, "Modifying the Ground Plane and Its Effect on Planar Inverted-F Antennas (PIFAs) for Mobile Phone Handsets," *IEEE Antennas Wireless Propag. Lett.*, vol. 2, pp. 226-229, 2003.

[21] H. Nakano, Y. Sato, H. Mimaki, and J. Yamauchi, "An inverted FL antenna for dual-frequency operation," *IEEE Trans. Antennas Propag*., vol. 53, no. 8, pp. 2417-2421, Aug. 2005.

[22] T. Tanaka, S. Hayashida, K. Imamura, H. Morishita, and Y. Koyanagi, "A Study on Miniaturization of Antenna for Handset Utilizing Magnetic Materials," *IEICE Trans. Commun*., vol. J87-B, no. 9, pp. 1327-1335, Sept. 2004. (in Japanese)

[23] H. Morishita, "Small Mobile Terminal Antennas: From Design Concept to Future Perspective," *IEICE Trans. Commun*., vol. J88-B, no. 9, pp. 1601-1612, Sept. 2005. (in Japanese)

[24] P. Jin, and R. W. Ziolkowski, "High-Directivity, Electrically Small, Low-Profile Near-Field Resonant Parasitic Antennas," *IEEE Antennas Wireless Propag. Lett.,* vol. 11, pp. 305-309, Mar. 2012.

[25] S. T. Fan, Y. Z. Yin, B. Lee, W. Hu, and X. Yang, "Bandwidth Enhancement of a Printed Slot Antenna With a Pair of Parasitic Patches," *IEEE Antennas Wireless Propag. Lett*., vol. 11, pp. 1230-1233, Oct. 2012.

[26] K-L. Wong, W-J. Chen, L-C. Chou, and M-R. Hsu, "Bandwidth Enhancement of the Small-Size Internal Laptop Computer Antenna Using a Parasitic Open Slot for Penta-Band WWAN Operation," *IEEE Trans. Antennas Propag*., vol. 58, no. 10, pp. 3431-3415, Jul. 2010.

[27] P. Hallbjorner, "The significance of radiation efficiencies when using S-parameters to calculate the received signal correlation from two antennas," *IEEE Antenna Propag. Lett*., vol. 4, pp. 97-99, Jun. 2005.

[28] K. Abe, H. Arai, T. Mitsui, and N. Takemura, "Beam Switched Antenna by Phase

Difference Feed," *IEICE Trans. Commun*., vol. J94–B, no. 2, pp. 156–163. (in Japanese)

[29] R. J. Garbacz, "Modal expansions for resonance scattering phenomena," *Proc. IEEE*, vol. 53, no. 8, pp. 856-864, Aug. 1965.

[30] R. F. Harrington, and J. R. Mautz, "The theory of characteristic modes for conducting bodies," *IEEE Trans. Antennas Propag*., vol. 19, no. 5, pp. 622-628, Sep. 1971.

[31] K. K. Kishor, and S. V. Hum, "A Two-Port Chassis-Mode MIMO Antenna," *IEEE Antennas Wireless Propag. Lett*., vol. 12, pp. 690-693, May 2013.

[32] G. Li, H. Zhai, Z. Ma, C. Liang, R. Yu, and S. Liu, "Isolation-Improved Dual-Band MIMO Antenna Array for LTE/WiMAX Mobile Terminals," *IEEE Antennas Wireless Propag. Lett*., vol. 13, pp. 1128-1131, Jun. 2014.

[33] L. Kang, H. Li, X. Wang, and X. Shi, "Compact Offset Microstrip-Fed MIMO Antenna for Band-Notched UWB Applications," *IEEE Antennas Wireless Propag. Lett*., vol. 14, pp. 1754-1757, Apr. 2015.

[34] Z. Ren, and A. Zhao, "Dual-Band MIMO Antenna With Compact Self-Decoupled Antenna Pairs for 5G Mobile Applications," *IEEE Access*, vol. 7, pp. 82288-82296, Jun. 2019.

[35] S. Nandi, and A. Mohan, "A Compact Dual-Band MIMO Slot Antenna for WLAN Applications," *IEEE Antennas Wireless Propag. Lett*., vol. 16, pp. 2457-2460, Jul. 2017.

[36] J. Deng, J. Li, L. Zhao, and L. Guo, "A Dual-Band Inverted-F MIMO Antenna With Enhanced Isolation for WLAN Applications," *IEEE Antennas Wireless Propag. Lett*., vol. 16, pp. 2270-2273, Jun. 2017.

[37] H. Huang, and J. Wu, "Decoupled Dual-Antenna With Three Slots and a Connecting Line for Mobile Terminals," *IEEE Antennas Wireless Propag. Lett.*, vol. 14, pp. 1730-1733, Apr. 2015.

[38] J-S. Sun, H-S. Fang, P-Y. Lin, and C-S. Chuang, "Triple-Band MIMO Antenna

for Mobile Wireless Applications," *IEEE Antennas Wireless Propag. Lett*., vol. 15, pp. 500-503, Jul. 2015.

[39] M. S. Khan, A-D. Capobianco, A. I. Najam, I. Shoaib, E. Autizi, and M. F. Shafique, "Compact ultra-wideband diversity antenna with a floating parasitic digitated decoupling structure," *IET Microw. Antennas Propag*., vol. 8, no. 10, pp. 747-753, Jul. 2014.

[40] L. Zhao, and K-L. Wu, "A Dual-Band Coupled Resonator Decoupling Network for Two Coupled Antennas," *IEEE Trans. Antennas Propag*., vol. 63, no. 7, pp. 2843-2850, Jul. 2015.

[41] F. Liu, J. Guo, L. Zhao, G-L. Huang, Y. Li, and Y. Yin, "Dual-Band Metasurface-Based Decoupling Method for Two Closely Packed Dual-Band Antennas," *IEEE Trans. Antennas Propag*., vol. 68, no. 1, pp. 552-557, Jan. 2020.

[42] R. Liu, X. An, H. Zheng, M. Wang, Z. Gao, and E. Li, "Neutralization Line Decoupling Tri-Band Multiple-Input Multiple-Output Antenna Design," *IEEE Access*, vol. 8, pp. 27018-27026, Feb. 2020.

[43] T. Miyasaka, H. Sato, and M. Takahashi, "A Dual-Band Decoupling Method of 2 Elements MIMO Antennas by Using a Short Stub and a Branch Element," *IEICE Trans. Commun*., vol. E102-B, no. 8, pp. 1763-1770, Aug. 2019.

[44] M. A. Fakih, A. Diallo, P. L. Thuc, R. Staraj, O. Mourad, and E. A. Rachid, "Optimization of Efficient Dual Band PIFA System for MIMO Half-Duplex 4G/LTE and Full-Duplex 5G Communications," *IEEE Access*, vol. 7, pp. 128881-128895, Sep. 2019.

[45] S. Zhang, B. K. Lau, Y. Tan, Z. Ying, and S. He, "Mutual Coupling Reduction of Two PIFAs With a T-Shape Slot Impedance Transformer for MIMO Mobile Terminals," *IEEE Trans. Antennas Propag*., vol. 60, no. 3, pp. 1521-1531, Mar. 2012.

[46] C-M. Luo, J-S. Hong, and M. Amin, "A decoupling method between two tri-band antennas for WLAN/WiMAX applications," *IEICE Elect. Express*, vol. 14, no. 11, pp. 1-6, May 2017.

[47] S. P. Biswal, and S. Das, “Two-element printed PIFA-MIMO antenna system for WiMAX and WLAN applications,” *IET Microw. Antennas Propag*., vol. 12, no. 14, pp. 2262-2270, Oct. 2018.

[48] A. Diallo, C. Luxey, P. L. Thuc, R. Staraj, and G. Kossiavas, “Enhanced two-antenna structures for universal mobile telecommunications system diversity terminals,” *IET Microw. Antennas Propag*., vol. 2, no. 1, pp. 93-101, Feb. 2018.

[49] C. Yu, S. Yang, Y. Chen, W. Wang, L. Zhang, B. Li, and L. Wang, “A Super-Wideband and High Isolation MIMO Antenna System Using a Windmill-Shaped Decoupling Structure,” *IEEE Access*, vol. 8, pp. 115767-115777, Jun. 2020.

[50] D. Sipal, M.P. Abegaonkar, and S.K. Koul, “Easily Extendable Compact Planar UWB MIMO Antenna Array,” *IEEE Antennas Wireless Propag. Lett.*, vol. 16, pp. 2328-2331, Jun. 2017.

[51] M. Alibakhshikenari, M. Khalily, B.S. Virdee, C.H. See, R.A.A-Alhameed, and E. Limiti, “Mutual-Coupling Isolation Using Embedded Metamaterial EM Bandgap Decoupling Slab for Densely Packed Array Antennas,” *IEEE Access*, vol. 7, pp. 51827-51840, Apr. 2019.

[52] M.S. Sharawi, “Current Misuses and Future Prospects for Printed Multiple-Input, Multiple-Output Antenna Systems,” *IEEE Antennas Propag. Mag*., vol. 59, pp. 162-170, Apr. 2017.

[53] D. Sarkar, and K.V. Srivastava, “A Compact Four-Element MIMO/Diversity Antenna With Enhanced Bandwidth,” *IEEE Antennas Wireless Propag. Lett*., vol. 16, pp. 2469-2472, Jul. 2017.

[54] W-J. Liao, C-Y. Hsieh, B-Y. Dai, and B-R. Hsiao, “Inverted-F/Slot Integrated Dual-Band Four-Antenna System for WLAN Access Points,” *IEEE Antennas Wireless Propag. Lett*., vol. 14, pp. 847-850, Dec. 2014.

[55] H. Lin, Q. Chen, Y. Ji, X. Yang, J. Wang, and L. Ge, “Weak-Field-Based Self-Decoupling Patch Antennas,” *IEEE Trans. Antennas Propag*., vol. 68, no. 6, pp. 4208-4217, Jun. 2020.

[56] Y. Li, C-Y-D. Sim, Y. Luo, and G. Yang, “High-Isolation 3.5 GHz Eight-Antenna

MIMO Array Using Balanced Open-Slot Antenna Element for 5G Smartphones," *IEEE Trans. Antennas Propag*., vol. 67, no. 6, pp. 3820-3830, Jun. 2019.

[57] G. Srivastava, and A. Mohan, "Compact MIMO Slot Antenna for UWB Applications," *IEEE Antennas Wireless Propag. Lett*., vol. 15, pp. 1057-1060, Oct. 2015.

[58] K-L. Wong, X-Q. Ye, and W-Y. Li, "Wideband Four-Port Single-Patch Antenna Based on the Quasi-TM1/2,1/2 Mode for 5G MIMO Access-Point Application," *IEEE Access*, vol. 10, pp. 9232-9240, Jan. 2022.

[59] W. Su, Q. Zhang, S. Alkaraki, Y. Zhang, X-Y Zhang, and Y. Gao, "Radiation Energy and Mutual Coupling Evaluation for Multimode MIMO Antenna Based on the Theory of Characteristic Mode," *IEEE Trans. Antennas Propag*., vol. 67, no. 1, pp. 74-84, Jan. 2019.

[60] Z. Ren, and A. Zhao, "Dual-Band MIMO Antenna With Compact Self-Decoupled Antenna Pairs for 5G Mobile Applications," *IEEE Access*, vol. 7, pp. 82288-82296, Jun. 2019.

[61] L. Sun, Y. Li, Z. Zhang, and H. Wang, "Self-Decoupled MIMO Antenna Pair With Shared Radiator for 5G Smartphones," *IEEE Trans. Antennas Propag*., vol. 68, no. 5, pp. 3423-3432, May 2020.

[62] R. Mathur, and S. Dwar, "8-port multibeam planar UWB-MIMO antenna with pattern and polarisation diversity," *IET Microw. Antennas Propag*., vol. 13, pp. 2297-2302, Oct. 2019.

[63] D. Gao, Z. Cao, X. Quan, M. Sun, S. Fu, and P. Chen, "A Low-Profile Decoupling Slot-Strip Array for 2 × 2 Microstrip Antenna," *IEEE Access*, vol. 8, pp. 113532-113542, Jun. 2020.

[64] K-L. Wu, C. Wei, X. Mei, and Z-Y. Zhang, "Array-Antenna Decoupling Surface," *IEEE Trans. Antennas Propag*., vol. 65, no. 12, pp. 6728-6738, Dec. 2019.

[65] A. Boukarkar, X. Q. Lin, Y. Jiang, L. Y. Nie, P. Mei, and Y. Q. Yu, "A Miniaturized Extremely Close-Spaced Four-Element Dual-Band MIMO Antenna System With Polarization and Pattern Diversity," *IEEE Antennas Wireless Propag. Lett*., vol.

17, no. 1, pp. 134-137, Nov. 2017.

[66] T. H. Nguyen, H. Morishita, Y. Koyanagi, K. Izui, and S. Nishiwaki, “Space-saving and broadband design of a small vertical U-shaped folded dipole antenna for dual-band WiMAX using a PSO algorithm,” *IEICE Commun. Express*, vol. 1, no. 3, pp. 89-94, Aug. 2012.

Research Achievements

Journal Papers

[1] Q. Q. Phung, T. H. Nguyen, N. Michishita, H. Sato, Y. Koyanagi, and H. Morishita, "Broadband design of U-shaped folded dipole antenna for WiMAX by using characteristic mode analysis," *IEICE Commun. Express*, vol. 8, no. 8, pp. 347-352, May 2019.

[2] Q. Q. Phung, T. H. Nguyen, N. Michishita, H. Sato, Y. Koyanagi, and H. Morishita, ''A Study on Decoupling Method for Two PIFAs Using Parasitic Elements and Bridge Line," *IEICE Trans. Commun*., vol. E104-B, no. 6, pp. 630-638, Jun. 2021.

[3] Q. Q. Phung, T. H. Nguyen, N. Michishita, H. Sato, Y. Koyanagi, and H. Morishita, ''Dual-Band Design and Decoupling Between Two Planar Inverted-F Antennas Using Linear Parasitic Elements and Bridge Line," *IET Microw. Antennas Propag*., vol. 16, no. 2-3, pp. 103-112, Feb. 2022.

[4] Q. Q. Phung, N. Michishita, H. Sato, Y. Koyanagi, and H. Morishita, ''Decoupling Method for Two Planar Inverted-F Antennas Using Inverted-L-Shaped Elements Based on Characteristic Mode Analysis," *Transaction of the Japan Society for Simulation Technology*, vol. 14, no. 1, pp. 1-8, 2022.

[5] Q. Q. Phung, T. H. Nguyen, N. Michishita, H. Sato, Y. Koyanagi, and H. Morishita, ''Decoupling Method for Four Closely Spaced Planar Inverted-F Antennas Using Parasitic Elements and Bridge Lines," *IEICE Trans. Commun*., 2023. (Conditional Acceptance)

[6] Q. Q. Phung, N. Michishita, H. Sato, Y. Koyanagi, and H. Morishita, ''Bandwidth Maintenance and Decoupling for Two Planar Inverted-F Antenna using Bridge Line," *Journal of Advanced Simulation in Science and Engineering*, 2023. (Conditional Acceptance)

International Conferences

[1] Q. Q. Phung, T. H. Nguyen, N. Michishita, H. Sato, Y. Koyanagi, and H. Morishita, "Characteristic Mode Analysis of U-Shaped Folded Dipole Antenna for WiMAX," *The 2019 International Workshop on Antenna Technology (iWAT)*, Mar. 2019.

[2] Q. Q. Phung, Y. Nakagawa, T. H. Nguyen, N. Michishita, H. Sato, Y. Koyanagi, and H. Morishita, "Decoupling of Two Planar Inverted-F Antennas by Using Parasitic Elements," *The 2019 Malaysia - Japan Workshop on Radio Technology (MJWRT 2019)*, Aug. 2019.

[3] Q. Q. Phung, N. Michishita, H. Sato, Y. Koyanagi, and H. Morishita, "A Study of Decoupling for Two Planar Inverted F Antennas," *The 2019 URSI - Japan Radio Science Meeting*, Sep. 2019.

[4] Q. Q. Phung, Y. Nakagawa, T.H. Nguyen, N. Michishita, H. Sato, Y. Koyanagi, and H. Morishita, "A Decoupling Method for Two PIFAs by Using Bridged Two Parasitic Elements," *2019 International Symposium on Antennas and Propagation (ISAP)*, Oct. 2019.

[5] Q. Q. Phung, N. Michishita, H. Sato, Y. Koyanagi, and H. Morishita, ''Quantitative Evaluation of the Decoupling Principle Between Two PIFAs by Using CMA," *2020 International Symposium on Antennas and Propagation (ISAP)*, Apr. 2021.

[6] Q. Q. Phung, T. Kai, N. Michishita, H. Sato, Y. Koyanagi, and H. Morishita, ''A Study of Decoupling Method Using Parasitic Elements for Two Planar Inverted-F Antennas," *2021 IEEE-APS Topical Conference on Antennas and Propagation in Wireless Communications (APWC)*, Sep. 2021.

[7] Q. Q. Phung, N. Michishita, H. Sato, Y. Koyanagi, and H. Morishita, ''Dual-Band Design and Decoupling for Two PIFAs Using Linear Parasitic Elements and Bridge Line," *2021 International Symposium on Antennas and Propagation (ISAP)*, Oct. 2021.

[8] Q. Q. Phung, N. Michishita, H. Sato, Y. Koyanagi, and H. Morishita, ''Decoupling Method for Two Planar Inverted-F Antennas Based on Current Modes on Ground

Plane," *2021 IEEE International Workshop on Electromagnetics (iWEM)*, Nov. 2021.

[9] Q. Q. Phung, N. Michishita, H. Sato, Y. Koyanagi, and H. Morishita, "Decoupling Method for Two Planar Inverted-F Antennas using Characteristic Mode Analysis," *2021 IEEE International Symposium on Antennas and Propagation and USNC-URSI Radio Science Meeting (APS)*, Dec. 2021.

[10] Q. Q. Phung, N. Michishita, H. Sato, Y. Koyanagi, and H. Morishita, "Decoupling Between Multiple Planar Inverted-F Antennas Without Adjusting Antenna Configuration," *2021 European Conference on Antennas and Propagation (EuCAP)*, Mar. 2022.

[11] Q. Q. Phung, N. Michishita, H. Sato, Y. Koyanagi, and H. Morishita, "Decoupling and Bandwidth Maintenance for Two Planar Inverted-F Antennas using Bridge Line," *The 41st JSST Annual International Conference on Simulation Technology*, Sep. 2022.

[12] Q. Q. Phung, N. Michishita, H. Sato, Y. Koyanagi, and H. Morishita, "Decoupling of Four Closely Spaced PIFAs Using Parasitic Elements and Bridge Lines," *2022 International Symposium on Antennas and Propagation (ISAP)*, Nov. 2022.

Technical Reports and Domestic Conferences

[1] Q. Q. Phung, N. Michishita, H. Sato, Y. Koyanagi, and H. Morishita, "Decoupling of Planar Inverted-F Antenna by Using Parasitic Elements," *IEICE Society Conference*, B-1-54, Sep. 2018. (in Japanese)

[2] Q. Q. Phung, N. Michishita, H. Sato, Y. Koyanagi, and H. Morishita, "A Simple Decoupling of Planar Inverted-F Antenna by Using Parasitic Elements," *IEICE General Conference*, B-1-98, Mar. 2019. (in Japanese)

[3] Q. Q. Phung, T. H. Nguyen, N. Michishita, H. Sato, Y. Koyanagi, and H. Morishita, "Decoupling of 2 Elements Planar Inverted-F Antenna by Using Parasitic Elements," *IEICE Society Conference*, BS-1-1, Sep. 2019. (in Japanese)

[4] Q. Q. Phung, N. Michishita, H. Sato, Y. Koyanagi, and H. Morishita, “A Consideration on Decoupling Method of 2 Elements Planar Inverted-F Antenna by Using Characteristic Mode Analysis,” *IEICE Society Conference*, B-1-65, Sep. 2020. (in Japanese)

[5] Q. Q. Phung, N. Michishita, H. Sato, Y. Koyanagi, and H. Morishita, “A Study on Decoupling Method for Two PIFAs Using Parasitic Elements and Consideration by Characteristic Mode Analysis,” *IEICE Technical Report*, AP2020-59, Sep. 2020. (in Japanese)

[6] Q. Q. Phung, N. Michishita, H. Sato, Y. Koyanagi, and H. Morishita, “Decoupling method for two PIFA elements considering the ground plane current by characteristic mode analysis,” *IEICE General Conference*, B-1-75, Mar. 2021. (in Japanese)

[7] Q. Q. Phung, N. Michishita, H. Sato, Y. Koyanagi, and H. Morishita, “A Study of Decoupling Method for Two Planar Inverted-F Antenna Elements Using Characteristic Mode Analysis,” *JSST Conference on Simulation Technology*, Apr. 2021. (in Japanese)

[8] Q. Q. Phung, N. Michishita, H. Sato, Y. Koyanagi, and H. Morishita, “Decoupling Method for Two PIFA Elements at Two Resonant Frequencies by Using Linear Parasitic Elements and Bridge Line,” *IEICE Society Conference*, B-1-71, Sep. 2021. (in Japanese)

[9] Q. Q. Phung, N. Michishita, H. Sato, Y. Koyanagi, and H. Morishita, “A Study on Decoupling Method Operating at Single and Dual-Frequency for Planar Inverted-F Antennas by Using Parasitic Elements,” *The 23rd AMT-ken Radio Terminal and Antenna System Measurement Technology*, Dec. 2021. (in Japanese)

[10] Q. Q. Phung, N. Michishita, H. Sato, Y. Koyanagi, and H. Morishita, “Decoupling Method for Four Planar Inverted-F Antennas using Parasitic and Bridge Elements,” *IEICE General Conference*, B-1-61, Mar. 2022. (in Japanese)

[11] Q. Q. Phung, N. Michishita, H. Sato, Y. Koyanagi, and H. Morishita, “A Study on Decoupling Method for Multiple Planar Inverted-F Antennas by Using Parasitic

Elements and Bridge Lines," *IEICE Technical Report*, AP2022-59, Jul. 2022. (in Japanese)

[12] Q. Q. Phung, N. Michishita, H. Sato, Y. Koyanagi, and H. Morishita, "Decoupling and Bandwidth Maintenance for Two-element Planar Inverted-F Antennas using Bridge Line," *IEICE Society Conference*, B-1-36, Sep. 2022. (in Japanese)

Other Research Activities

Awards

[1] Young Engineering Award of *Technical Committee on Antennas and Propagation of IEICE* (電子情報通信学会アンテナ・伝播研究専門委員会若手奨励賞), Dec. 2020.

[2] Student Presentation Award of *The 41st JSST Annual International Conference on Simulation Technology*, Sep. 2022.